QUANTUM LIQUIDS AND QUANTUM CRYSTALS

Complexes in rare-gas solid solutions

A. I. Karasevskiĭ[a)]

G. V. Kurdyumov Institute of Metal Physics of the National Academy of Sciences of Ukraine, pr. Vernadskogo 36, Kiev 03142, Ukraine

(Submitted October 22, 2004; resubmitted June 2, 2005)

It is shown that complexes—equilibrium nanoclusters of impurity atoms—can form in dilute rare-gas solid solutions consisting of two species of atoms with substantially different radii; the thermodynamic stability of these complexes is due to relaxation of the excess elastic energy when the impurity atoms combine into a cluster. Two types of complexes can occur: vacancy complexes (VCs) and cluster complexes (CCs). In the VC case, impurity atoms are bound in the first coordination sphere of a vacancy. The VCs are separate formations, and their equilibrium concentration can be significantly higher than that of isolated vacancies. In the CC case, clusters of n impurity atoms with a volume close to that occupied by $n-1$ host atoms (in the clustering of n atoms of smaller radius than the host) or $n+1$ host atoms (in the clustering of n atoms of larger radius) can form. An analysis is made of the particular case of a dilute solution of ^{4}He in ^{3}He, where, on account of the mass difference of ^{3}He and ^{4}He, the effective radii of the atoms in the crystal are different, giving rise to elastic stresses around a ^{4}He impurity atom in the crystal. © *2005 American Institute of Physics*. [DOI: 10.1063/1.2144449]

INTRODUCTION

Some types of rare-gas atoms are miscible in the solid state, and the solid solutions that form can separate, as the temperature is lowered, into phases consisting of practically pure constituents. If the radii of the constituent atoms are substantially different, then in the region of low concentration of one constituent the elastic stresses arising around the atoms of that constituent can lead to the formation of complexes—equilibrium nanoclusters of impurity atoms, the thermodynamic stability of which is due to a relaxation of the excess elastic energy when those atoms combine into a cluster. This relaxation can be due to two causes: the transition of an impurity atom into the first coordination sphere of a vacancy, and the formation of an n-atom cluster having a volume close to that occupied by $n-1$ (in the clustering of n atoms of smaller radius) or $n+1$ (in the clustering of n atoms of larger radius) host atoms.[1,2] Since the energy benefit from the relaxation of elastic energy is relatively small, favorable conditions for cluster formation exist at low temperatures, when the positive contribution to the free energy of the system due to the decrease of the configurational entropy of the solution is also small, although it is necessary that the diffusion mobility of the atoms in the solution remain sufficiently high. All of these conditions are well satisfied for ^{4}He–^{3}He binary solid solutions, which have a high mobility of the atoms at low temperatures, and the effective radii of the atoms in the crystal differ because of the mass difference of ^{3}He and ^{4}He, giving rise to elastic stresses around a ^{4}He impurity in a ^{3}He crystal or a ^{3}He impurity in a ^{4}He crystal. For the sake of definiteness our discussion of complex formation in this paper will be done for the case of ^{3}He–^{4}He solid solutions; the results are applicable for any binary solid solution with a sufficiently high atomic mobility.

In Sec. I we investigate vacancy complexes (VCs) in which the impurity atoms are bound in the first coordination sphere of a vacancy. Here the VCs are separate formations and, as will be shown below, the concentration of such VCs can be significantly higher than that of isolated vacancies.

In Sec. II we consider the formation of clusters of $n+1$ impurity atoms—cluster complexes (CCs)—with a displacement volume of n host atoms. For example, $n+1$ ^{4}He atoms situated at n sites of the ^{3}He crystal. As we shall show, in decomposing ^{3}He–^{4}He solutions the most favorable process will be the formation of such CCs near the decomposition curves.

I. VACANCY COMPLEXES

The transition of a ^{4}He impurity atom into the first coordination sphere of a vacancy in the ^{3}He crystal will lead to partial relaxation of the excess elastic energy, making the region around a vacancy in the ^{3}He crystal energetically favorable for ^{4}He impurity atoms. This mechanism of cluster formation around a vacancy for impurity atoms having a crystallographic radius differing strongly from the atoms of the host crystal was first considered in Ref. 1, where such formations were called complexes.

For complexes in ^{3}He–^{4}He solid solutions we shall assume that when i atoms of the ^{4}He impurity pass into the first coordination sphere of a vacancy, the energy of vacancy formation u_0 in the pure ^{3}He crystal changes additively by $i\Delta u$, i.e., the energy of formation of a complex of the ith tssype, consisting of a vacancy and i atoms of ^{4}He in the first coordination sphere of that vacancy, is equal to

$$u_i = u_0 + i\Delta u, \tag{1}$$

where $i=0,1,\ldots,z$.

Following Ref. 1, the change of the free energy of the ^{3}He crystal upon dissolution of a small number of ^{4}He atoms in it can be written as

$$\Phi = \Phi_0 + v_0 N_4 + TN_4 \ln \frac{N_4}{eG} + + \sum_{i=0}^{z} \left[u_i n_i + Tn_i \ln \frac{n_i}{eGW(i)} \right], \tag{2}$$

where N_4 is the total number of impurity atoms not bound to vacancies, v_0 is the change of the thermodynamic potential of the crystal when the ^{4}He impurity atoms are located near the ^{3}He crystal lattice sites not connected to vacancies, and G is the total number of lattice sites. The factor

$$W(i) = \frac{z!}{i\,!\,(z-i)!} \tag{3}$$

takes into account the possible permutations of the ^{3}He and ^{4}He atoms in the first coordination sphere of the vacancy. The equilibrium values of N_4 and n_i are determined from the condition that the thermodynamic potential (2) be minimum with respect to N_4 and n_i for a fixed number N_0 of ^{4}He impurity atoms in the system,

$$N_0 = N_4 + \sum_{i=0}^{z} i n_i, \tag{4}$$

which is taken into account with the aid of a Lagrange multiplier λ. After minimizing (2) with respect to N_4 and n_i we obtain

$$c_{^4\mathrm{He}} = \frac{N_4}{G} = c_0 \mathrm{e}^{-\lambda_1/T}, \tag{5}$$

$$c_i = \frac{n_i}{G} = \frac{z!}{i\,!\,(z-i)!} c_0^i c_v \mathrm{e}^{-i\lambda_1/T} \mathrm{e}^{-i\Delta w/T}. \tag{6}$$

Here $c_v = \mathrm{e}^{-u_0/T}$ is the equilibrium concentration of vacancies in the pure crystal, and $\Delta w = \Delta u - v_0$ is the change of the free energy of the crystal upon the transition of an impurity atom from the bulk into the first coordination sphere of a vacancy. For greater clarity we have introduced in (5) and (6) the renormalized Lagrange multiplier

$$\lambda_1 = v_0 + T \ln c_0 - \lambda, \tag{7}$$

where $c_0 = N_0/G$ is the mean impurity concentration in the crystal. It follows from Eq. (5) that for such a choice of Lagrange multiplier the value of λ_1 determines the degree of deviation of the concentration of impurities not bound to vacancies from its mean value in the crystal. Taking Eq. (6) into account, we can write the total concentration of complexes in the crystal in the form

$$\bar{c} = \sum_{i=0}^{z} c_i = [1 + c_0 \mathrm{e}^{-\lambda_1/T} \mathrm{e}^{-\Delta w/T}]^z c_v. \tag{8}$$

Equally simple expressions are also obtained for the total concentration of impurity atoms in complexes

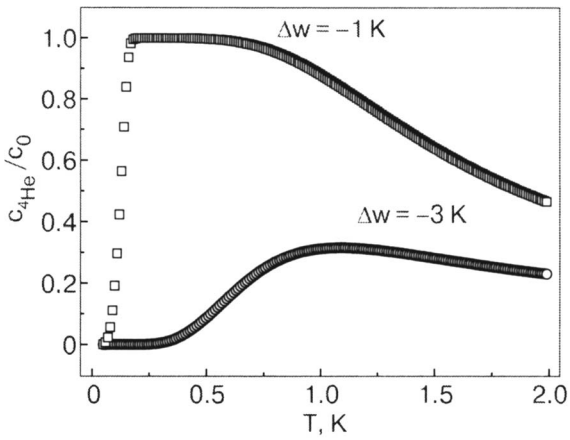

FIG. 1. Temperature dependence of the concentration of free ^{4}He impurity atoms in the ^{3}He crystal (c_0=0.02, u_0=6 K).

$$\sum_{i=0}^{z} i c_i = z c_0 \mathrm{e}^{-\lambda_1/T} \mathrm{e}^{-\Delta w/T} [1 + c_0 \mathrm{e}^{-\lambda_1/T} \mathrm{e}^{-\Delta w/T}]^{z-1} c_v \tag{9}$$

and the balance Eq. (4) for determining the Lagrange multiplier:

$$\mathrm{e}^{\lambda_1/T} = 1 + z \mathrm{e}^{-\Delta w/T} [1 + c_0 \mathrm{e}^{-\lambda_1/T} \mathrm{e}^{-\Delta w/T}]^{z-1} c_v. \tag{10}$$

The theoretical results (5)–(10) permit one to describe the state of a dilute ($c_0 \ll 1$) solution with allowance for a possible change of energy (1) of impurity atoms in the first coordination sphere of a vacancy. As an example, Figs. 1–3 show the results obtained for the equilibrium values of various parameters characterizing the complexes in a solution in the temperature interval 0.05–2 K at c_0=0.02 and for an energy of vacancy formation in the pure ^{3}He crystal u_0 =6 K and a relatively weak interaction of impurity atoms with a vacancy, Δw=−1 and −3 K. It should be stressed that the values of the parameters and the results presented in Figs. 1–3 are purely for illustration. The parameter Δw in ^{3}He −^{4}He solid solutions the results of Ref. 3 can be evaluated using the results of Ref. 3, where a calculation of the interaction of vacancies with various lattice defects in solid ^{4}He

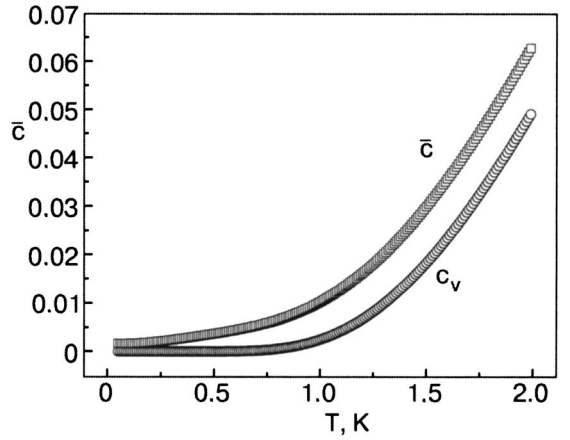

FIG. 2. Temperature dependence of the total concentration $\bar{c}$ of complexes in a crystal in comparison with the equilibrium vacancy concentration c_v(Δw=−3 K, c_0=0.02, u_0=6 K).

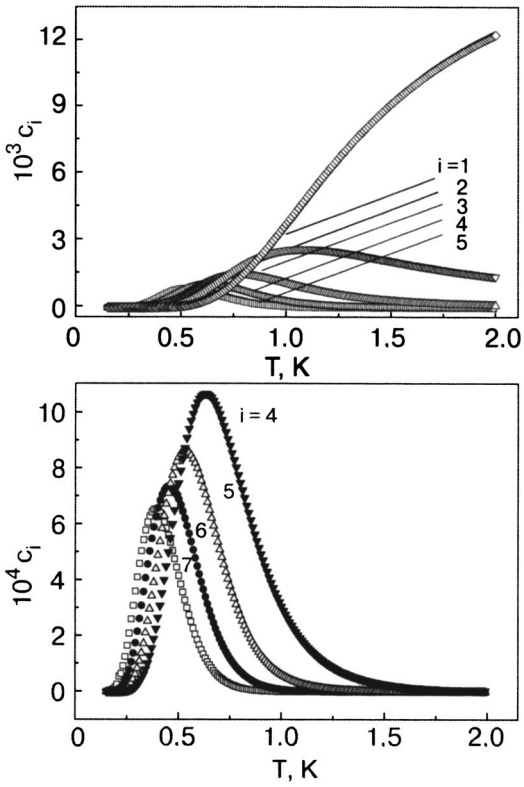

FIG. 3. Temperature dependence of the concentration of multiatomic complexes for $\Delta w=-3$ K, $c_0=0.02$, $u_0=6$ K.

was carried out. In the general case one must determine Δw on the basis of a statistical description of the relaxation of the medium near a vacant lattice site.

The formation of vacancy complexes—bound states of i impurity atoms and a vacancy—depletes the supply of free impurities in the solution, i.e., it leads to a decrease of the ratio $c_{^4\mathrm{He}}/c_0$. Figure 1 shows the curve of $c_{^4\mathrm{He}}/c_0$ for two values of Δw, from which it follows that for a relatively large value of $|\Delta w|/T>1$ and low temperatures $T\leqslant 0.5$ K, practically all the impurity atoms are found in complexes. For $T\leqslant 1$ K the concentration of complexes will be significantly higher than the concentration of vacancies in the crystal (Fig. 2), and the complexes will in essence be the main type of equilibrium low-temperature defect in the crystalline solution. Indeed, in the case of a relatively large negative value of Δw the change of energy upon formation of a complex consisting of i impurity atoms, $u_c=u_0+i\Delta w$, can turn out to be negative. In that case in the low-temperature region, where the contribution of the configurational entropy to the free energy of complex formation is small, the thermodynamically favorable process in the solid solution will be the formation not of vacancies but of vacancy complexes containing a rather large number of impurity atoms surrounding a vacancy. It follows from Eqs. (5) and (10) that the transition of impurity atoms to complexes occurs in a rather narrow temperature interval $\Delta T\sim\Delta w$ (Fig. 1). With increasing temperature the multiatomic VCs decompose (Figs. 1 and 3), and in a dilute solid solution at high temperatures the main types of defects are isolated vacancies, at which, because $\Delta w<0$, impurity atoms can be "adsorbed" in the first coordination sphere (Fig. 3), i.e., the character of the formation of VCs changes with temperature, as is manifested in the nonmonotonic dependence of the curves in Fig. 1. The cause of the formation of vacancy complexes of ^{4}He atoms in the ^{3}He crystal could be the change in energy of the impurity atoms in the first coordination sphere of a vacancy, which is formally taken into account by means of the parameter Δw. As was assumed in Ref. 1, one of the causes of such a lowering of the energy is the partial relaxation of the excess elastic energy arising in the crystal on account of the distortion of the lattice by an impurity with a smaller or larger crystallographic radius. In the continuum approximation this energy has the value[4]

$$\delta E\approx\frac{3E}{(1+\sigma)}v\left[\frac{R_3}{R_4}-1\right]^2, \tag{11}$$

where $v=4\pi R_3^3/3$, E and σ are Young's modulus and Poisson's ratio for the ^{3}He crystal, and R_3 and R_4 are the crystallographic radii of the ^{3}He and ^{4}He atoms. For $E=2\times10^8$ dyn/cm^2, $\sigma=0.5$, $R_3=3.77\times10^{-8}$ cm, and $R_3/R_4\approx1.06$, one gets $\delta E\approx2.57$ K.

Besides the relaxation of elastic energy, substitution of a host atom by an impurity atom in the first coordination sphere of a vacancy will also lead to a change of the energy of the atoms surrounding the vacant lattice site. It can be assumed that compression of the medium around a vacant site will prevent an atom of large crystallographic radius from entering that region (the ^{3}He atoms in the case of the isotypic solution ^{4}He$-^3$He) but will favor the substitution of host atoms by atoms of smaller radius (^{4}He). This is possibly the reason for the absence of ^{3}He clusters upon the thermocycling of dilute solid solutions of ^{3}He in ^{4}He.[5,6]

II. CLUSTER COMPLEXES

If a cluster of n atoms of ^{4}He is formed in a dilute solid solution of ^{4}He in ^{3}He, then at a certain value n_1 the volume of the cluster can be equal (close to) the volume occupied by n_1-1 ^{3}He atoms. At a certain value $n_2>n_1$ a cluster with a volume equal to that of n_2-2 ^{3}He atoms forms, etc. In each of these cases a cluster of n_i ($i=1, 2, \ldots$) atoms of ^{4}He will cause hardly any elastic deformation of the surrounding medium, and the formation of such a cluster will be accompanied by the relaxation of the excess elastic energy of the individual atoms forming the cluster. Obviously the values of n_i will depend on the molar volumes per ^{4}He and ^{3}He atom:

$$n_i=i\frac{V_{^3\mathrm{He}}}{(V_{^3\mathrm{He}}-V_{^4\mathrm{He}})}.$$

Thus, at a pressure $P=30.6$ bar, when $V_{^3\mathrm{He}}=24.6$ cm^3/mole and $V_{^4\mathrm{He}}=20.54$ cm^3/mole, one has $n_1\approx6$, $n_2\approx12$, etc. An increase of the cluster size from n_i to n_{i+1} in the cell formed by n_i-i host atoms is accompanied by a monotonic increase of the elastic strain of the surrounding medium with increasing n. However, at a certain value of n, increasing the size of the cell will lead to a decrease of the elastic energy, which goes to zero for a cluster of n_{i+1} atoms in a cell formed by $n_{i+1}-(i+1)$ host atoms. Thus the transition from a cluster with n_i to a cluster with n_{i+1} requires overcoming a potential barrier separating these two metastable states of the solution. It should be noted that the argu-

ments given above are valid for a continuous medium, and the results can change substantially when the crystal structure of both the host and the inclusions is taken into account.

The metastability of the cluster state in the solution is due to the presence of excess surface energy at the cluster–host boundary, and also the work $R[c]>0$ necessary to create a region with a high concentration of impurity atoms in a homogeneous dilute solution.[7] On the decomposition curve $R[c]=0$, and the excess energy of the clusters with respect to the segregation of a bulk phase will be determined by the surface energy, which is small in ^{3}He–^{4}He, and near the decomposition curve a significant number of clusters can form, with the characteristic feature that they contain a fixed number of atoms n_i. Because of the microscopic size of VCs and CCs in ^{3}He–^{4}He solid solutions, the answer to the question of which of the types of complexes is formed in these solutions can be obtained only with a statistical treatment of the formation of complexes in ^{3}He–^{4}He solid solutions. In the case of VCs such a statistical treatment must include a description of the structure of the vacancy and a determination of the change of the energy of impurity atoms when they substitute for atoms of the first coordination sphere of vacancies found in a compressed or dilatated state.

It should be mentioned again that ^{3}He–^{4}He solid solutions are objects favorable for complex formation. This is because of the significant difference of the crystallographic radii of the ^{3}He and ^{4}He atoms and the high diffusion mobility of these atoms at low temperatures, when relatively weak influences cause appreciable changes in the concentration of the solution. Since in the present treatment the quantum nature of the ^{3}He and ^{4}He atoms was manifested only in a difference of their crystallographic radii, all of the results obtained above can be used for studying complexes in other systems, e.g., in solid solutions of heavy rare gases.

In closing the author thanks V. N. Grigor'ev and E. Ya. Rudavskii for fruitful discussion and substantive comments.

[a)]E-mail: akaras@imp.kiev.ua

[1]M. A. Krivoglaz, Fiz. Tverd. Tela (Leningrad) **12**, 2445 (1970) [Sov. Phys. Solid State **12**, 1955 (1971)].
[2]M. A. Krivoglaz, Fiz. Met. Metalloved. **57**, 1057 (1984).
[3]S. E. Kal'noi and M. A. Strzhemechnyi, Fiz. Nizk. Temp. **8**, 1025 (1982) [Sov. J. Low Temp. Phys. **8**, 515 (1982)].
[4]L. D. Landau and E. M. Lifshitz, *Theory of Elasticity*, 2nd ed., Pergamon Press, Oxford (1970), Nauka, Moscow (1965).
[5]A. N. Ganshin, V. N. Grigor'ev, V. A. Maĭdanov, A. A. Penzev,É. Ya. Rudavskiĭ, A. S. Rybalko, and E. V. Syrnikov, JETP Lett. **73**, 289 (2001).
[6]V. Maidanov, A. Ganshin, V. Grigor'ev, A. Penzev, E. Rudavskii, A. Rybalko, and E. Syrnikov, J. Low Temp. Phys. **126**, 133 (2002).
[7]L. D. Landau and E. M. Lifshitz, *Statistical Physics*, 2nd ed., Pergamon Press, Oxford (1969), Nauka, Moscow (1964).

Translated by Steve Torstveit

Thermodynamics of quasi-one-dimensional deposits on carbon nanobundles

T. N. Antsygina, I. I. Poltavsky, and K. A. Chishko[a)]

B. Verkin Institute for Low Temperature Physics and Engineering, National Academy of Sciences of Ukraine, pr. Lenina 47, Kharkov 61103, Ukraine

T. A. Wilson and O. E. Vilches[b)]

Department of Physics, University of Washington, Seattle, Washington 98194-1560, USA
(Submitted June 17, 2005)

The low-temperature thermodynamics of helium adsorbed in the outer grooves of carbon nanobundles is investigated theoretically in a lattice-gas model with the use of the Green's function formalism. The proposed model describes both the formation of a one-dimensional (1D) condensate on the bottoms of the grooves and also the formation of two secondary chains in the groove (a three-chain structure) and thus is adequate for interpreting the behavior of the adsorbate over a rather wide range of coverages in the initial stage of deposition. The temperature dependence of the density of the deposit is obtained for the primary chain and secondary chains. The energy, heat capacity, and heat of adsorption are found as functions of temperature, and the total density of the 1D adsorbate is obtained for several different values of the binding energy with the substrate for atoms deposited in the primary and secondary positions. The adsorption isotherms (the total density of adsorbate as a function of external pressure) are calculated for various temperatures. Experimentally measured adsorption isotherms are presented for ^{4}He deposited on bundles of single-walled carbon nanotubes. The measurements were made in the temperature range 2–15 K. Those experiments and previously published data on the adsorption isotherms of methane are interpreted using a theoretical model developed in this paper. © *2005 American Institute of Physics*. [DOI: 10.1063/1.2144450]

I. INTRODUCTION

Low-dimensional cryocrystals obtained by depositing atoms or molecules from the gas phase on different types of substrates are under active experimental and theoretical investigation at the present time.[1,2] A large percentage of the papers on this subject involve the study of the structure and thermodynamics of two-dimensional (2D) systems in the form rare-gas monolayers[2–9] on atomically smooth flat surfaces of graphite and metals. A recent achievement in this field is the preparation and experimental study of systems formed during deposition of molecules or atoms on the inner and outer surfaces of carbon bundles.[10–17]

A nanobundle is a sheaf of carbon nanotubes[18] with a hexagonal close-packed structure in the cross section perpendicular to the tubes.[19–21] The diameter of the tubes (from 5 to 14Å) and the number of tubes in an individual bundle (from tens to hundreds) depend on the technology used to prepare the carbon samples. The deposits are laid down in several possible positions. First, in the intratube channels, second, the intertube channels, and, finally, the outer surface of the bundles. Intratube filling is possible only in nanobundles consisting of open nanotubes. The deposition in the intertube channels, owing to their restricted size, is possible only for small atoms and molecules (helium, neon, hydrogen).[12] Although theoretical estimates[22] show that these position are energetically favorable,[23] their role in real systems remains in dispute.[10,12]

Of particular interest is the interpretation of effects associated with the deposition of particles on the outer surface of a nanobundle. Typically in such deposition there is a progression of stages with increasing number of adsorbed particles, from the 1D crystal to a three-chain structure, then to a multilayer quasi-1D structure, and, finally, to a two-dimensional structure at large occupations. Of course, this progression of structures is reflected in the thermodynamic characteristics of the system measured directly in experiment. Thus it is of interest to study the thermodynamics of deposits on nanobundles theoretically to provide a suitable interpretation of the observed effects.

Of the considerable number of theoretical papers on the topic of our discussion, many are devoted to calculations of the adsorption potentials and the mechanisms of localization of the deposits inside and on the outer surface of the bundles,[19–22,24–27] and also to phonon excitations in continuous deposits.[28] Only a few papers discuss the individual aspects of the thermodynamic behavior of the systems of interest to us,[29–31] and the findings of most of the theoretical papers cited are based exclusively on the use of numerical methods of computer simulation. Thus there is an urgent need to develop models and approaches that would permit one to obtain analytical results in the thermodynamics of low-dimensional deposits.

In Ref. 32 an analytical approach in the lattice-gas model was used to investigate the thermodynamics of a 1D system formed in the grooves of a carbon nanobundle in the initial stage of deposition of an atomic (helium) deposit in them, and it was shown that the theoretical results obtained are in quantitative agreement with the experimental data.[10] In the present paper we propose a model that can describe adequately the thermodynamics of an atomic deposit not only during the formation and consolidation of a 1D condensate on the bottom of the grooves of a nanobundle but also in the

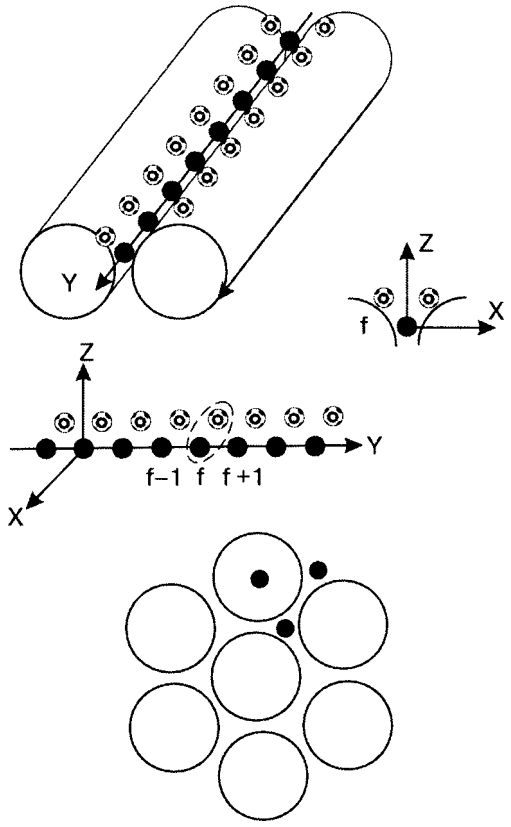

FIG. 1. Configuration of the system.

initial stage of formation of the three-chain structure.

II. STATEMENT OF THE PROBLEM

Let us consider a closed system containing N particles distributed between two subsystems. The particles deposited on the outer surface of the bundles form a low-dimensional subsystem (adsorbate). The particles enclosed in the free volume of an isolated cell containing nanobundles belong to the three-dimensional (3D) subsystem (adsorbent). The 3D subsystem will be described by the model of an ideal lattice gas.[33] In such an approach that subsystem is simply a reservoir of particles to be deposited on the bundles.

The specific part of the problem lies in the description of the low-dimensional subsystem. Here the most favorable positions are in the grooves between two nanotubes, and in the initial stage of deposition the particles are adsorbed predominantly at those positions, forming 1D linear chains. As the occupation of the first row increases, two new chains in symmetric positions parallel to it begin to form and develop, resulting in the formation of a three-chain structure (Fig. 1).

We will be interested in the case corresponding to the initial stage of formation of the upper chains, when the number of particles in them is comparatively small, so that the interparticle interaction in the upper chains can be neglected. We shall assume that the Hamiltonian of the system can be written in lattice-gas form. We divide the total number of lattice sites B that can be occupied by particles of the system into three groups. The first group are those sites (the total number of which is denoted B_3) occupied by the particles in the volume, the second consists of all possible sites (B_1) corresponding to particle positions in the lower chain (groove), and the third group to those sites ($2B_1$) that correspond to particle positions in the two upper chains. The fraction of the total constituted by sites of the lower chain is denoted as $\xi(\xi=B_1/B, B=3B_1+B_3)$. The distribution of particles between the volume and the three-chain subsystem (which will be referred to below as the low-dimensional subsystem) at a fixed temperature must be found from the corresponding equilibrium conditions. We note that in the initial adsorption stage of interest to us here, the pressure and density of the 3D gas are so small that the 3D atmosphere can be treated to good accuracy as an ideal gas irrespective of its composition; this justifies the assumption of ideality of the 3D subsystem.

The Hamiltonian of the low-dimensional subsystem has the form

$$H=\varepsilon_0\sum_f n_f+U\sum_f n_f n_{f+1}+\varepsilon_1\sum_f n_f n_{f+1}(A_f+B_f), \qquad (1)$$

where ε_0 and ε_1 are the well depths for particles belonging to the lower and upper chains, respectively, U is the interaction potential of the particles in the lower chain, and n_f, A_f, and B_f are the occupation numbers of the positions in the lower chain and two upper chains, respectively, which take values of 0 or 1. The index f labels the cells of the low-dimensional subsystem. Hamiltonian (1) takes into account explicitly that the deposition of particles in a site f of the upper chains of a cell is possible only under the condition that the positions f and $f+1$ in the lower chain are occupied by atoms.

The low-dimensional subsystem is found in contact with a 3D ideal gas, the thermodynamic potential (per site) of which has the form[33]

$$\Omega_{3D}=-T\ln[1+\exp(\beta\mu)], \qquad (2)$$

where $\beta=1/T$, and μ is the chemical potential (we are using a system of units in which Boltzmann's constant is equal to unity). The two subsystems are found in thermodynamic equilibrium with each other, i.e., they have equal temperatures T and chemical potentials μ. The chemical potential as a function of temperature can be found from the condition of conservation of the total number N of particles in the system,

$$\xi n_{\rm ads}+(1-3\xi)n_{3D}=x. \qquad (3)$$

Here $x=N/B$, $n_{\rm ads}=n+n_{uc}$ is the density of the adsorbate in the low-dimensional subsystem, $n=\langle n_f\rangle$ (the angle brackets denote thermodynamic averaging), $n_{uc}=\langle A_f\rangle+\langle B_f\rangle$, and n_{3D} is the density of particles in the 3D subsystem, equal to

$$n_{3D}=-\frac{\partial\Omega_{3D}}{\partial\mu}=f(0), \qquad (4)$$

where $f(y)$ is the Fermi distribution function,

$$f(y)=\{1+\exp[\beta(y-\mu)]\}^{-1}.$$

We will be interested in the thermodynamic functions of the low-dimensional subsystem: the mean energy E and heat capacity C_V (per site), and also the heat of adsorption $Q_{\rm ads}$:[34]

$$E=\varepsilon_0 n+Uc_2+2\varepsilon_1 b_2, \quad C_V=\frac{\partial E}{\partial T},$$

$$Q_{\rm ads} = T^2\left(\frac{\partial \ln P}{\partial T}\right)_N. \tag{5}$$

We introduce the following notation:

$$c_2 = \langle n_{f+1} n_f\rangle, \quad b_2 = \langle A_f n_{f+1} n_f\rangle = \langle B_f n_{f+1} n_f\rangle, \tag{6}$$

where P is the pressure of a 3D ideal lattice gas,

$$P = \frac{B_3}{v_{3D}} T \ln[1+\exp(\beta\mu)], \tag{7}$$

where v_{3D} is the volume of the 3D subsystem. The heat of adsorption $Q_{\rm ads}$ is the energy necessary for the transfer of a particle from the low-dimensional to the 3D subsystem. For $T\to 0$ and $x\to 0$ the value of $Q_{\rm ads}$ should approach ε_0.

Together with the aforementioned quantities, an experimental study will also determine a family of adsorption isotherms, i.e., the number of adsorbed particles as a function of pressure at various temperatures. From that family of curves one can recover the so-called isosteric heat of adsorption $Q_{\rm st}$,[35]

$$Q_{\rm st} = T^2\left(\frac{\partial \ln P}{\partial T}\right)_{B_1, n_{\rm ads}}. \tag{8}$$

We note that the isosteric heat of adsorption $Q_{\rm st}$ coincides with the binding energy ε_0 of the particles with the substrate in the limit when the temperature and density of the adsorbate approach zero.

III. SYSTEM OF EQUATIONS FOR THE AVERAGES

Our goal is to calculate the averages n, c_2, and b_2 in terms of which the thermodynamic characteristics (5) of the system are expressed. To solve the problem we use the method of two-time Green's functions.[36] To find $n=\langle c_f^+ c_f\rangle$ it is necessary to write the equation of motion for the spectral components of the anticommutator Green's function

$$G_f = \langle\langle c_f | c_f^+\rangle\rangle_\omega, \tag{9}$$

where c_f^+ and c_f are the Fermi creation and annihilation operators in the lower chain. Appearing on the right-hand side of the equation of motion are Green's functions of higher order, for which one should also construct equations of motion, so that a chain of equations is formed. In this case, because of the form of the system Hamiltonian (1), the chain is broken, resulting in a system of nine equations:

$$(\Lambda + 2\varepsilon_1 + 2U)G_f = \frac{1}{2\pi} + UK_f(1) + \varepsilon_1 K_f(S), \tag{10}$$

$$(\Lambda + 2\varepsilon_1 + U)K_f(1) = \frac{n}{\pi} + UR_f(1,1) + \varepsilon_1[K_f(S) + R_f(1,S)], \tag{11}$$

$$(\Lambda + 2\varepsilon_1)R_f(1,1) = \frac{n^2}{\pi} + 2\varepsilon_1 R_f(1,S), \tag{12}$$

$$(\Lambda + \varepsilon_1 + U)K_f(S) = \frac{2b_1}{\pi} + UR_f(1,S) + 2\varepsilon_1[K_f(\Gamma) + 2R_f(1,\Gamma)], \tag{13}$$

$$(\Lambda + \varepsilon_1)R_f(1,S) = \frac{2\lambda_1}{\pi} + 6\varepsilon_1 R_f(1,\Gamma), \tag{14}$$

$$(\Lambda + U)K_f(\Gamma) = \frac{\tau}{\pi} + UR_f(1,\Gamma) + \varepsilon_1 R_f(S,\Gamma), \tag{15}$$

$$\Lambda R_f(1,\Gamma) = \frac{\lambda_2}{\pi} + \varepsilon_1 R_f(S,\Gamma), \tag{16}$$

$$(\Lambda - \varepsilon_1)R_f(S,\Gamma) = \frac{2\lambda_3}{\pi} + 2\varepsilon_1 R_f(\Gamma,\Gamma), \tag{17}$$

$$(\Lambda - 2\varepsilon_1)R_f(\Gamma,\Gamma) = \frac{\lambda_4}{\pi}, \tag{18}$$

where $\Lambda = \omega - \varepsilon_0 - 2\varepsilon_1 - 2U$. In Eqs. (10)–(18) we have introduced the functions

$$K_f(P) = \langle\langle (P_f n_{f+1} + P_{f-1} n_{f-1}) c_f | c_f^+\rangle\rangle_\omega,$$

$$R_f(P,Q) = R_f(Q,P) = \langle\langle (P_f Q_{f-1} + Q_f P_{f-1})\,\eta_f c_f | c_f^+\rangle\rangle_\omega$$

(where the arguments P and Q are combinations of occupation numbers) and the operators

$$S_f = A_f + B_f, \quad \Gamma_f = A_f B_f, \quad \eta_f = n_{f+1} n_{f-1},$$

and the averages

$$b_1 = \langle A_f n_f\rangle = \langle B_f n_f\rangle = \langle A_f n_{f+1}\rangle = \langle B_f n_{f+1}\rangle,$$

$$\tau = \langle \Gamma_f n_f\rangle = \langle \Gamma_f n_{f+1}\rangle,$$

$$\lambda_1 = \langle A_f \eta_f\rangle = \langle B_f \eta_f\rangle = \langle A_{f-1}\eta_f\rangle = \langle B_{f-1}\eta_f\rangle,$$

$$\lambda_2 = \langle \Gamma_f \eta_f\rangle = \langle \Gamma_{f-1}\eta_f\rangle = \langle A_f A_{f-1}\eta_f\rangle = \langle B_f B_{f-1}\eta_f\rangle = \langle A_f B_{f-1}\eta_f\rangle = \langle B_f A_{f-1}\eta_f\rangle,$$

$$\lambda_3 = \langle \Gamma_f A_{f-1}\eta_f\rangle = \langle \Gamma_f B_{f-1}\eta_f\rangle = \langle A_f \Gamma_{f-1}\eta_f\rangle = \langle B_f \Gamma_{f-1}\eta_f\rangle,$$

$$\lambda_4 = \langle \Gamma_f \Gamma_{f-1}\eta_f\rangle.$$

In writing the system of equations we have neglected in Eq. (12) the correlations between the occupation numbers of particles at sites found a distance of two steps along the chain, i.e., we have assumed that the values of n_{f+1} and n_{f-1} are statistically independent, so that

$$\langle \eta_f\rangle = \langle n_{f+1} n_{f-1}\rangle = n^2. \tag{19}$$

The accuracy of this approximation is estimated in the Appendix.

Solving the system of equations (10)–(18) with relation (19) and using the functions G_f and $K_f(1)$, one can find the averages n and c_2. We note that Eqs. (10)–(18) contain the averages b_1, τ, and λ_i, which cannot be determined with the aid of the Green's functions that appear in this system. To close the system it must be supplemented with the equations for the Green's functions, which will permit us to find the quantities indicated. As can be seen from the definition of the averages b_1, τ, and λ_i, each of them contains at least one of the operators $A_f = a_f^+ a_f$ or $B_f = b_f^+ b_f$ (a_f^+, b_f^+, a_f, and b_f are the creation and annihilation operators for particles in the upper

chains). This makes it possible to calculate averages with the use of Green's function of the type $\langle\langle \hat{L}a_f | a_f^+ \rangle\rangle_\omega$ and $\langle\langle \hat{L}b_f | b_f^+ \rangle\rangle_\omega$ (where $\hat{L}$ is an operator that depends on the occupation numbers of particles at the sites of the upper and lower chains) and thereby to simplify the calculation considerably. We introduce the following notation for the Green's functions we seek:

$$X_f(P) = \langle\langle P_{f-1} n_f a_f | a_f^+ \rangle\rangle_\omega, \quad Y_f = \langle\langle n_{f+1} n_f a_f | a_f^+ \rangle\rangle_\omega,$$

$$Z_f(P) = \langle\langle P_{f-1} \eta_f a_f | a_f^+ \rangle\rangle_\omega, \quad W_f = \langle\langle B_f \Gamma_{f-1} \eta_f a_f | a_f^- \rangle\rangle_\omega.$$

Doing the necessary calculations, we obtain

$$X_f(1) = F(n, c_2), \quad Y_f = F(c_2, c_2), \quad X_f(B) = F(b_1, b_2),$$

$$Z_f(1) = F(n^2, c_3), \quad Z_f(A) = F(\lambda_1, s_1),$$

$$Z_f(\Gamma) = F(\lambda_2, s_2), \quad W_f = F(\lambda_3, s_3),$$

where

$$F(a,b) = \frac{1}{2\pi}\left(\frac{a-b}{\omega} + \frac{b}{\omega - \varepsilon_1}\right), \quad s_m = c_3 f^m(\varepsilon_1),$$

$$c_3 = \langle \eta_f n_f \rangle.$$

With the aid of the functions X, Z, and W and the dispersion relations,[36] we can express b_1, τ, and λ_i, which appear in Eqs. (10)–(18), and b_2, which is needed to determine the mean energy (5), in terms of the quantities n, c_2, and c_3 as follows:

$$b_1 = \Phi(n, c_2), \quad b_2 = \Phi(c_2, c_2), \quad \tau = \Phi(b_1, b_2),$$

$$\lambda_1 = \Phi(n^2, c_3), \quad \lambda_{m+1} = \Phi(\lambda_m, s_m), \quad m = 1,2,3,$$

where the function $\Phi(a,b)$ has the form

$$\Phi(a,b) = (a-b)f(0) + bf(\varepsilon_1). \tag{20}$$

On the other hand, the averages n, c_2, and c_3 are determined directly with the aid of the Green's functions, which are found from Eqs. (10)–(18). As a result, we arrive at a system of self-consistent equations for n, c_2, and c_3:

$$n = (1-n)^2 f(\varepsilon_0) + 2c_2 - c_3, \tag{21}$$

$$c_2 = [n(1-n) + \tau - 2b_1 + 2\lambda_1 - \lambda_2] f(\varepsilon_0 + U) + 2(b_1 - \tau - \lambda_1 + \lambda_2) f(\varepsilon_0 + \varepsilon_1 + U) + (\tau - \lambda_2) f(\varepsilon_0 + 2\varepsilon_1 + U) + c_3, \tag{22}$$

$$c_3 = (n^2 - 4\lambda_1 + 6\lambda_2 - 4\lambda_3 + \lambda_4) f(\varepsilon_0 + 2U) + 4(\lambda_1 - 3\lambda_2 + 3\lambda_3 - \lambda_4) f(\varepsilon_0 + \varepsilon_1 + 2U) + 6(\lambda_2 - 2\lambda_3 + \lambda_4) f(\varepsilon_0 + 2\varepsilon_1 + 2U) + 4(\lambda_3 - \lambda_4) f(\varepsilon_0 + 3\varepsilon_1 + 2U) + \lambda_4 f(\varepsilon_0 + 4\varepsilon_1 + 2U). \tag{23}$$

Relations (21)–(23) must be supplemented by the equation (3) for determining the chemical potential. The averages $\langle A_f \rangle$ and $\langle B_f \rangle$ appearing in (3) are calculated according to the scheme described above. As a result, Eq. (3) becomes

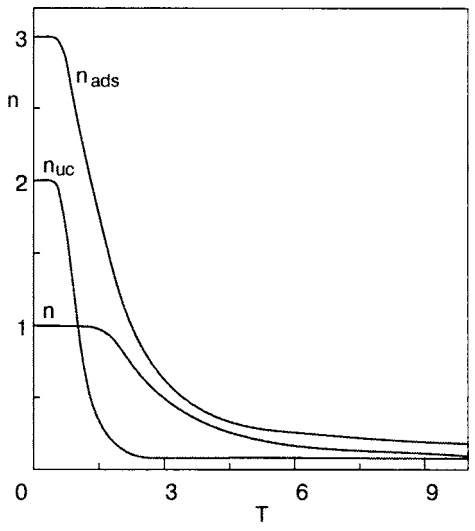

FIG. 2. Temperature dependence of the mean densities of the adsorbate in the lower chain n and in the upper chains n_c and also of the total adsorbate density $n_{\text{ads}} = n + n_{uc}$.

$$\xi n + 2\xi\Phi(1, c_2) + (1 - 3\xi) f(0) = x. \tag{24}$$

The system of equations (21)–(24) in the general case can be solved only numerically.

IV. THERMODYNAMIC FUNCTIONS OF THE SYSTEM

Solving the system of Eqs. (21)–(24), we find the chemical potential μ and the averages n, c_2, and b_2 in terms of which the thermodynamic functions (5) of the adsorbate are expressed. It is of interest to analyze the character of the dependences of these quantities for different values of the system parameters ε_0 and ε_1, since they are directly determined by both the interaction of the adsorbate with the bundle and by the geometry of the surface onto which the deposition occurs.

In this Section we choose as the unit of measurement for the energy the interparticle interaction energy U while retaining the same notation as before for variables of the corresponding dimensions. To do the calculations we must also specify the values of the parameters ξ and x. In a real experiment the parameter ξ depends not only on the structure of the bundles but also on the free volume of the experimental cell and is therefore to some degree arbitrary. In all the calculations of this Section we assume $\xi = 0.01$, which apparently corresponds to the real experimental conditions.[10] Finally, we shall assume that the mean density of particles in the system is unchanging and take its value to be $x = 0.04$, i.e., such that for a specified total number of particles N there manifestly exists a temperature region in which all of the positions of the low-dimensional subsystem are filled by adsorbate.

Figure 2 shows the temperature dependence of the adsorbate densities $n(T)$ and $n_{uc}(T)$ in the lower and upper chains, respectively, and also the total density of the adsorbate $n_{\text{ads}}(T)$ at a fixed value of the total number of particles in the system. It is seen in Fig. 2 that the groove is filled faster than the upper chains. This is completely understandable, since, first, the inequality $|\varepsilon_0| > |\varepsilon_1|$ holds, and, second, the filling of each of the positions in the upper chain is possible only under the condition that the neighboring positions

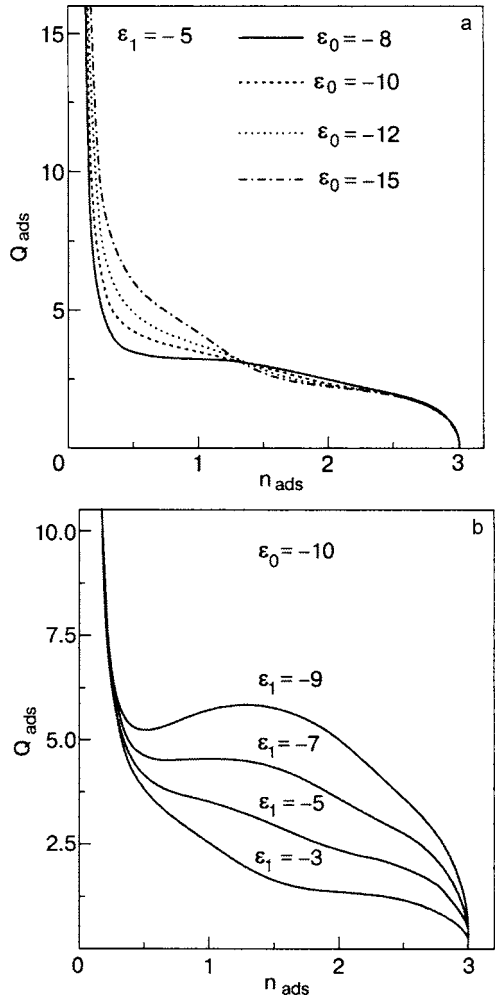

FIG. 3. Dependence of the heat of adsorption on the total adsorbate density for various values of ε_0 (a) and ε_1 (b).

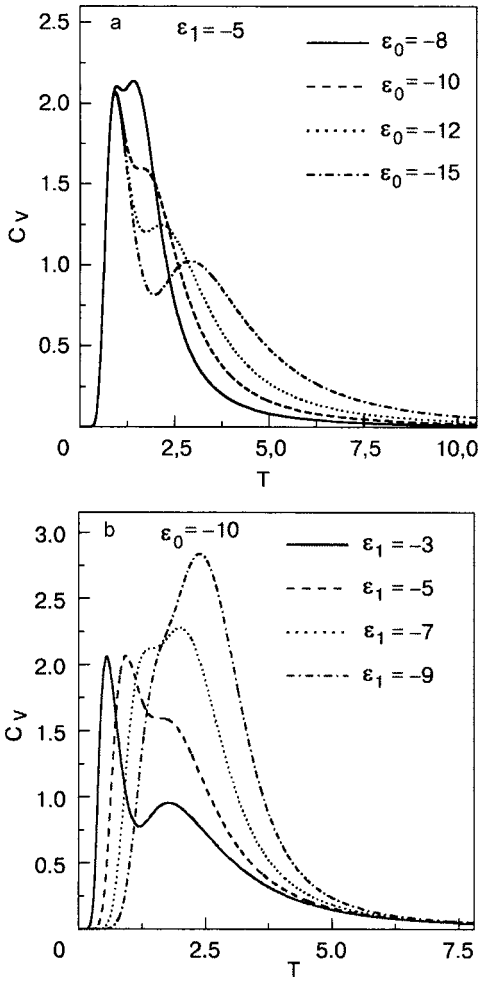

FIG. 4. Temperature dependence of the heat capacity for different values of ε_0 (a) and ε_1 (b).

in the lower chain are filled. Accordingly, the total adsorbate density $n_{\text{ads}}(T) \to 3$ for $T \to 0$ if $x > 3\xi$, as is the case in our problem. With increasing density of particles in the system an expansion of the temperature region near zero in which n and n_{uc} are close to the limiting values occurs.

For the experimental study of the systems under discussion the main thermodynamic quantities are usually presented as functions of the adsorbate density n_{ads}. Figure 3a shows a family of curves of the heat of adsorption Q_{ads} as a function of n_{ads} for different values of ε_0 and a fixed value $\varepsilon_1 = -5$, and Fig. 3b shows the same functions for different ε_1 and a fixed $\varepsilon_0 = -10$. It is seen in Fig. 3a that at small n_{ads} (high temperatures) the heat of adsorption is progressively larger the larger the ratio $\varepsilon_0/\varepsilon_1$, whereas for n_{ads} greater than about 1.25, on the contrary, Q_{ads} decreases with increasing $\varepsilon_0/\varepsilon_1$. The curves in Fig. 3b show that Q_{ads} increases with increasing ratio $\varepsilon_1/\varepsilon_0 < 1$, and as it approaches unity the $Q_{\text{ads}}(n_{\text{ads}})$ curves exhibit a maximum near $n_{\text{ads}} \simeq 1.5$. Such behavior of Q_{ads} is due to the change of the relative contributions to this quantity from the particles of the lower and upper chains as the ratio between the energies ε_1 and ε_0 changes. Indeed, at low occupations the contribution of the lower chain is always predominant, and the more so the larger the ratio $\varepsilon_0/\varepsilon_1$. With increasing n_{ads} the lower chain is rapidly filled and ceases to influence the variation of the system energy, and accordingly the formation of the heat of adsorption is due to the particles of the upper chains (Fig. 2). The energy of localization in the upper chain, $|\varepsilon_1|$, is smaller than $|\varepsilon_0|$, but the upper row has twice as many positions for adsorption, so that for comparable values of $|\varepsilon_1|$ and $|\varepsilon_0|$ a maximum appears on the $Q_{\text{ads}}(n_{\text{ads}})$ curve because of the predominant contribution of atoms deposited in the upper chains (see Fig. 3b).

The temperature dependence of the heat capacity of the low-dimensional subsystem (normalized by B_1) at different values of ε_0 and fixed $\varepsilon_1 = -5$ is shown in Fig. 4a, and the same curves for different ε_1 and fixed $\varepsilon_0 = -10$ are presented in Fig. 4b. The behavior of the heat capacity changes substantially with changing ratio $\varepsilon_0/\varepsilon_1$. At comparatively large $|\varepsilon_0|$ the heat capacity has a pronounced double-peak character, the broad, high-temperature peak being due to the filling of the groove and the narrow, low-temperature peak to the deposition of particles in the upper chains. With decreasing ratio $\varepsilon_0/\varepsilon_1$ the two peaks grow in amplitude and draw closer together. Such behavior of the heat capacity is explained by the circumstance that the positions of the peaks correspond to the regions of the fastest variation of n_{ads} with temperature.

Figure 5 shows the dependence of the heat of adsorption and heat capacity on the mean density x of particles in the system for three different values of the temperature and at

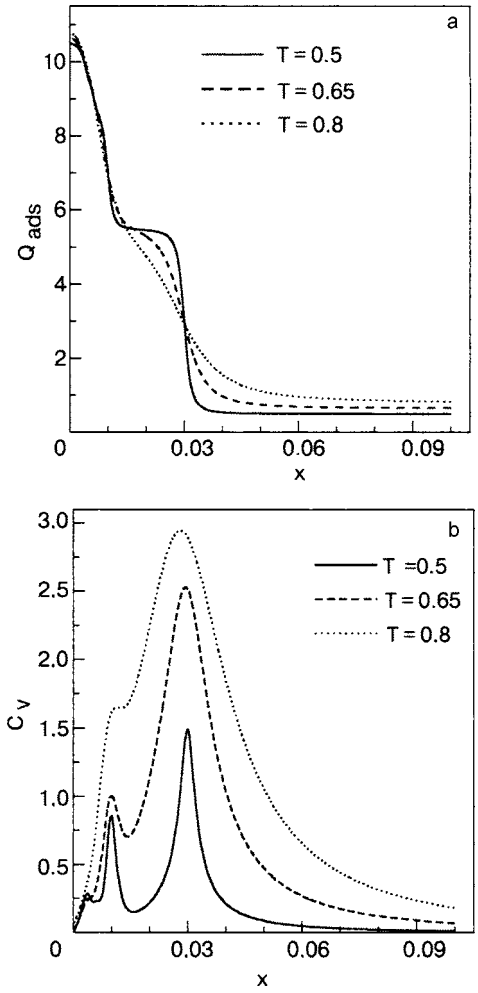

FIG. 5. Dependence of the heat of adsorption (a) and heat capacity (b) on the density of particles at different temperatures.

fixed parameters $\varepsilon_0=-10$ and $\varepsilon_1=-5$. It is seen from the curves that Q_{ads} and C_V have features at $x\simeq\xi$ and $x\simeq 3\xi$. Specifically, the $Q_{\text{ads}}(x)$ curves exhibit steps at those values of x, and the $C_V(x)$ curves have maxima that become more pronounced as the temperature is lowered. This is due to details of the filling process in the low- and high-energy positions at different temperatures. Apparently at low T the particles settle predominantly in the positions of the groove, and the transition to the upper chains is a rather sharp one. At high temperatures, naturally, the picture is smeared.

Moreover, at temperatures below $T\sim 0.5$ and low densities, $x<\xi$, the $CV(x)$ curves acquire a third peak, the parameters of which are wholly determined by the value of the interatomic interaction U. The presence of a maximum of the heat capacity at $T\sim U$ is a known property of the 1D lattice gas.[33,37]

Figure 6 shows the dependence of the isosteric heat Q_{st} on the number of adsorbed particles. One can obtain a theoretical evaluation of Q_{st} without having to use the adsorption isotherms, the method commonly used to extract Q_{st} from experimental data. In the theoretical case one can find it by supplementing the system of Eqs. (21)–(24) by the condition of constancy of the number of particles adsorbed on the nanobundle, $n_{\text{ads}}=\text{const}$, and assuming that x, the total number of particles in the system, is variable. As is seen in Fig. 6,

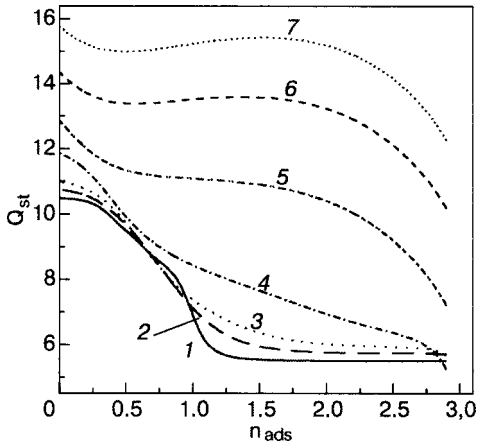

FIG. 6. Dependence of the isosteric heat on the adsorbate density at different temperatures: 0.5 (*1*), 0.75 (*2*), 1 (*3*), 2 (*4*), 5 (*5*), 8 (*6*), and 10 (*7*).

with decreasing temperature $Q_{\text{st}}(n_{\text{ads}}\to 0)$ approaches ε_0, i.e., it approaches the limiting value corresponding to the binding energy with a groove of a nanobundle, in complete agreement with the physical meaning of Q_{st}.

Thus the analysis carried out in this Section shows that the variation of each of the system parameters ε_0, ε_1, and U has a different influence on the character of the behavior of the thermodynamic quantities. This means that in a comparison of theory with experiment one can achieve agreement only for a unique choice of the values of these parameters.

V. EXPERIMENTAL MEASUREMENTS OF ^{4}He ADSORPTION ISOTHERMS ON NANOBUNDLES

The adsorption isotherms are the conventional tool used to study the physical properties of adsorbates on substrates. The experimental setup consists of a cell in which the adsorbent is placed, connected to a reservoir in which known doses of a gas are prepared for introduction into the system. The cell is held at a low temperature T (the temperature of measurement) and has a free volume V_C in addition to the surface on which the adsorbate settles. The reservoir has a volume V_I and is held at room temperature. The two volumes V_C and V_I should be calibrated for precise determination of the amount of physisorbed gas (deposited on the adsorbent surface) as the difference between the total amount of gas admitted to the system and the amount of gas remaining in the free volume V_C+V_I of the measurement system.

An experiment consists of M successive stages in which metered doses of the gas, prepared beforehand in the reservoir at room temperature, are admitted from the volume V_I into the system. Thus, prior to the start of the mth measurement stage ($m=1,\ldots,M$) a known gas dose $N_I^{(m)}$ is contained in a volume V_I at room temperature and at pressure $P_I^{(m)}$. The mth stage of the experiment starts when the volume V_I is connected to the measurement cell and the system is held for a time necessary to reach equilibrium. After that, the final pressure $P_F^{(m)}$ established in the free volume of the system, V_C+V_I, is measured and the amount of physisorbed gas $N_{\text{ads}}^{(m)}$ is measured. For quantitative description of the adsorbate it is convenient to switch from $N_{\text{ads}}^{(m)}$ to a quantitative $V_{\text{ads}}^{(m)}$ having the meaning of the volume of gas adsorbed after the admission of the mth dose and measured in cubic centimeters

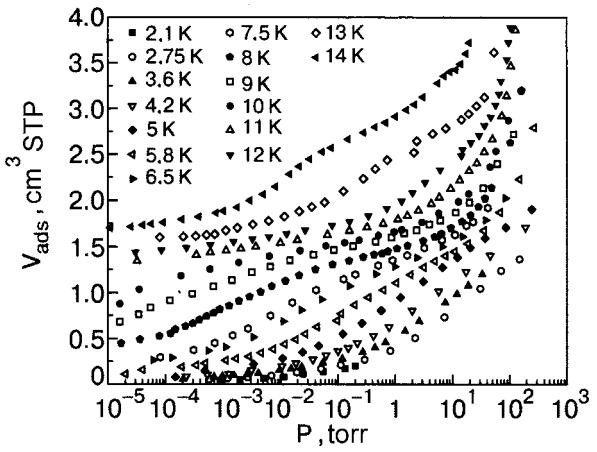

FIG. 7. Adsorption isotherms for ^{4}He, obtained experimentally at different temperatures.

under standard conditions (ccSTP), i.e., at $T_0=273$ K and $P_0=760$ torr. Assuming that the gas filling the free volume of the system is ideal, one can calculate $V_{\text{ads}}^{(m)}$ by the formula

$$V_{\text{ads}}^{(m)} = \alpha \sum_{j=1}^{m} (P_I^{(j)} - P_F^{(j)}) - \gamma P_F^{(m)},$$

where $\alpha=(T_0/T)(V_I/P_0)$ and $\gamma=(T_0/T)(V_C/P_0)$. For equilibrium gas pressures below approximately 2 torr one must introduce corrections in this formula to take into account the presence of thermomolecular effects. For this we shall use the procedure proposed in Ref. 38.

The adsorbent used in our experiments contained 20 mg of unpurified carbon single-walled nanotube bundles (SWNTBs) prepared at Montpellier.[39] The diameter of the bundles, according to scanning electron microscope data, was 10 nm. Neutron-diffraction measurements[40] showed that the nanobundles had a close-packed structure with an average distance between nanotubes of 1.7 nm and contained from 30 to several hundred nanotubes, with an average of from 30 to 50 nanotubes/nanobundle. The purity of the SWNTB sample was around 80%; neutron diffraction reveals the presence in the adsorbent of islands of a catalyst and graphitized particles. It is known from recent neutron diffraction data[41] that the surface density of ^{4}He in a completely perfect monolayer on the lateral surface of a nanobundle is 8.9 atoms/nm^2, so that the specific surface in our adsorbent is at least 240 m^2/g. From the isotherms obtained for other gases deposited on purified nanobundles it is known that their specific surface is larger than 400 m^2/g.

Figure 7 shows a set of our measured ^{4}He adsorption isotherms on SWNTB, plotted as the adsorbed gas volume $V_{\text{ads}}^{(m)}$ (in ccSTP) versus the pressure $P_F^{(m)}$, with corrections for thermomolecular effects. Eight of the isotherms of this set have been published previously.[10]

The set of isotherms measured using a sufficiently small step in T can be used to calculate the isosteric heat of adsorption Q_{st} defined according to Eq. (8). In practice the isotherms $V_{\text{ads}}^{(m)}(\ln P_F^{(m)})$ were processed on a computer, and the results were plotted in the form of $\ln P$ as a function of $1/T$ at constant V_{ads} and then differentiated. The results of the evaluation of Q_{st} in the temperature interval from 5.8 to 14 K show[10] that after the initial stage of deposition, when the heat of adsorption is rapidly decreasing (from values $Q_{\text{st}}\sim 230$ K) with increasing coverage, the $Q_{\text{st}}(n_{\text{ads}})$ curve goes out onto a broad plateau at $Q_{st}\sim 125$ K, which is 12% lower than the values corresponding to adsorption on flat graphite, $Q_{\text{st}}\sim 140$ K.[42] This was to be expected, since the initial adsorption occurs predominantly in the grooves on the outer surface of the nanobundle and imperfect intertube positions[23] (if such there are, due, e.g., to a spread in the values of the diameters of the tubes making up the nanobundle), and then on the graphitelike surface of the nanotubes. This outer surface consists of only one carbon layer and, furthermore, it is curved, and both of these factors can decrease the attraction to it in comparison with flat graphite. These results agree with the previously published data.[16,17]

VI. DISCUSSION OF THE RESULTS. COMPARISON OF THEORY AND EXPERIMENT

The theory constructed in the present paper permits calculation of all the important physical quantities characterizing the thermodynamics of atomic deposits on the outer surfaces of nanobundles. It is of interest to compare the results of the theory with the experimental data presented in the previous Section and with other published data. Here we discuss the interpretation of the ^{4}He adsorption isotherms presented in Fig. 7 and also the CH_4 adsorption isotherms obtained in Ref. 43 for the temperature interval 159.88–194.68 K. We have calculated the adsorption isotherms for both systems using expression (7) for the pressure and compared the results of the calculation with the experimental data mentioned.

For interpreting the helium results we took from the family of isotherms in Fig. 7 those corresponding to the temperature interval 6.5–14 K, since the low-temperature curves of this family correspond to high-density coverages, for which our theory is invalid. We note that although the proposed model was initially constructed for atomic deposits, it can also be applied to methane, which was studied in Ref. 43, since the temperatures at which those measurements were made are significantly greater than the rotational constant of methane, $B=7.56$ K,[44] so that the rotational degrees of freedom of the molecules being deposited are completely excited, and the molecules can be treated as spherically symmetric objects.

The results of a comparison of the theory and experiment are shown in Figs. 8 and 9, and the values of the system parameters determined from the best fit of the theoretical and experimental curves. For comparison of the results of the theory with the experimental data we first chose the values of ε_0 and ε_1. Data have been published only for ε_0 (Refs. 22, 43, 45, and 46, which was calculated numerically and estimated from experiment, while there are no indications as to the possible values of ε_1 and U. One can only say that the relation $|\varepsilon_1|<|\varepsilon_0|$ should hold, since the particles of an upper row are clearly less strongly bound to the substrate than is the adsorbate at the bottom of a groove. The problem of estimating U has not been discussed before. Our analysis has shown that the best quantitative agreement of theory and experiment for the whole family of curves in Figs. 8 and 9 can be obtained only under the assumption that there is a

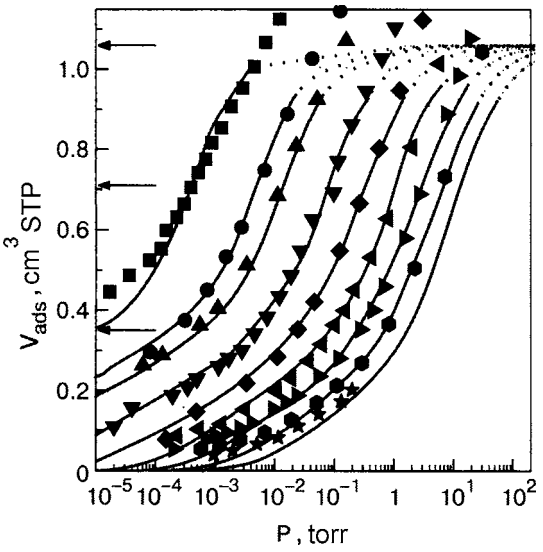

FIG. 8. ^{4}He adsorption isotherms. The symbols represent experimental data of the presence system at temperatures T[K], from left to right): 6.5, 7.5, 8, 9, 10, 11, 12, 13, 14. The curves are the proposed theory. The dotted curves denote the region in which the theory becomes inapplicable. The arrows indicate the number of positions in one, two, and three chains.

repulsion between particles ($U>0$). This is not surprising, since in the region of adsorbate densities of interest to us, the number of occupied positions in the lower chain is rather large, and the mean distances between particles are small, so that the main role is played by the repulsion between adsorbate particles on adjacent sites. Then the system as a whole is stabilized by the strong attraction to the substrate.

We note that in the initial stage of filling of the lower chain, when the number of adsorbate molecules is small and the distances between them are large, the properties of the system are determined predominantly by the attraction between molecules.[32]

Obtaining an estimate of the parameter ξ and the ratio B_3/v_{3D} which appear in expression (7) is problematic because the free volume of the experimental system and the surface area of the nanobundles accessible for adsorption are not known to sufficient accuracy. However, analysis showed that the results of the fitting are not very sensitive to the concrete value of ξ, and what is fundamentally important is that for any fixed ξ the value of x took on values from 0 to $x>3\xi$, at which the total amount of the the gas exceeds the capacity of the low-dimensional subsystem. The ratio B_3/v_{3D} was determined from the condition of best agreement of theory and experiment.

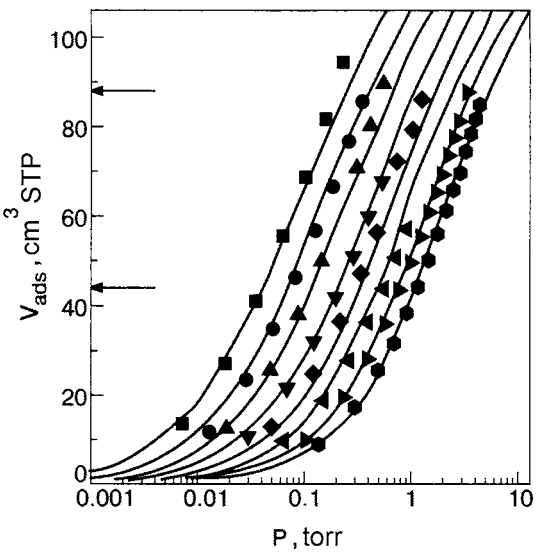

FIG. 9. Adsorption isotherms for methane. The symbols are the experimental data of Ref. 43 at temperatures T[K]: 169, 164, 159, 174, 179, 184, 189, and 194. The curves are the present theory. The arrows indicate the number of positions in one of the two chains.

TABLE I. Values of the parameters of the system for comparison of theory with experiment.

System	ε_0, K	ε_1, K	U, K
^{4}He	−195	−118	17
CH_4	−3030	−2590	5

For converting from the dimensionless units of the theory to the dimensional density of the adsorbate (in cm^3 at standard conditions, ccSTP) we use the fact that the number of adsorbate particles corresponding to the complete filling of three chains ($n_{ads}=3$) can be estimated from experiment.[11,43] This makes it possible to establish uniquely the correspondence between the units of measurement of the density.

It should be emphasized that for the indicated *unique* choice of numerical values of the system parameters (see Table I) the family of calculated adsorption isotherms *automatically* lies on the corresponding families of experimental curves (Figs. 7 and 8) all the way to pressures at which the model considered becomes inapplicable and one must take into account consideration the presence of 2D positions, the interparticle interaction in the upper chains, etc. Here the values which we found for ε_0 in both the helium and methane cases are in good agreement with the values obtained independently from experiment[43,46] and by computer simulation.[22,45]

The results of a comparison of the temperature-averaged calculated curve of Q_{st} for a helium deposit with the corresponding dependence obtained experimentally in Refs. 10 and 11 are presented in Fig. 10.

VII. CONCLUSION

The theory constructed in the present paper gives a good quantitative description of the experimental data actually observed; in particular, it correctly reproduces the behavior of the adsorption isotherms and isosteric heat of adsorption in the vicinity of the transition from the completion of deposition on the bottom of the grooves to the formation of a deposit in the upper chains. The proposed model is effective because it adequately reflects the mechanics of filling of the positions of the upper row, and that fact, on the one hand, makes it possible to achieve real qualitative agreement of the theory and experiment and, on the other hand, suggests a way to describe other effects accompanying the processes of formation of atomic or molecular adsorbates on nanobundles. The model can be generalized to take into account the intertube and intratube deposition and also the presence of higher-order positions—multichain quasi-1D and

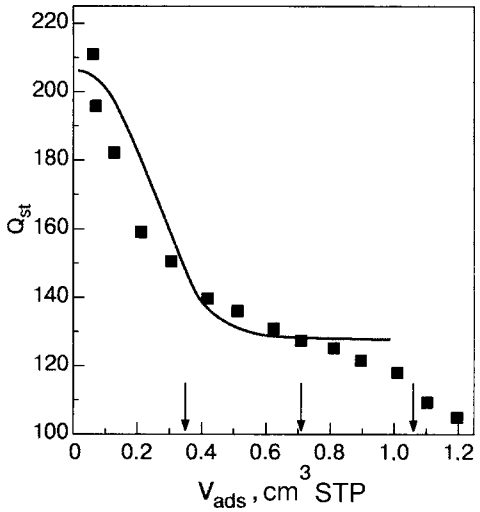

FIG. 10. Isosteric heat as a function of the adsorbate density. The symbols are experimental data.[10] The curve is the proposed theory. The arrows show the number of positions in one, two, and three chains.

quasi-2D. Furthermore, the intraparticle interaction can be taken into account in a more consistent manner.

An advantage of the proposed method is that it enables one to estimate the value of the binding energy ε_0 on the basis of experimental data at rather high adsorbate densities, i.e., in the region where measurements can be made to high accuracy. In addition, the proposed theory can be used to estimate such important parameters of the system as ε_1 and U. In this regard we note that, because the parameters indicated are responsible for the character and position of the anomalies of the thermodynamic quantities as functions of the adsorbate density, the accuracy of their extraction from the experimental data is all the higher the lower the temperature at which the measurements are made, since the anomalies of the thermodynamic functions of the system become more pronounced. This also means that for a deeper investigation of the systems of interest to us, it is vital to extend the experiment to the low-temperature region.

The authors are grateful to the National Science Foundation (U.S.) for support of this study (Grants DMR 0245423 and DMR 98-76763, Kharkov Exchange Supplement).

APPENDIX

Let us investigate the accuracy of the assumption that the quantities n_{f+1} and n_{f-1} are statistically independent. To do this, we consider the case when the particles can be adsorbed only in the lower chain of sites ($\varepsilon_1=0$) or are found in the 3D subsystem. Then the Hamiltonian of the 1D subsystem has the form

$$H_1=\varepsilon_0\sum_f n_f+U\sum_f n_f n_{f+1}. \tag{A1}$$

The problem of calculating the thermodynamic functions of the system in the model of (A1) admits an exact solution (see, e.g., Refs. 33 and 47, and a solution can also be obtained by the Green's function method with the use of approximation (19); this allows one to estimate the accuracy of the approximation.

The exact expression for the thermodynamic potential (per site) of the 1D subsystem, corresponding to the grand canonical ensemble, has the form[33]

$$\Omega_{1D}=-T\ln\lambda, \tag{A2}$$

where

$$\lambda=\frac{1}{2}[1+R+\exp(\alpha+K)],$$

$$R=\sqrt{[1-\exp(\alpha+K)]^2+4\exp\alpha},$$

$$\alpha=\frac{\mu-\varepsilon_0}{T},\ K=-\frac{U}{T}. \tag{A3}$$

The mean value $n=\langle n_f\rangle$ is equal to

$$n=-\frac{\partial\Omega_{1D}}{\partial\mu}=\frac{1}{2}\left[1+\frac{\exp(\alpha+K)-1}{R}\right], \tag{A4}$$

and the correlator $c_2=\langle n_f n_{f+1}\rangle$ is given by the relation

$$c_2=\frac{\partial\Omega_{1D}}{\partial U}=\frac{n}{\lambda}\exp(\alpha+K).$$

The chemical potential is found from the equation expressing conservation of the total number of particles in the system:

$$x=\xi_0 n+(1-\xi_0)f_F(0), \tag{A5}$$

where $x=N/B, \xi_0=B_1/B, B=B_1+B_3$.

On the other hand, the mean values of n and c_2 for the 1D subsystem can be calculated using the Green's function method. Doing the calculation in the standard way, we obtain the following system of three equations:

$$(\omega-\varepsilon_0)\langle\langle c_f|c_f^+\rangle\rangle_\omega=\frac{1}{2\pi}+2U\langle\langle n_{f-1}c_f|c_f^+\rangle\rangle_\omega, \tag{A6}$$

$$(\omega-\varepsilon_0-U)\langle\langle n_{f+1}c_f|c_f^+\rangle\rangle_\omega=\frac{n}{2\pi}+U\langle\langle \eta_f c_f|c_f^+\rangle\rangle_\omega,$$

$$(\omega-\varepsilon_0-2U)\langle\langle \eta_f c_f|c_f^+\rangle\rangle_\omega=\frac{\langle\eta_f\rangle}{2\pi}.$$

System (A6) is not closed, since the last of the equations contains the average $\langle\eta_f\rangle$ on the right-hand side, and it cannot be calculated using the Green's functions appearing in (A6). However, if the correlator is decoupled according to Eq. (13), then the system (A6) is closed. Solving the resulting system of equations and using the dispersion relation,[36] we find the desired averages n and c_2:

$$(1-n)^2 f_F(\varepsilon_0)+2n(1-n)f_F(\varepsilon_0-U)+n^2 f_F(\varepsilon_0+2U)-n=0. \tag{A7}$$

$$c_2=n(1-n)f_F(\varepsilon_0+U)+n^2 f_F(\varepsilon_0+2U). \tag{A8}$$

Equations (A5) and (A7) form a system for finding the values of μ and n.

The mean energy E_{1D} of the two-dimensional subsystem is given by

$$E_{1D}=\varepsilon_0 n+Uc_2 \tag{A9}$$

and can be found using both the exact and the approximate expressions for n and c_2. Analysis shows that both the mean

energy and the heat capacity (the characteristic that is most sensitive to temperature variation) calculated with the use of the decoupling (19) are practically no different from the exact values: the error is less than one-tenth of a percent in the entire temperature region. Consequently, it can be assumed that the use of the Green's function method with the indicated decoupling permits one to solve the problem under discussion to rather high accuracy.

[a)]E-mail: chishko@ilt.kharkov.ua
[b)]E-mail: vilches@phys.washington.edu

[1]I. F. Lyuksyutov, A. G. Naumovets, and V. L. Pokrovskiĭ, *Two-Dimensional Crystals* [in Russian], Naukova Dumka, Kiev (1988).
[2]J. G. Dash, Fiz. Nizk. Temp. **1**, 839 (1975) [Sov. J. Low Temp. Phys. **1**, 401 (1975)].
[3]G. A. Stewart and J. G. Dash, J. Low Temp. Phys. **5**, 1 (1971).
[4]M. Bretz, G. B. Huff, and J. G. Dash, Phys. Rev. Lett. **28**, 729 (1972).
[5]M. Bretz, J. G. Dash, D. C. Hickernell, E. O. McLean, and O. E. Vilches, Phys. Rev. A **8**, 1589 (1973).
[6]R. L. Elgin and D. L. Goodstein, Phys. Rev. A **9**, 2657 (1974).
[7]D. S. Greywall, Phys. Rev. B **47**, 309 (1993).
[8]J. T. Birmingham and P. L. Richards, J. Low Temp. Phys. **109**, 267 (1997).
[9]T. N. Antsygina, K. A. Chishko, and I. I. Poltavsky, J. Low Temp. Phys. **126**, 15 (2002).
[10]T. Wilson and O. E. Vilches, Physica B **329–333**, 278 (2003).
[11]T. Wilson and O. E. Vilches, Fiz. Nizk. Temp. **29**, 975 (2003) [Low Temp. Phys. **29**, 732 (2003)].
[12]S. Talapatra, A. Zambano, S. E. Weber, and A. D. Migone, Phys. Rev. Lett. **85**, 138 (2000).
[13]J. C. Lasjounias, K. Biljakovič, Z. Benes, J. E. Fischer, and P. Monceau, Phys. Rev. B **65**, 113409 (2002).
[14]T. Wilson, A. Tyburski, M. R. DePies, O. E. Vilches, D. Becquet, and M. Bienfait, J. Low Temp. Phys. **126**, 403 (2002).
[15]Y. H. Kahng, R. B. Hallock, E. Dujardin, and T. W. Ebbesen, J. Low Temp. Phys. **126**, 223 (2002).
[16]W. Teizer, R. B. Hallock, E. Dujardin, and T. W. Ebbesen, Phys. Rev. Lett. **82**, 5305 (1999).
[17]W. Teizer, R. B. Hallock, E. Dujardin, and T. W. Ebbesen, Phys. Rev. Lett. **84**, 1844 (2000).
[18]P. J. F. Harris, *Carbon Nanotubes and Related Structures*, Cambridge Univ. Press (1999).
[19]A. Čiber and H. Buljan, Phys. Rev. B **66**, 075415 (2002).
[20]A. Čiber, Phys. Rev. B **66**, 205406 (2002).
[21]M. M. Calbi, M. W. Cole, S. M. Gatica, M. J. Bojan, and G. Stan, Rev. Mod. Phys. **73**, 857 (2001).
[22]G. Stan, M. J. Bojan, S. Curtarolo, S. M. Gatica, and M. W. Cole, Phys. Rev. B **62**, 2173 (2000).
[23]W. Shi and J. K. Johnson, Phys. Rev. Lett. **91**, 015504 (2003).
[24]A. Čiber, Phys. Rev. B **67**, 165426 (2003).
[25]A. Čiber, Phys. Rev. B **68**, 033406 (2003).
[26]M. Boninsegni, S.-Y. Lee, and V. H. Crespi, Phys. Rev. Lett. **86**, 3360 (2001).
[27]J. Boronat, M. C. Gordillo, and J. Casulleras, J. Low Temp. Phys. **126**, 199 (2002).
[28]M. T. Cvitaš and A. Čiber, Phys. Rev. B **67**, 193401 (2003).
[29]M. W. Cole, V. H. Crespi, G. Stan, C. Ebner, J. M. Hartman, S. Moroni, and M. Boninsegni, Phys. Rev. Lett. **84**, 3883 (2000).
[30]M. M. Calbi and M. W. Cole, Phys. Rev. B **66**, 115413 (2002).
[31]M. C. Gordillo, J. Boronat, and J. Casulleras, Phys. Rev. Lett. **85**, 2348 (2000).
[32]T. N. Antsygina, I. I. Poltavsky, and K. A. Chishko, J. Low Temp. Phys. **138**, 223 (2005).
[33]T. L. Hill, *Statistical Mechanics: Principles and Selected Applications*, McGraw-Hill, New York (1956), Izd-vo Inostr. Lit., Moscow (1960).
[34]L. D. Landau and E. M. Lifshitz, *Statistical Physics*, 2nd ed., Pergamon Press, Oxford (1969), Nauka, Moscow (1964).
[35]J. G. Dash, *Films on Solid Surfaces*, Academic Press (1975).
[36]D. N. Zubarev, *Nonequilibrium Statistical Thermodynamics*, Consultants Bureau, New York (1974), Nauka, Moscow (1971).
[37]T. N. Antsygina, V. A. Slyusarev, and K. A. Chishko, Fiz. Nizk. Temp. **21**, 583 (1995) [Low Temp. Phys. **21**, 453 (1995)].
[38]T. Takaishi and Y. Sensui, Trans. Faraday Soc. **59**, 2503 (1963).
[39]C. Journet, W. K. Maser, P. Bernier, A. Loiseau, M. Lamy de la Chapelle, S. Lefrant, P. Deniard, R. Lee, and J. E. Fisher, Nature (London) **388**, 756 (1997).
[40]M. Bienfait, P. Zeppenfeld, N. Dupont-Pavlovsky, M. Muris, M. R. Johnson, T. Wilson, M. DePies, and O. E. Vilches, Phys. Rev. B **70**, 035410 (2004).
[41]J. Pearce, M. A. Adams, O. E. Vilches, M. R. Johnson, and H. R. Glyde, Phys. Rev. Lett. **99**, 185302 (2005).
[42]G. Vidali, G. Ihm, H.-Y. Kim, and M. W. Cole, Surf. Sci. Rep. **12**, 133 (1991).
[43]S. E. Weber, S. Talapatra, C. Journet, A. Zambano, and A. D. Migone, Phys. Rev. B **61**, 13150 (2000).
[44]V. G. Manzhelii, Yu. A. Freiman, M. L. Klein, and A. A. Maradudin (eds.), *Physics of Cryocrystals*, AIP Press, Woodbury, NY (1996).
[45]M. Aichinger, S. Kilić, E. Krotscheck, and L. Vranješ, Phys. Rev. B **70**, 155412 (2004).
[46]S. Talapatra and A. D. Migone, Phys. Rev. B **65**, 045416 (2002).
[47]R. J. Baxter, *Exactly Solved Models in Statistical Mechanics*, Academic Press, New York (1982), Mir, Moscow (1985).

Translated by Steve Torstveit

Kinetic processes at the triple points on the melting curve of ^{4}He

E. O. Vekhov,[a] N. P. Mikhin, A. V. Polev, and É. Ya. Rudavskiĭ

B. I. Verkin Institute for Low Temperature Physics and Engineering of the National Academy of Science of Ukraine, pr. Lenina 47, Kharkov 61103, Ukraine

(Submitted May 19, 2005; resubmitted June 7, 2005)

The kinetics of a bcc–hcp structural phase transition on the melting curve of ^{4}He near the triple points (bcc–hcp–He II and bcc–hcp–He I) in the temperature range 1.25–2.0 K is investigated. The capillary blocking method is used to make the samples, and high-precision pressure measurement is used to investigate the kinetics. It is established that far from the triple points exponential functions describe the pressure change accompanying a temperature change on the melting curve. Anomalous behavior of the pressure and temperature of the sample is observed at a transition through the triple points. This attests to remelting of the crystal at a structural phase transition. © *2005 American Institute of Physics*. [DOI: 10.1063/1.2144451]

I. INTRODUCTION

A characteristic feature of the phase diagram of ^{4}He is the presence of a very narrow region of a bcc phase near the melting curve (Fig. 1). This was discovered in 1961 from acoustic measurements[1] and then identified in x-ray experiments.[2] Subsequent investigations of the heat capacity and P–V–T measurements[3–5] yielded reliable information about the thermodynamic parameters characterizing this system. As one can see in Fig. 1, there are two triple points on the melting curve of ^{4}He. At these points the liquid, fcc, and hcp phases are in equilibrium with one another—the bottom triple point A (BTT) and the top triple point B (TTT). The third triple point C is obtained as a result of the intersection of the melting curve and line of phase transitions into a superfluid state (λ line). Consequently, at the BTT superfluid helium (He II) is in equilibrium with the bcc and hcp phases, and at the TTT normal helium (He I) is in equilibrium with these phases.

The first experiments investigating the kinetics of phase transitions at triple points appeared only recently.[6–8] In Ref. 6 the optical method was used to establish that the phase transition occurs differently in TTT and BTT. In the course of the transition through the TTT, on heating and cooling, a new crystal phase nucleates inside the existing crystal, giving rise at first to clouding and then breakdown of the crystal. The authors suppose that this transition is reminiscent of a martensite transformation. But they believe that at the BTT the state of the initial crystal plays no role in the phase transistion, since the new crystalline phase grows in a superfluid liquid. Optical observations of nucleation at a transition from He II into the hcp phase at temperatures $T<T_A$ have shown that at first a metastable bcc phase appears. Then this phase vanishes and a new hcp phase appears in the liquid.[9]

New and important information about the kinetics of a phase transition between two phases—bcc and hcp—with sharply different crystal structure was obtained using pulsed nuclear magnetic resonance.[7,8] Since NMR on ^{3}He nuclei was used, the object of investigation was a weak solid solution of ^{3}He and ^{4}He; the phase diagram of this solution is close to that shown in Fig. 1. The spin-echo method made it possible to separate the contributions of all coexisting phases to the diffusion processes. It was established that besides the contributions corresponding to the equilibrium phases—bcc, hcp, and a bulk liquid, an additional diffusion process characterized by an anomalously high value of the diffusion coefficient appears. The diffusion coefficient is close to the corresponding value for liquid helium, but diffusion itself is spatially bounded. This behavior could be due to the appearance of liquid drops in the course of the bcc-hcp transition.

At the present time there is no clear understanding of the kinetic processes that are bring about the bcc-hcp transition. The present work was undertaken to obtain new experimental data on the kinetics of phase transitions at the triple points on the melting curve of ^{4}He. It was considered desirable to use the high-precision pressure measurement method, which has been used successfully to investigate the kinetics of another phase transition—separation of helium isotopes in solid solutions,[10] and has proven to be very informative.

II. MEASUREMENT CELL AND EXPERIMENTAL PROCEDURE

The experiments were performed in the cell shown in Fig. 2. The copper case of the cell 1 had a 10 mm in diameter and 1.5 mm high disk-shaped cavity, where the experimental sample was placed. The bottom of the cavity consisted of the mobile membrane of a Straty-Adams capacitive pressure gauge 3.[11] The cell was attached to the cold duct 4, which was weakly thermally coupled to the source of refigeration (degree chamber, which is not shown in Fig. 2). The weak thermal coupling consisted of a stainless steel tube filled with a small quantity of ^{4}He gas, so that the cell and the degree chamber would be coupled primarily via a helium film on the inner surface of the tube.

The samples investigated were made by the capillary blocking method at an initial temperature which was chosen so that the samples would consist of a mixture of a crystal and liquid with a composition corresponding to different sections of the ^{4}He phase diagram. A thermal stabilizer maintained the cold duct at a constant temperature to within 2–3 mK. This ensured that the temperature of the cold duct had the prescribed value (from 1.25 to 2.0 K). The temperature of the degree chamber remained low (~1.3 K) and its operational stability remained undisturbed even when the

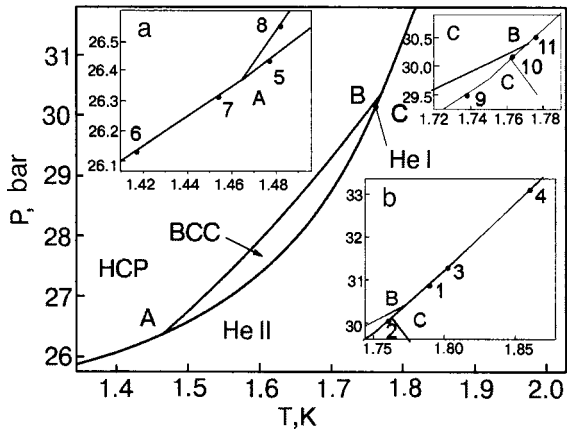

FIG. 1. Section of the phase diagram of He in the region of existence of the bcc phase. *A*—bottom triple point (T_1=1.464 K, P_1=26.36 bar), *B*—top triple point (T_2=1.772 K, P_2=30.40 bar), *C*—point of intersection with the λ line (T_λ=1.762 K, P_λ=30.13 bar). The insets a and b show on a magnified scale the sections near the triple points. The points 1-11 correspond to the states which were investigated in the present work.

thermal stabilizer heated the cell up to ≈2 K. This made it possible to avoid undesirable phenomena due to possible remelting accompanying the solid-helium "plug" punching through the filling capillary. Since the contact between the filling capillary and the degree chamber was good, such a "plug" usually formed near the degree chamber. Several tens of samples with 50–60% of each sample consisting of a solid phase were investigated.

The characteristic equalization time of the cell and degree-chamber temperatures was several seconds with the thermal stabilizer not operating. In an experiment the cell was usually cooled or heated in 10–100 mK steps, using the heat stabilizer. In this case the relaxation time of the cold-duct temperature was 1–3 s and the relaxation time of the sample temperature was 20–50 s. The state of the experimental system was recorded by measuring the pressure of the sample in the cell with an essentially constant volume to within 0.003 bar.

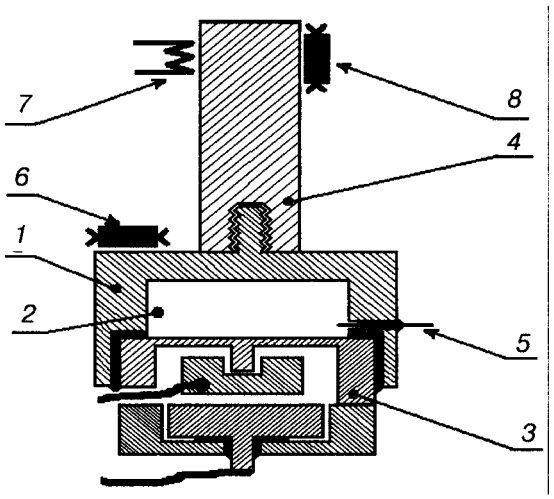

FIG. 2. Diagram of the measuring cell: 1–case, 2–sample volume, 3–capacitive pressure gauge, 4–cold duct, 5–filling capillary, 6–cell-resistance thermometer, 7–heater, 8–resistance thermometer for thermal stabilization.

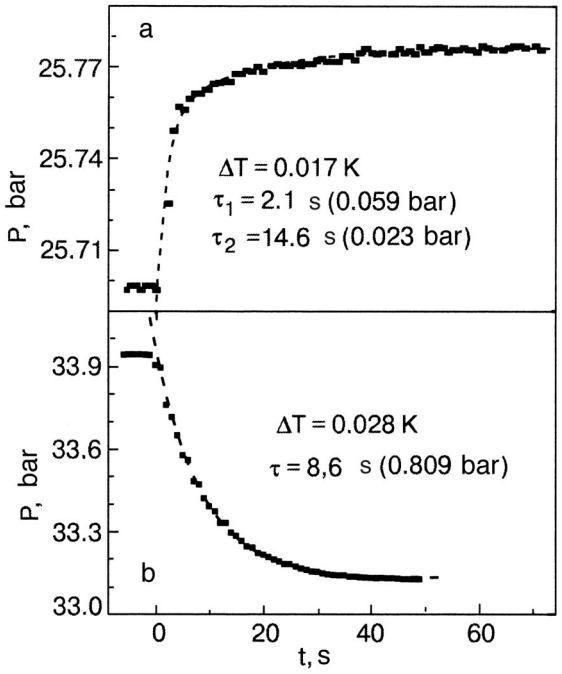

FIG. 3. Kinetics of the change in pressure accompanying stepped heating (a) on the melting curve below BTT (initial temperature 1.29 K) and stepped cooling (b) above the TTT (initial temperature 1.88 K). The dashed line shows the corresponding fit of the exponential functions (1) to the experimental data.

III. KINETICS OF PRESSURE CHANGE WITH A CHANGE IN TEMPERATURE ALONG THE MELTING CURVE

A. Far from the triple points

When a two-phase system is heated or cooled on the melting curve far from the triple points the corresponding time variation of the pressure $P(t)$ at constant volume has the form of smooth curves without any appreciable anomalies. The typical time dependences $P(t)$ are presented in Fig. 3 for two sections of the melting curve—below BTT (hcp+He II) (Fig. 3a) and above TTT (hcp+He I) (Fig. 3b). Analysis showed that all time dependences can be described by a superposition of two exponential functions:

$$P(t) = P_0 \pm \Delta P\left[\alpha \exp\left(-\frac{t}{\tau_1}\right) + (1-\alpha)\exp\left(-\frac{t}{\tau_2}\right)\right], \quad (1)$$

where P_0 is a finite pressure, ΔP is the total change in pressure, τ_1 and τ_2 are time constants characterizing each exponential process, α and $1-\alpha$ are the weights of each process. The + and − signs correspond to cooling and heating of the system, respectively.

In all cases below the λ point on the melting curve the time constant of the first exponential process is τ_1=1–8 s and its specific contribution to ΔP is α=0.6–0.9. The time constant τ_2 of the other, slower process ordinarily equals several tens of seconds and its contribution to ΔP is much smaller. This can be explained qualitatively if the first process is attributed to fast equalization of the temperatures of the superfluid liquid and cell case (estimates show that this time is several seconds, taking account of the Kapitsa jump) and the corresponding crystallization (on cooling) or melting (on heating) in accordance with the phase diagram. The latter is confirmed by the large (60–90%) relative contribution of

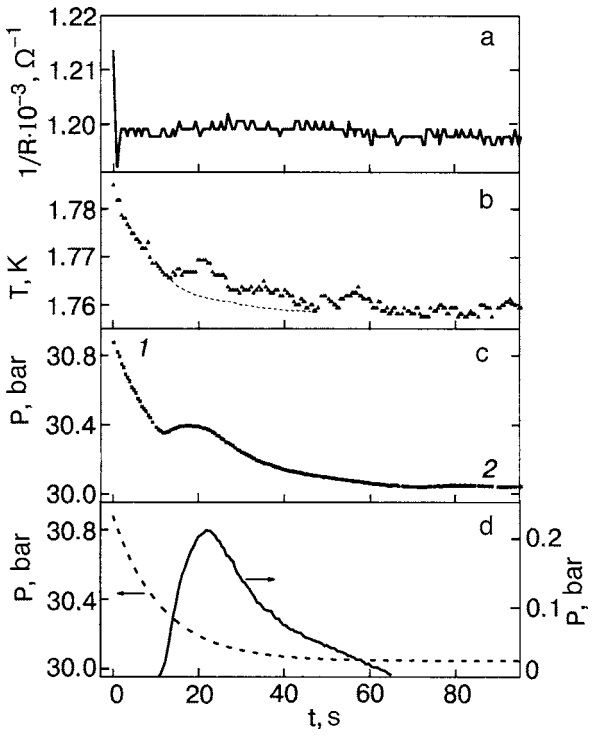

FIG. 4. Variation of the indications of the resistance thermometer on the cold duct (a), variation of the sample temperature (b), kinetics of pressure variation (c) and a fit of the latter (d) (the dashed line is the exponential variation of the pressure and the solid line is the additional contribution to the pressure) on cooling through the TTT. The numbers 1 and 2 in Fig. 4c correspond to inset b in Fig. 1.

this process to the total change in pressure ΔP. The second (slow) process is probably due to the final thermal relaxation of the entire system.

Above TTT the pressure change is described well by a single exponential function with relaxation time 10–20 s. In this case the liquid phase is not superfluid, which greatly increases the equalization time of the liquid and cell-case temperatures, and here the Kapitsa jump becomes negligible. Since the heat of melting (crystallization) becomes greater in this temperature range, this likewise increases the characteristic time of the first process. The second process accelerates somewhat compared with the analogous process below the λ point (as the relative fraction of the crystal phase in the system decreases), and both processes are essentially indistinguishable. The experiments with stepped heating of the two-phase system above the TTT showed that as temperature increases from 1.8 to 1.9 K, i.e. the amount of the crystal decreases, the time constant does indeed decrease by 32–40%.

B. Top triple point

At a transition through the top triple point the time dependence $P(t)$ undergoes a series of anomalies which differ in character for cooling and heating of the two-phase system. The kinetics of the temperature change and the corresponding pressure change for stepped cooling, i.e. at a transition from the state "liquid+hcp" (point 1, Fig. 1) into the state "liquid+bcc" (point 2, Fig. 1), is shown in Fig. 4. The transition through the TTT is set by the change in the thermal stabilization current, i.e. by the cooling of the cold duct 4 (Fig. 2), whose temperature within each cooling step is maintained constant for several minutes (Fig. 4a), until the pressure stops changing and reaches a stationary value (Fig. 4c). As Fig. 4c shows, the time dependence $P(t)$ differs radically from the smooth exponential dependences observed far from the triple point (Fig. 3). Analysis of the observed time dependence $P(t)$ showed that it can be described by a superposition of an exponental function (1) and a nonmonotonic function with a maximum (Fig. 4d). This character of the anomaly is ordinarily observed at temperatures 5–20 mK below the TTT, can contain one or two maxima, and is easily reproduced.

The time dependences presented above show that on cooling below the TTT the transition hcp→bcc starts without a delay. However, it does not occur all at once but rather in portions which can be initiated by temperature, i.e. by successive cooling steps, and by the wait time.

The maxima in the time dependence $P(t)$, i.e. an additional positive contribution to the pressure $dP(t)$, could be due to, first, the formation from a supercooled metastable hcp phase of a looser bcc phase and, second, the fact that the hcp-bcc transition is preceded by melting of the hcp crystal.

We note that a pressure increase is accompanied by a heat effect (Fig. 4b)—an increase of the temperature of the sample. Such an effect has also been observed when the calorimetric measurements were performed near the bcc-hcp transition.[5]

The conclusion about remelting can be confirmed by estimating the corresponding transition heats.[12] If it is assumed that the hcp-bcc transition occurs without remelting of the crystal, then two processes should occur. The first (main) process—crystallization of the liquid into the bcc phase due to a decrease of the temperature—releases the latent heat of crystallization ($\approx +7.2$ J/mole) and proceeds throughout the entire cooling time; it should not give rise to time-local thermal effects. The second process—a structural hcp-bcc transition (HB process)—should result in heat absorption (≈ -0.6 J/mole). Then the observed time dependence $T(t)$ (Fig. 4b), where time-local heating of the system can be seen, cannot be explained on the basis of such a model.

When remelting of the crystal phase is taken into account the second process is regarded as a superposition of two other processes: melting of the initial hcp phase (HL process), which is accompanied by heat absorption (≈ -8.0 J/mole), and crystallization of the liquid formed into a bcc phase (LB process) with heat release ($\approx +7.2$ J/mole). Since the HL and LB processes occur against the background of the above-mentioned crystallization of the liquid as a result of a decrease of temperature (main process), a time-local temperature increase is ultimately observed.

As far as the experimentally observed time-local pressure increase is concerned, it is consistent with the remelting model.

Using the known values of the compressibility and molar volumes we find that the positive contribution of the HL process to the pressure dominates over the negative contribution from the LB process, even taking account of the main crystallization process.

The remelting of the crystal in the course of a structural phase transition between two sharply differing crystal lattices

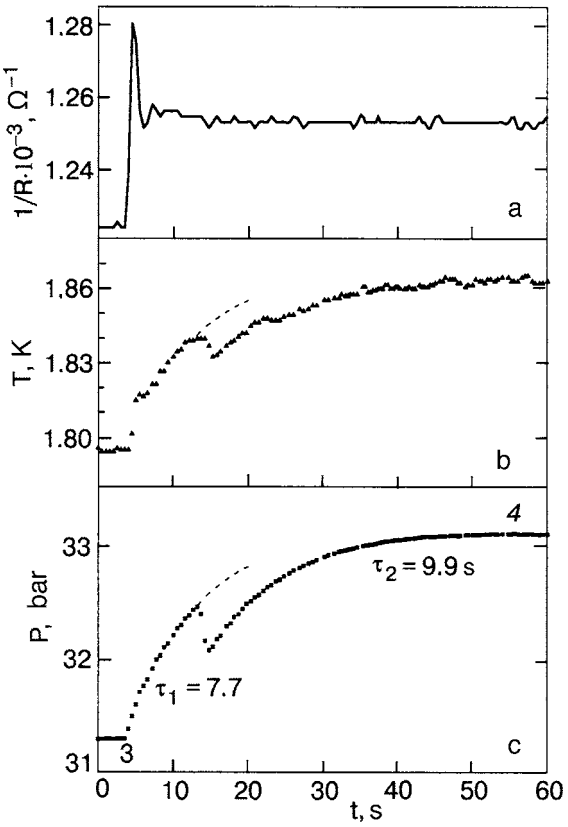

FIG. 5. Variation of the indications of the resistance thermometer on the cold duct (a), variation of the sample temperature (b), and kinetics of pressure variation (c) on heating above TTT. The numbers 3 and 4 in Fig. 5 correspond to inset b in Fig. 1.

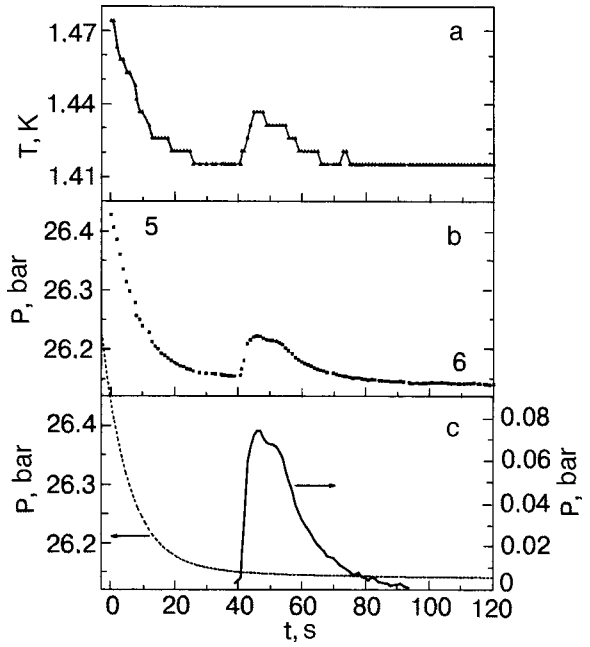

FIG. 6. Kinetics of the change in pressure of the sample (a), pressure (b), and corresponding fit of the change in pressure (c) (dashed line—exponential pressure change, solid—additional contribution to the pressure). The numbers 5 and 6 in Fig. 6b correspond to inset a in Fig. 1.

also occurs on heating through the TTT, i.e. accompanying a bcc-hcp transition. The kinetics of the change in temperature and pressure of the two-phase mixture is displayed in Fig. 5. The transition through the TTT is set by the heating of the cold duct 4 (Fig. 2), whose temperature is maintained constant within each heating step by the thermal stabilizer. The corresponding pressure change is initially exponential, following the change of the sample temperature. On the phase diagram this corresponds to a transition from the point 2 to the point 3 on the melting curve (Fig. 1). The temperature at the point 3 was stabilized and maintained constant for 30–40 min, and the pressure in the system remained unchanged. The phase transition and the associated pressure anomalies (Fig. 5c) were initiated only by subsequent heating of the system from the point 3 to the point 4. Ordinarily, the excess heating of the system needed to start the phase transition was up to 100 mK. The bcc-hcp transition was observed in the form of a sharp pressure drop by $\sim$0.5 bar, after which the pressure once again continues to increase exponentially.

We underscore that the sharp pressure drop is accompanied by an appreciable heat effect (Fig. 5b)—a decrease of the sample temperature. Such an unusual kinetics can be explained by the fact that initially the bcc phase melts, and part of the liquid formed crystallizes into the hcp phase.

Estimates show that the heat effect due to heat absorption (accompanying melting of the bcc phase) is $\sim$1.5 times greater than the heat release accompanying crystallization of the hcp phase from the liquid formed. However, if the melting of the crystal is neglected, then the restructuring of the lattice from bcc into hcp will give a positive heat effect, which contradicts the experimental results.

C. Bottom triple point

The character of the pressure and temperature anomalies on cooling of the two-phase system "liquid+bcc" through the BTT is presented in Fig. 6. On cooling from the point 5 to the point 6 (Fig. 1) the temperature of thermal stabilization decreases by a step and then is maintained constant, and the sample temperature increases by $\approx$20 mK in $\approx$40 sec. At the same time the sample pressure increases by $\approx$0.75 bar and the system reaches a static state (point 6) in 40–50 sec.

The following processes should occur when the system is cooled below the BTT: the main process of crystallization of the liquid in proportion to the cooling along the melting curve, which is accompanied by a decrease of the sample pressure and heat release, and a bcc-hcp transition (BH process), which is accompanied by a pressure decrease and heat release. None of these processes can explain the time-local pressure increase observed in Fig. 6. Just as in the case of the TTT, such a time dependence $P(t)$ can be described by a superposition of an exponential function (1) and a nonmonotonic additional contribution to the pressure.

The anomalous pressure increase can be explained by assuming that the bcc-hcp transition at the BTT likewise occurs through melting of the bcc phase (BL process) and subsequent crystallization of the liquid into the hcp phase (LH process). The heat effect of the LH process (heat release) is approximately 20% greater than the heat effect of the BL process (heat absorption). As far as the local pressure increase is concerned, it cannot be explained without using the

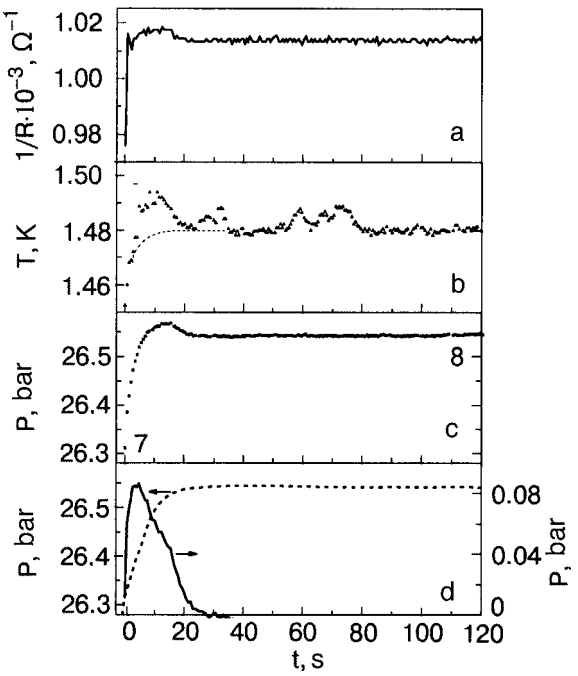

FIG. 7. Variation of the indications of the resistance thermometer on the cold duct (a), variation of the sample temperature (b), kinetics of pressure variation (c) and a fit of the latter (d) (the dashed line is the exponential variation of the pressure and the solid line is the additional contribution to the pressure) on cooling through the BTT. The numbers 7 and 8 in Fig. 7c correspond to inset a in Fig. 1.

remelting model, and when such a model is used the observed effect in ΔP can be explained by assuming that the BL process occurs before the LH process.

The behavior of the pressure on heating through the BTT, i.e. at a transition from the state "liquid+hcp" into the state "bcc+hcp," is shown in Fig. 7. It should be noted that on heating through the BTT, in our experiments, the system did not immediately pass into the final equilibrium state corresponding to the melting curve. Instead, it always arrived on the bcc-hcp equilibrium curve. The initial state corresponds to the point 7 on the melting curve below the BTT (Fig. 1), and the final state corresponds to the point 8 on the bcc-hcp equilibrium line. Since the initial state corresponds to the two-phase system "hcp+liquid" and the final state corresponds to the system "hcp+bcc," the system could pass into such a state by crystallization of an equilibrium liquid into the bcc phase. However, this would be accompanied by a pressure drop, which contradicts the phase diagram and experiment. Agreement with the experiment can be obtained by assuming that a hcp-bcc transition occurs and is accompanied by a pressure increase. The kinetics of this process is shown in Figs. 7c and 7d, where, together with an exponential pressure increase, a short-time (during the first 15–20 s) additional pressure increase, as a result of which the function $P(t)$ has a clear maximum, is also observed. Once again, the additional contribution to the pressure can be explained by melting of the hcp phase (HL process) with heat absorption (≈ -1.7 J/mole) followed by crystallization of this liquid into the bcc phase (LB process) with heat release ($\approx +1.4$ J/mole). Apparently, crystallization of the equilibrium liquid at a transition through the BTT makes the main contribution to the local heating of the system. Without using the remelting model the hcp-bcc transition would give local cooling of the system, which contradicts experiment.

IV. DISCUSSION

Analyzing the above-described behavior of the pressure on passing through triple points on the melting curve, we note that the character of the time dependence $P(t)$ is the same in all cases except for heating through the TTT: an additional contribution $dP(t)$ to the pressure, due to a structural phase transition, against the background of an exponential pressure decrease (on cooling) or exponential pressure increase (on heating), which was characteristic for a change in pressure far from the triple points, is observed. Such an additional contribution is a nonmonotonic function of time with a maximum, and this process occurs within a limited time frame 20–30 s.

The observed additional pressure increase accompanying a phase transition can be explained by the fact that the appearance and growth of a new phase (bcc or hcp) are due to partial or complete melting of the old crystalline phase. This result is confirmed by the appearance of the corresponding heat effects accompanying melting and crystallization of the phases. This result also agrees with NMR studies of the kinetics of bcc-hcp transitions in weak solid solutions of ^{3}He and ^{4}He,[7,8] where formation of a liquid phase (in the form of drops) with coexistence of both crystalline modifications was observed. Remelting at a bcc-hcp transition was observed by the acoustic method in even earlier work.[13]

The assumption that the melting of the initial crystal at a bcc-hcp transition is consistent with optical observations,[6] where the observed clouding of the initial crystal on passage through the TTT can be attributed to the formation of droplets. As far as the BTT is concerned, the authors observed directly the melting of one phase and crystallization of another phase. This process could also be due to the influence of the superfluidity of the liquid phase, which is manifested at the BTT on heating and cooling and at the TTT only on cooling. The latter is due to the fact that the λ point on the melting curve lies only 10 mK below the TTT, and on cooling the system ordinarily (in our experiments) falls in the region of existence of the superfluid phase. In this case the heat exchange due to the transfer of heat released on melting of the old phase occurs very rapidly through the "super-heat-conducting" superfluid liquid. On account of the high heat transmission the anomalous pressure change starts without any appreciable delay in temperature, and the pressure itself changes evenly.

The observed time dependence $P(t)$ on heating through the TTT, when the liquid phase (He I) is a normal liquid with no thermal conductivity, is of a different character. In this case an appreciable delay is observed in the onset of the phase transition (by 1–2.5 bar in pressure) and instead of a gradual pressure change at the bcc-hcp transition the pressure is observed to undergo a sharp jump (Fig. 5c). Against this background the pressure increase due to melting of the initial crystal is not always noticeable (especially if the amount of the crystalline phase is small), though the change in the temperature of the sample (Fig. 5b) clearly shows cooling of the sample as a result of the absorption of the heat of the bcc-

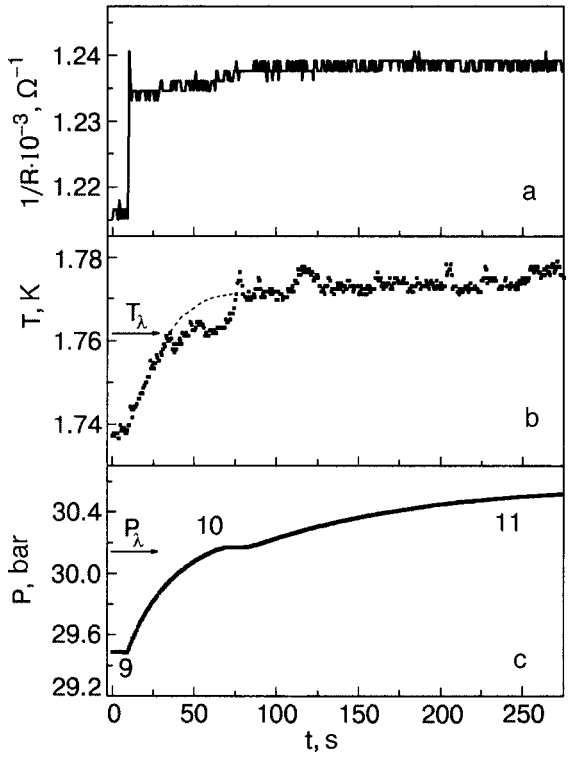

FIG. 8. Variation of the indications of the resistance thermometer on the cold duct (a), variation of the sample temperature (b), kinetics of pressure variation (c) on heating through the point C. The numbers 9, 10, and 11 in Fig. 8c correspond to inset c in Fig. 1.

normal liquid transition (against this background the heat released as a result of the bcc-hcp transition is approximately an order of magnitude smaller).

The presence of a superfluid transition on the melting curve (point C in Fig. 1) also gives rise to special features in the kinetics of the change in temperature of the sample and the pressure (Fig. 8). When the system is heated through the point C the exponential growth of temperature and pressure is replaced at this point by a small plateau lasting for 10–20 s. The physical reason for this effect is the very high heat capacity of the liquid near the λ point.

Another possible effect of superfluidity is manifested in the kinetics of the pressure change far from the triple points (see Sec. III A). Below the λ point on the melting curve, where the liquid phase is He II, the pressure variation $P(t)$ is described by a superposition of two exponential processes—a fast process, which estimates show to be associated with rapid cooling (heating) of He II and therefore with crystallization (melting) on the liquid-crystal boundary, and a slow process due to slow thermal relaxation of the crystal. Above the λ point, when the liquid is He I, the fast process slows down, and the pressure change is described by a single exponential function with a large time constant.

We call attention to the fact that the kinetics of the pressure change at both triple points is asymmetric with respect to the direction of temperature change. The phase transition on heating through the TTT and cooling through BTT, i.e. at a transition from the bcc into the hcp phase, occurs with an appreciable delay in temperature (pressure), while in the opposite direction the phase transition starts immediately when the triple point is reached. The fact that the transition from the bcc into the hcp phase occurs with greater difficulty than in the opposite direction has been observed previously.[6,9] This could be due to the fact that the surface tension of the system "hcp-liquid" is almost 25% higher than that of the system "bcc-liquid."

We thank V. N. Grigor'ev for a helpful discussion, V. A. Maĭdanov for providing the experimental cell, and A. P. Birchenko for assistance in the experiments.

This work was supported by the Ukrainian Foundation for Fundamental Research 02.07/00391 (project No. F12-7/286-2004).

[a)]E-mail: vekhov@ilt.kharkov.ua

[1]J. H. Vignos and H. A. Fairbank, Phys. Rev. Lett. **6**, 265 (1961).
[2]A. F. Schuch and R. L. Mills, Phys. Rev. Lett. **8**, 469 (1962).
[3]D. O. Edwards and R. C. Pandorf, Phys. Rev. **144**, 143 (1966).
[4]E. R. Grilly, J. Low Temp. Phys. **11**, 33 (1973).
[5]J. K. Hoffer, W. R. Gardner, C. G. Waterfield, and N. F. Phillips, J. Low Temp. Phys. **23**, 63 (1976).
[6]Y. Okuda, H. Fujii, Y. Okumura, and H. Mackana, J. Low Temp. Phys. **121**, 725 (2000).
[7]N. Mokhin, A. Polev, and É. Rudavskiĭ, JETP Lett. **73**, 470 (2001).
[8]A. Polev, N. Mikhin, and E. Rudavskii, J. Low Temp. Phys. **127**, 279 (2002).
[9]T. A. Johnson and C. Elbaum, J. Low Temp. Phys. **107**, 317 (1997).
[10]A. N. Gan'shin, V. A. Maĭdanov, and N. F. Omelaenko, Fiz. Nizk. Temp. **24**, 815 (1998) [Low Temp. Phys. **24**, 611 (1998)].
[11]G. C. Straty and E. D. Adams, Rev. Sci. Instrum. **40**, 1393 (1969).
[12]B. N. Esel'son, V. N. Grigor'ev, V. G. Ivantsov, and É. Ya. Rudavskiĭ, *Properties of Liquid and Solid Helium*, Izd-vo Standartov, Moscow (1978).
[13]N. Grigor'ev, N. E. Dyumin, and S. V. Svatko, Fiz. Nizk. Temp. **15**, 253 (1989) [Low Temp. Phys. **15**, 142 (1989)].

Translated by M. E. Alferieff

Conductivity of a two-dimensional electronic crystal over ^{3}He–^{4}He liquid solutions

V. E. Sivokon',[a] K. A. Nasedkin, and Yu. P. Monarkha

B. I. Verkin Institute for Low Temperature Physics and Engineering of the National Academy of Sciences of Ukraine, pr. Lenina 47, Kharkov 61103, Ukraine

(Submitted June 17, 2005; resubmitted July 5, 2005)

Experimental data on and a theoretical analysis of the conductivity of a two-dimensional Wigner crystal (WC) on the surface of weak solutions of quantum liquids ^{3}He–^{4}He ($x<0.25\%$ ^{3}He) are presented. The conductivity is determined using resonance excitation of low-frequency coupled longitudinal phonon-ripplon modes of a WC. A strong temperature dependence of the resistance of a WC, differing substantially from that found previously for a nondegenerate electron gas, is found. At the same time the experimental dependence of the resistance on the impurity concentration is found to be quite weak, which shows that the scattering of transverse phonons by ripplons plays the dominant role in the resistance of a two-dimensional WC for $x<0.25\%$. © *2005 American Institute of Physics*. [DOI: 10.1063/1.2144452]

A Wigner crystal (WC) on the surface of liquid helium is a two-dimensional electronic system, whose dynamical properties are determined by the translational symmetry and the processes occurring on the surface of the quantum liquid. The characteristic features of the interaction of electrons with the surface of liquid helium under the conditions of Wigner crystallization result in the possibility of excitation of coupled electron-ripplon oscillations, whose observation was the first experimental evidence of crystallization in a system of surface electrons.[1] The study of the resonance spectra of coupled oscillations was found to be a convenient method to determine the complex conductivity of an electronic crystal, whose reactive part is associated with the effective mass of the electron and whose active part reflects the relaxational processes occurring when an electronic crystal moves along a helium surface.[2]

The theoretical investigations of the interaction of electrons with the surface of liquid helium under conditions of crystallization of the electrons made it possible to, specifically, calculate the frequency of coupled resonances[3,4] and analyze the special features of the motion of an electronic crystal along the liquid-vapor interface.[5] Subsequently, it was established that the resonance frequencies, calculated using a self-consistent approach,[4] and the corresponding reactive part of the conductivity agree quantitatively with the experimental data.[6] At the same time, serious difficulties arise in describing the width of the electron-ripplon resonances in the conductivity of a WC because the electron-ripplon system is under strong-coupling conditions. For liquid ^{4}He the dissipative mechanism due to damping of capillary waves[5] is ineffective because of the smoothness of the damping coefficient, and therefore it cannot be explained by the experimentally obtained values of the width of the coupled electron-ripplon resonances.[6] A theoretical analysis of the direct scattering of the phonons of a two-dimensional WC by ripplons[7] shows that two-phonon processes predominate under strong-coupling conditions, since the interaction resulting in single-phonon processes is already included in the renormalization of the phonon spectrum. Under these conditions the conductivity of the WC depends on the frequency of the external field. Consequently, in order to compare theory with experiment the temperature dependence of the resonance frequency of coupled phonon-ripplon modes, which becomes strongly distorted even with a very low ^{3}He impurity concentration, must be taken into account consistently.

To determine the nature of the broadening of the electron-ripplon resonances and the mechanism of dissipative losses of an electronic crystal it is of great interest to perform experimental investigations of its conductivity where not only the parameters of the crystal itself but also the properties of the liquid substrate are changed in a controllable manner. An attempt to analyze the role of the surface in dissipative processes in an electronic crystal was made in Ref. 8, where the spectra of coupled electron-ripplon resonances in a crystal with prescribed parameters (surface electron density $n_e=1.3\cdot 10^9$ cm^{-2}, clamping electric field $E_\perp=600$ V/cm) over ^{3}He–^{4}He solutions with 0.025% and 0.25% ^{3}He were studied experimentally. At low temperatures the ^{3}He atoms fill the Andreev surface levels, which changes the surface tension.[9] It was found that when ^{3}He is added the frequencies of the resonances (0, 1) in the experimental cell shift to lower frequencies and the resonance curves become somewhat broader. A method making it possible to determine the mobility of the crystal according to the measured resonance curves was proposed. In this method, together with a system of equations describing the experimental cell, the theoretical response function of the crystal moving along the surface of a liquid, as proposed in Ref. 5, was used; this made it possible to calculate the width of the resonance line as a function of the real part of the reciprocal of the conductivity and, comparing it to that found experimentally, to find the mobility of the crystal. It was established that the mobility of the crystal over a solution is somewhat lower than over pure ^{4}He, but this result was not discussed, since it was not clear how accurate the proposed method for analyzing the data is and also in view of the fact that the ^{4}He data used in such an analysis were preliminary and were obtained under conditions which were not adequately controlled.

Subsequently, detailed investigations were performed of the conductivity of an electronic crystal over pure helium for a wide range of values of the parameters.[2] The conductivity of the electronic crystal in this work was determined by ana-

lyzing the signal obtained from a measuring cell containing the electronic crystal under the action of a guiding field with frequency equal to the frequency of the coupled resonance (0, 1). At the same time, to determine the complex conductivity it is sufficient to use the equations describing the experimental cell, and there is no need to use the theoretical response function explicitly. The results of the calculations for the experimental data obtained in Ref. 2 on the mobility of a WC agree well with the published data. In the work it was proposed that the broadening of the electron-ripplon resonances of the conductivity of the crystal could be due to defects of the crystal structure (dislocations). In this connection it was necessary to analyze once again the role of the surface of the liquid in dissipative processes of a WC, using a new method for determining the conductivity[2] and new data on the conductivity of an electronic crystal over pure ^{4}He. Such an analysis is the objective of the present work.

In this work the spectra of coupled electron-ripplon oscillations in electronic crystals with surface density $1.3\cdot10^9$ cm^{-2} over pure ^{4}He and ^{3}He–^{4}He solutions with ^{3}He concentrations 0.025% and 0.25% are investigated in the temperature range 80–400 mK. The experimental cell and the computational scheme for calculating the conductivity of the electronic crystal from the measured components of the response of the system to an exciting electric voltage are described in Ref. 10. The cell consists of a flat circular capacitor, whose gap contains a layer of liquid helium with electrons on its surface. A constant voltage, clamping the electrons to the surface of the liquid, is applied to one of the capacitor plates. The second plate is a composite structure and contains the input and output electrodes. An ac voltage is applied to the input electrode, and the current is measured on the output electrode. The relation between the output current and the input voltage is

$$J=(G_1+\mathrm{i}\omega G_2)V\mathrm{e}^{\mathrm{i}\omega t}. \tag{1}$$

The complex conductivity of an electronic layer can be determined for the cell geometry from the experimentally measured quantities G_1 and G_2:

$$G_1=f_1(\chi_1,\chi_2,\omega,A),\quad G_1=f_2(\chi_1,\chi_2,\omega,A)+G_0, \tag{2}$$

where $\chi_1=\mathrm{Re}\,\sigma_{\mathrm{eff}}^{-1}$, $\chi_2=\mathrm{Im}\,\sigma_{\mathrm{eff}}^{-1}$, A and G_0 are coefficients which are determined by the geometry of the cell, and f_1 and f_2 are certain functions which are quite complicated. The measurements were performed at frequencies corresponding to the excitation of coupled electron-ripplon oscillations in the cell. In the course of the measurements the frequency dependence of the amplitude and phase of the current at fixed temperatures and with fixed amplitudes of the exciting voltage were measured.

Figure 1 shows the resonance spectra of a crystal with $n_e=1.3\cdot10^9$ cm^{-2} over a ^{3}He–^{4}He solution containing 0.25% ^{3}He. The spectra were measured for different temperatures in the range 80–400 mK. The melting temperature of this crystal is 760 mK. Figure 1 shows most clearly the resonance features corresponding to the excitation of the resonance mode (0, 1), but the next harmonic (0, 2) can also be seen. Similar spectra were measured for the same type of crystal over pure ^{4}He (atomic impurity ^{3}He about $5\cdot10^{-7}$) and a solution with 0.25% ^{3}He.

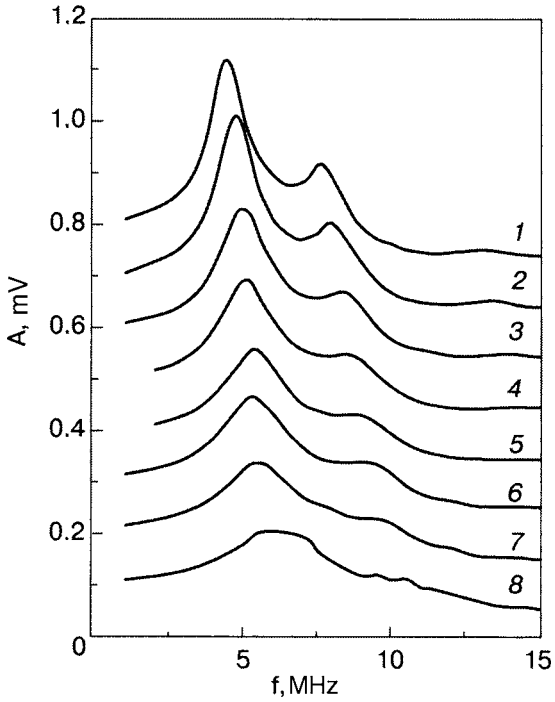

FIG. 1. Resonance spectra of coupled electron-ripplon oscillations of a two-dimensional WC with density $n_e=1.3\cdot10^9$ cm^{-2} over the surface of a solution with ^{3}He concentration 0.25% at different temperatures T, mK: 81 (1), 98 (2), 134 (3), 164 (4), 195 (5), 221 (6), 258 (7), and 348 (8).

The temperature dependences of the (0, 1) resonance frequencies are presented in Fig. 2. The experimental data are compared with the results of a theoretical calculation. Previously, a model taking account of coupling only with ripplons whose wave vector has the same magnitude as the shortest vector g_1 of the reciprocal electronic lattice was used to describe the coupled phonon-ripplon modes. This model correctly describes the position of the electron-ripplon resonances only near the melting temperature T_m of a WC. At much lower temperatures the coupling with ripplons with wave vector $|\mathbf{q}|=g_n$ with $n>1$ must be taken into account

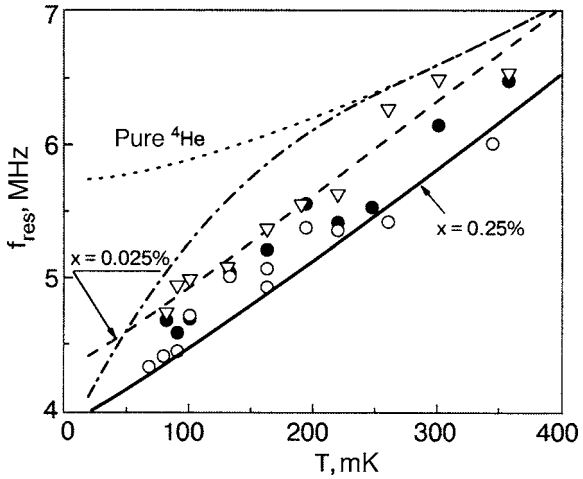

FIG. 2. Temperature dependence of the resonance frequency of coupled longitudinal phonon-ripplon modes over ^{3}He–^{4}He solutions with different concentrations: pure ^{4}He (dotted line–theoretical calculation), ^{4}He technical purity (▽—experimental data, dotted-dashed line—theoretical calculation), $x=0.025\%$ (●—experimental data, dashed line—calculation), and $x=0.25\%$ (○—experimental data, solid line—theory).

even for a low-frequency mode $\omega<\omega_1$ (here $\omega_1=\omega_q$ with $q=g_1$, and $\omega_q=\sqrt{\alpha/\rho}q^{3/2}$ is the dispersion law for capillary waves of a liquid with density ρ and surface tension α). The required generalization is easily found for the case where the frequency dependence of the contribution of terms with $|\mathbf{q}|=g_n$ for $n>1$ to the effective mass of an electron can be neglected: $\Sigma_{n=2}^{\infty}C_n$, where the coefficients C_n characterize the degree of phonon-ripplon coupling with $q=g_n$.[5] This approximation is applicable for modes with $\omega<\omega_1$. As a result, the dispersion law for a low-frequency coupled mode assumes the following form:

$$\Omega_{l,k}^2=\frac{\omega_{l,k}^2+M_d\omega_1^2-\sqrt{(\omega_{l,k}^2+M_d\omega_1^2)^2-4(M_d-C_1)\omega_{l,k}^2\omega_1^2}}{2(M_d-C_1)}, \tag{3}$$

where $\omega_{l,k}$ is the spectrum of longitudinal oscillations of a WC over a flat surface, $M_d=\Sigma_{n=1}^{\infty}C_n$ is the effective mass of the dimple (normalized to the free-electron mass m_e), formed on the surface of liquid helium under each electron because of the electron-ripplon interaction. In the limit $M_d\to C_1$ the relation (1) becomes the well-known result of the simplified model of Refs. 3 and 4.

The coefficients C_n are proportional to the Debye-Waller factor $\exp(-g^2\langle u_f^2\rangle/4)$ for the high-frequency modes of a WC and therefore have a strong temperature dependence. We found C_n following the results of a self-consistent approach:[11] the mean-square displacements $\langle u_f^2\rangle$ of the electrons at the lattice sites and the Debye-Waller factor can be described by the simplified model,[4] since it correctly reflects both limiting cases $T\to T_m$ and $T\to 0$. However, it should be kept in mind that a quite large number of terms with $n>1$ must be included in the corresponding lattice sums over $\mathbf{g}_n$. The results of the calculation of the resonance frequency using the relation (3) with wave vector $k=k_0$, set by the geometry of the cell, are presented in Fig. 2. The calculation employed the measured values of the surface tension for a solution with the corresponding ^{3}He concentration[9] or linear interpolation based on existing data for the two closest concentrations. At low temperatures the data obtained for all solutions strongly deviate from the curve calculated for ideally pure ^{4}He. When the temperature dependence of the surface tension of weak solutions is taken into account the theoretical calculation is much closer to the experimental data, especially for controlled concentrations 0.025% and 0.25% (dashed and solid lines). Obviously, the more accurate theory correctly describes the position of the low-frequency electron-ripplon resonances, in agreement with the expected properties of the surface of the solution.

The energy losses of the crystal are characterized by the real component of the conductivity σ. The quantity $\mathrm{Re}(1/\sigma)$ for all series of measurements in the present work is determined similarly to the way this was done for pure helium in Ref. 2. The results of an analysis of the complex response of the crystal as a function of temperature at the frequency of the mode (0, 1) are presented in Fig. 3. The data differ strongly from the resistance of a nondegenerate electron gas (dashed line, calculated for $x=0.25\%$) and have a different temperature dependence (in strong clamping fields $1/\sigma$ increases with decreasing temperature because the surface tension of the solution decreases). There is also a substantial

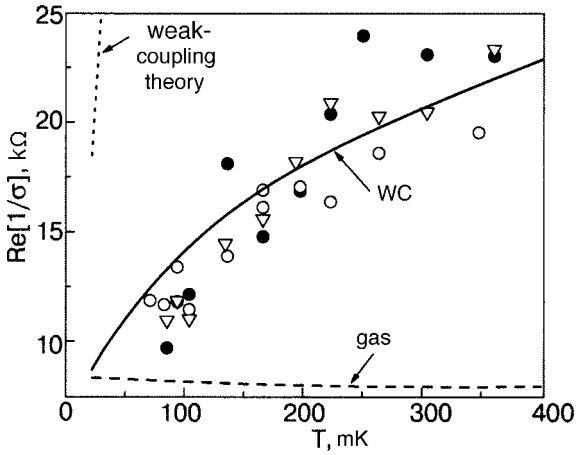

FIG. 3. Temperature dependence of the resistance $[\mathrm{Re}(1/\sigma)]$ over a two-dimensional WC over ^{4}He of technical grade purity (▽) and solutions with $x=0.025\%$ (●) and $x=0.25\%$ (○). Dotted line—calculation in the weak-coupling approximation; dashed line—calculation for a nondegenerate two-dimensional electron gas; solid line—calculation using Eqs. (4)–(6), obtained for a WC with $x=0.25\%$.

discrepancy between the experimental data and the resistance of a WC calculated in the weak-coupling approximation (dotted line, $x=0.25\%$). The fact that this estimate is high was explained in the strong-coupling theory[7] by the facts that the terms of the interaction Hamiltonian which are responsible for the single-phonon scattering by ripplons are already included in the renormalization of the spectrum of the WC and relaxation of the momentum of the electrons at low frequencies is determined only by multiphonon scattering processes.

For high-frequency coupled phonon-ripplon modes ($\omega>\omega_f$, where ω_f is the limiting frequency of optical phonons) the effective frequency of collisions in which two transverse phonons of a WC participate has the form[7]

$$\nu_{2f}^{(\mathrm{f})}=\frac{\pi n_e}{8\alpha m_e\omega_f}\sum_{\mathbf{g}}\alpha_g^2\tilde{V}_g^2, \tag{4}$$

where

$$\alpha_g=\frac{g^2T}{4\pi m_e c_t^2 n_e};\quad \tilde{V}_g=\tilde{V}_g\exp(-g^2\langle u_f^2\rangle/4);$$

c_t is the velocity of transverse phonons of a two-dimensional WC on a flat substrate, and V_g is a function that describes the electron-ripplon interaction Hamiltonian (in the limit of strong clamping fields $V_g\to eE_\perp$).

Processes in which low-frequency coupled modes participate make a somewhat larger contribution:[7]

$$\nu_{2f}^{(8)}=\frac{\pi n_e}{16\alpha m_e}\sum_{|\mathbf{g}|=g_1}\alpha_g^2\frac{J(\omega_g-\omega)}{|\omega_g-\omega|}\tilde{V}_g^2. \tag{5}$$

Here the function $J(\omega)$ depends logarithmically on the size of the system and is approximately described by the formula

$$J(\omega)\approx\ln\left(\frac{\omega_f|\omega|}{c_tk_0\sqrt{\omega_1^2-\omega^2}}\right),$$

where k_0 is determined by the size of the experimental cell (in concrete calculations we used the more accurate formula presented in Ref. 7).

For sufficiently high concentrations (greater than or of the order of 0.25%) the scattering of quasiparticles of the solution by the WC-induced sublattice of the surface dimples must also be taken into account. For pure ^{3}He this effect results in a strong resistance of the dimples characterized by an effective collision frequency:[11]

$$\upsilon_D = \frac{2\kappa}{m_e n_e} \sum_{\mathbf{g}} g_x^2 |\xi_g|^2, \tag{6}$$

where ξ_g are the Fourier components of the displacements $\xi(\mathbf{r})$ of the helium surface. In the absence of an energy gap in the spectrum of the impurity atoms

$$\kappa = \frac{1}{2\pi^2\hbar^3} \int_0^\infty f(p) p^3 dp,$$

where $f(p)$ is the equilibrium quasiparticle momentum distribution function. The case of degenerate statistics of pure ^{3}He is analyzed in Ref. 11. For this case the coefficient κ is independent of the temperature and is determined by the value of the momentum of the quasiparticles on the Fermi surface. For the weak solutions studied in the present work the impuriton gas is nondegenerate and the coefficient $\kappa = n_3 \sqrt{2m_3^* T/\pi}$ increases with temperature (n_3 is the number of impurity atoms per unit volume of the solution and m_3^* is the effective mass of the impurity quasiparticles).

The total resistance of the WC is determined by the sum of the dimple contribution (6) and the electronic contributions (4) and (5). The former depends very strongly and the latter to a much lesser degree on the impurity concentration. Calculation shows that the electronic contribution to the resistance can even increase somewhat as concentration decreases. The presence of an appreciable electronic contribution greatly decreases the concentration dependence of the total resistance. The result of the calculation for impurity concentration 0.25% is presented in Fig. 3 (solid line). The theoretical estimates show that under these conditions ($x = 0.25\%$) the electronic and dimple contributions are approximately of the same order of magnitude.

It should be noted that good numerical agreement between theory and experiment obtains only for the concentration 0.25%. For lower concentrations the agreement between theory and experiment is only qualitative. The numerical discrepancy could be due to breakdown of the ballistic nature of the regime for quasiparticles scattered by dimples. This regime was used in the derivation of Eq. (6) and could break down because of the scattering of impurities by phonons. Another possible explanation is due to the asymptotic character of the expansion of the electronic dynamical structure factor used in the derivation of Eq. (5).

It should also be noted that comparing the data found in the present work for $\mathrm{Re}(1/\sigma)$ with previously obtained data on the resonance width[6] shows good agreement only for the 0.25% solution. For the 0.025% solution there is a discrepancy by approximately a factor of 2. This discrepancy can hardly be explained by the unreliability of the previously obtained data for technical-grade ^{4}He, since a two-fold discrepancy exists for quite reliable solutions with 0.025% and 0.25% ^{3}He for which measurements were performed under identical conditions. Apparently, the discrepancy is due to the fact that the mobility is not determined accurately enough from the resonance width.

Experiments with the free surface of a weak solution are also possible for substantially higher concentrations of the He impurity (right up to values of the order of 6%). Under these conditions, according to the theoretical relations presented, the dimple resistance should be much greater than the electronic resistance, even if the gas of ^{3}He quasiparticles is degenerate at low temperatures. An experimental investigation of the resistance of WC with such concentrations is of great interest for determining the contributions of surface and volume excitations of the solution and are planned for the future.

We thank Yu. Z. Kovdrya and S. S. Sokolov for discussion of the results obtained in this work.

[a)]E-mail: sivokon@ilt.kharkov.ua

[1]C. C. Grimes and G. Adams, Phys. Rev. Lett. **42**, 795 (1979).
[2]V. E. Sivokon', Fiz. Nizk. Temp. **30**, 509 (2004) [Low Temp. Phys. **30**, 377 (2004)].
[3]D. S. Fisher, V. I. Halpern, and P. M. Platzman, Phys. Rev. Lett. **42**, 798 (1979).
[4]Yu. P. Monarkha and V. B. Shikin, Fiz. Nizk. Temp. **9**, 913 (1983) [Low Temp. Phys. **9**, 471 (1983)].
[5]Yu. P. Monarkha, Fiz. Nizk. Temp. **6**, 685 (1980) [Low Temp. Phys. **6**, 331 (1980)]; Yu. P. Monarkha, Fiz. Nizk. Temp. **7**, 692 (1981) [Low Temp. Phys. **7**, 338 (1981)].
[6]V. E. Sivokon', V. V. Donetsko, Yu. Z. Kovdrya, and V. N. Grigor'ev, Fiz. Nizk. Temp. **22**, 1107 (1996) [Low Temp. Phys. **22**, 845 (1996)].
[7]Yu. P. Monarkha, Fiz. Nizk. Temp. **29**, 910 (2003) [Low Temp. Phys. **29**, 682 (2003)].
[8]V. V. Donetsko, V. E. Sivokon', Yu. Z. Kovdrya, and V. N. Grigor'ev, Fiz. Nizk. Temp. **23**, 1028 (1997) [Low Temp. Phys. **23**, 772 (1997)].
[9]D. O. Edwards and W. F. Saam, in: *Progress in Low Temperature Physics* 7A, D. F. Brewer (ed.), North-Holland (1978).
[10]V. E. Sivokon', V. V. Donetsko, S. S. Sokolov, Yu. Z. Kovdrya, and V. N. Grigor'ev, Fiz. Nizk. Temp. **22**, 716 (1996) [Low Temp. Phys. **22**, 549 (1996)].
[11]Yu. P. Monarkha and K. Kono, J. Phys. Soc. Jpn. **66**, 3901 (1997).

Translated by M. E. Alferieff

SUPERCONDUCTIVITY, INCLUDING HIGH-TEMPERATURE SUPERCONDUCTIVITY

Generalized permeability of a type II superconductor

V. K. Ignatjev[a)]

Volgograd State University, ul. 2-ya Prodol'naya 30, Volgograd 400062, Russia
(Submitted February 13, 2004; resubmitted June 24, 2005)

A generalized electric displacement is constructed for a superconductor in the mixed state by averaging the microscopic fields over a system of Abrikosov vortices moving with a velocity varying in time and space, with the vortex and transport currents of the superconducting component and the conduction current of the normal component taken into account. Expressions are obtained for the linear and nonlinear generalized permeability. It is shown that bulk waves, including longitudinal ones, can exist in a superconductor and that spatial dispersion is manifested even in the rf region of the spectrum and has a substantial influence on higher-harmonic generation. © *2005 American Institute of Physics*. [DOI: 10.1063/1.2144453]

INTRODUCTION

Interest in the electrodynamics of type II superconductors has not slackened in the half century since the publication of Ginzburg and Landau's paper.[1] The magnetic flux in such superconductors is transported by the diffusion[2,3] of Abrikosov vortices[4] which form both a comparatively regular lattice[5] and a peculiar vortex liquid[6,7] and even a vortex plasma,[8] the order parameter in the mixed state of the superconductor being strongly dependent on the coordinates.[9] The dynamics of an isolated vortex has been well studied both theoretically[10] and experimentally.[11] The losses arising in the normal conduction of the core and the irreversible changes of the order parameter in the viscous motion of the vortices were taken into account in Ref. 12, and the loss due to polarization of the medium by the field of a moving vortex was taken into account in Ref. 13. The balance equations for the forces have usually been derived thermodynamically,[10] i.e., they pertain, strictly speaking, to the equilibrium state.

The mixed state of a type II superconductor can be treated in a thermodynamic approach as an equilibrium state of the system of Abrikosov vortices, rectilinear or curved, characterized as a system of isolated particles, e.g., by a sort of chemical potential.[14] In the description of the reaction of the system of vortices to an external electromagnetic influence (transport current or variable magnetic field) a kinetic approach[9] has mainly been used, leading, for example, to an equation of the kinetic state known as the modified Bean model.[15]

Calculation of the response of a superconductor in the mixed state to an alternating electromagnetic field is usually done under the assumption that the vortex lattice moves as a whole, i.e., all of the vortices move with a velocity that varies in time but is uniform in space.[9,12,16,17] Such a vibrational approach to the motion of the lattice has been used for studies of the frequency dependence of the reflection coefficient,[17] the surface impedance,[18] and the susceptibility,[19] harmonic generation,[9] and the appearance of steps on the current–voltage characteristic.[16]

Models of the critical and resistive states have been well confirmed experimentally in the quasistationary regime, e.g., at frequencies relevant to commercial application.[11,14,20] At the same time, in the rf region substantial deviations from the classical model have been observed, particularly in ceramic superconductors, for which the diameter of the vortex lines can be significantly larger than in metallic superconductors.[21] It was shown in Ref. 22 that the surface resistance of a high-T_c superconductor (HTSC) is several orders of magnitude larger than is predicted by the theory. The frequency dependence of the surface impedance deviates substantially from the linearity predicted by the model of the critical state.[15] The superconducting current density also has a feature near the surface of the superconductor.[23]

In optics the features of the surface impedance and the corresponding reflection anomalies can be caused by spatial dispersion of the susceptibility,[24] which is manifested when the wavelength is comparable to the characteristic scale of the nonlocality. In the mixed state of a superconductor the corresponding scale can be the size of a vortex or the period of the vortex lattice, and therefore for ceramic superconductors the nonlocality affects the surface impedance and the nonlinear susceptibility even at low frequencies.[18] In the rf region the influence of spatial dispersion on the susceptibility of the superconductor, both the linear and nonlinear, can be of a resonance character. As we shall show below, the nonlocality itself can cause nonlinearity of the susceptibility of a superconductor; this effect is not observed in crystal optics.

The elastic properties of the vortex lattice have been investigated in detail both theoretically and experimentally.[14] As to the complex susceptibility of type II superconductors, however, only the frequency dependence has been analyzed, and the dependence on the wave vector was not taken into consideration,[25] although such topics as flux creep and the corresponding temperature dependence of the absorption[26] and the hysteretic dependence of the critical current on the instantaneous value of the magnetic field[27,28] have been taken into account. Actually, in such an approach the dynamics of the vortex lattice is treated as a vibrational and not a wave process. That approach can be used to determine the frequency dispersion relation of the lattice vibrations,[29] but effects of interaction of the electromagnetic wave with quasi-

elastic waves, which are well known in acoustooptics and spin-wave electronics, vanish. As we shall show below, a wave propagating in the vortex lattice is not purely longitudinal, like a bulk acoustic wave, but is mixed, like a spin wave.[30] Accordingly, the dispersion characteristics of such a wave are far richer than for an acoustic wave.

It should be noted that spatial dispersion in insulators gives rise to new normal waves.[31] Such an effect can also be expected in superconductors, the dispersion characteristics of such waves being easily controlled electrically, since the period of the vortex lattice depends on the external magnetic field. Previously such a possibility was known only for spin waves.[30] The propagation of electromagnetic and spin waves in a layered superconductor–ferrite–superconductor structure was studied in Ref. 32. It was shown that the dispersion characteristics of spin waves can be controlled efficiently, but the wave characteristics due to spatial dispersion in the superconductor itself were not taken into account. Incorporation of spatial dispersion can expand the functional capabilities of superconductor electronics.[33]

The analysis of electromagnetic process in type II superconductors is complicated by the impossibility of separating the magnetization current and conduction (transport) current even in the dc case, since they are created by the motion of the whole condensate of Cooper pairs.[10,14] Therefore, by analogy with the optics one can describe the state of the superconductor by a linear functional of the electric field—the generalized polarization vector $\mathcal{P}$, the derivative of which is equal to the averaged total microscopic current $\mathbf{j}=\rho\mathbf{v}$ in the medium, including both the conduction current and the local magnetization and polarization currents of the bound charges, which can be neglected in the rf region:[34]

$$\frac{\partial\mathcal{P}(\mathbf{r})}{\partial t}=\langle\mathbf{j}\rangle=\frac{1}{V}\int_V\mathbf{j}(\mathbf{r}+\mathbf{r}_1)d^3r_1,$$

$$\mathcal{P}(\mathbf{r},t)=\int_0^\infty\int_{-\infty}^\infty\tilde{\chi}(\mathbf{r},\mathbf{r}_1,t_1)\mathbf{E}(\mathbf{r}-\mathbf{r}_1,t-t_1)d^3r_1dt_1$$
$$=\frac{1}{(2\pi)^4}\int_{-\infty}^\infty\int_{-\infty}^\infty\hat{\chi}(\mathbf{r},\mathbf{k},\omega)\mathcal{E}(\mathbf{k},\omega)\exp(i\mathbf{k}\cdot\mathbf{r}$$
$$-i\omega t)d\omega\ d^3k,$$

$$\mathcal{E}(\mathbf{k},\omega)=\int_{-\infty}^\infty\int_{-\infty}^\infty\mathcal{E}(\mathbf{r},t)\exp(-i\mathbf{k}\cdot\mathbf{r}+i\omega t)dt\ d^3r,$$

$$\hat{\chi}(\mathbf{r},\mathbf{k},\omega)=\int_0^\infty\int_{-\infty}^\infty\tilde{\chi}(\mathbf{r},\mathbf{r}_1,t_1)\exp(-i\mathbf{k}\cdot\mathbf{r}_1$$
$$+i\omega t_1)dt_1\ d^3\ R_1. \qquad (1)$$

Here V is a physically small volume, containing a large number of structural units, in which the variation of the fields can be neglected. In Eq. (1) the medium is assumed isotropic and homogeneous but stationary. Then the electromagnetic field in the medium is described by three vectors, **E**, **B**, and the generalized electric displacement $\mathcal{D}=\mathbf{E}+4\pi\mathcal{P}$, and Maxwell's equations without external currents and charges take the form[34]

$$\text{div}\ \mathbf{B}=0,\quad \text{div}\ \mathcal{D}=0,$$

$$c\ \text{curl}\ \mathbf{E}=-\partial\mathbf{B}/\partial t,\ c\ \text{curl}\ \mathbf{B}=\partial\mathcal{D}/\partial t. \qquad (2)$$

Here **E** and **B** are macroscopic, i.e., the microscopic fields **e** and **b** averaged over the physically small volume:

$$\mathbf{E}(\mathbf{r})=\langle\mathbf{e}(\mathbf{r})\rangle=\frac{1}{V}\int_V\mathbf{e}(\mathbf{r}+\mathbf{r}_1)d^3r_1,$$

$$\mathbf{B}(\mathbf{r})=\langle\mathbf{b}(\mathbf{r})\rangle=\frac{1}{V}\int_V\mathbf{b}(\mathbf{r}+\mathbf{r}_1)d^3r_1. \qquad (3)$$

Equation (1) is a constitutive relation of the medium. The dependence of the total current on the alternating magnetic field in that relation is taken into account through the third equation in (2) as

$$\mathbf{B}(t)=-c\int_0^t\text{curl}\ \mathbf{E}(t_1)dt_1+\mathbf{B}(0).$$

The static magnetic field $\mathbf{B}_0=\mathbf{B}(0)$ is usually introduced into the generalized susceptibility as a parameter.

The boundary conditions for the vectors **E**, **B**, and $\mathcal{D}$ are obtained from Eqs. (2) in the usual way:[34]

$$E_{2\tau}=E_{1\tau},\quad B_{2n}=B_{1n},\quad \mathcal{D}_{2n}=\mathcal{D}_{1n},$$

$$B_{2\tau}-B_{1\tau}=4\pi i_v/c, \qquad (4)$$

where i_v is the linear density of the total surface current induced in the medium, including the magnetization current. The fourth condition corresponds to continuity of the field **H** at the boundary of the superconductor. However, the thermodynamic definition[14,35] of the field **H** used in the description of the mixed state of the superconductor is valid only for the equilibrium state and not for a dissipative resistive state. Furthermore, the construction of the field energy in a dispersive medium is a rather complex problem, while at the same time the relation of the field **H** with the generalized electric displacement $\mathcal{D}$ has been obtained under rather general conditions.[34]

WAVE EQUATION FOR THE MIXED STATE

The Ginzburg–Landau equations[1] were obtained by minimizing the free energy, and they and the Abrikosov vortex equation[4] that follows from them describe a stationary state in thermodynamic equilibrium. Nonstationary processes in type II superconductors are described by the microscopic Gor'kov–Eliashberg equations.[36] These equations are obtained by the methods of quantum electrodynamics with the use of a diagram technique and permit the solution of numerous problems of nonstationary superconductivity in which the interaction of the Cooper condensate with electron–hole excitations and nonequilibrium phonons is taken into account.[9,16,37]

For analysis of the reaction of a system of Abrikosov

vortices to an external electromagnetic field one usually derives from the microscopic equations the dynamic (time-dependent) Ginzburg–Landau equations for the order parameter, which demonstrate the macroscopic quantum properties of the superconductor.[37] In that way expressions have been obtained for the coefficient of viscosity of moving vortices and the flux-flow resistance over a wide range of temperatures and for any alloy.[38,39] However, in the presence of a propagating electromagnetic wave whose wavelength in the medium is comparable to the period of the vortex lattice, the vortex velocity field is nonuniform in both space and time, and therefore the relation between the electric and magnetic fields averaged in the sense of Eq. (3) will be more complicated than is assumed in a treatment of laminar flux flow.[12] These features, in turn, can have a substantial influence on the dispersion characteristics of the waves.

The influence of transport processes and spatial dispersion on the propagation of electromagnetic waves has been well studied in plasma electrodynamics.[40] To construct the kinetic equations of a plasma in such a case one uses the Bogolyubov method of a hierarchy of scales,[41] which under certain assumptions allows one to ignore the internal structure of the particles of the plasma and describe their motion classically. In the rf region, when the energy of a quantum is much less than the gap width, the mixed state of the superconductor can also be treated as a plasmalike medium.[8] Then a region of the order of the coherence length ξ will contain many cells of the crystal lattice and many Cooper pairs. The role of the second scale is played by the characteristic vortex size $\lambda \gg \xi$. Therefore the construction of the macroscopic fields for a type II superconductor in a magnetic field that is uniform along the z axis can be carried out in two steps.

First one averages Eqs. (1) and (3) over a volume V in the form of a cylinder with its generator along the z axis and with a diameter of the order of ξ. Such an averaging makes the problem two-dimensional and "smoothes out" the spatial nonuniformities of the fields while preserving the nonlocality due to the interaction of the Abrikosov vortices. In the second step a statistical averaging over the ensemble of Abrikosov vortices is carried out. Since the characteristic lag time $\tau \sim \Delta/\hbar$ for recovery of the order parameter in a moving vortex[42] is much less than the wave period, the Cooper condensate can be assumed to be in microscopic equilibrium, in which case the quantity $-2e\varphi/\hbar$, where φ is the scalar potential, coincides with the derivative of the phase θ of the order parameter.[37]

The dynamics of the classical particles in a plasmalike medium is conveniently described by Lagrange's equations. In the framework of the simplifying assumptions made, the Cooper condensate in the superconductor can be characterized by a general scalar potential and regarded as a Lagrangian system. It is therefore of interest to obtain the time-dependent Ginzburg–Landau equations for such a system by the methods of the Lagrangian formalism. We construct a nonrelativistic Lagrangian of a superconducting condensate, using the classical expression for the free energy of the superconductor in an electromagnetic field:[1,12,43–45]

$$\mathcal{L} = \frac{ieh}{2cm}(\psi \nabla \psi^* - \psi^* \nabla \psi)\cdot \mathbf{A} - \frac{h^2}{4m}\nabla \psi \cdot \nabla \psi^* - \frac{e^2}{c^2 m}A^2|\psi|^2 + 2e|\psi|^2\varphi + \frac{ih}{2}\left(\psi\frac{\partial \psi^*}{\partial t} - \psi^*\frac{\partial \psi}{\partial t}\right) - \alpha|\psi|^2 - \frac{\beta}{2}|\psi|^4 + \frac{1}{8\pi}\left|\frac{1}{c}\frac{\partial \mathbf{A}}{\partial t} + \nabla\varphi\right|^2 - \frac{1}{8\pi}|\mathrm{curl}\ \mathbf{A}|^2. \quad (5)$$

Here we have used the expression[46] for the potential energy of a variable charge in a fixed potential and have taken into account that

$$\mathbf{e} = -\frac{1}{c}\frac{\partial \mathbf{A}}{\partial t} - \nabla\varphi. \quad (6)$$

We write Lagrange's equation for a continuous medium in the form[43]

$$\frac{\partial \mathcal{L}}{\partial q_i} - \frac{\partial}{\partial t}\frac{\partial \mathcal{L}}{\partial(\partial q_i/\partial t)} - \frac{\partial}{\partial x}\frac{\partial \mathcal{L}}{\partial(\partial q_i/\partial x)} - \frac{\partial}{\partial y}\frac{\partial \mathcal{L}}{\partial(\partial q_i/\partial y)} - \frac{\partial}{\partial z}\frac{\partial \mathcal{L}}{\partial(\partial q_i/\partial z)} = \frac{\partial F}{\partial(\partial q_i/\partial t)}. \quad (7)$$

The field functions $q_i(\mathbf{r},t)$ for the Lagrangian (5) are the order parameter ψ^* and the components of the vector potential A_x, A_y, A_z. On the right-hand side of Eq. (7) is the derivative of the dissipative function with respect to the corresponding generalized velocity,[47] since the superconducting component and the electromagnetic field do not form a closed system. Its interaction with the crystal lattice and the normal component lead to energy dissipation for the electromagnetic field in the cores of the moving vortices.[42] The rate of energy of the system corresponds to twice the value of the dissipative function. Neglecting the lag in the recovery of the order parameter in a moving vortex,[42] we shall assume that the dissipation is due to the current of the normal component and set $F = |\mathbf{e}|^2\sigma_n/2$, where σ_n is the conductivity of the normal component.

After calculating the corresponding derivatives of the Lagrangian (5) and dissipative function, substituting them into Eq. (7), and performing some straightforward vector transformations with Eq. (6) taken into account, we obtain

$$i\hbar\frac{\partial \psi}{\partial t} = \left\{-\frac{1}{4m}\left(i\hbar\nabla + \frac{2e}{c}\mathbf{A}\right)^2 + 2e\varphi - \alpha - \beta|\psi|^2\right\}\psi, \quad (8)$$

$$\mathrm{curl\ curl}\ \mathbf{A} = -\frac{8\pi e^2}{c^2 m}|\psi|^2\mathbf{A} + \frac{i2\pi e\hbar}{cm}(\psi\nabla\psi^* - \psi^*\nabla\psi) + \frac{4\pi}{c}\sigma_n\mathbf{e} + \frac{1}{c}\frac{\partial \mathbf{e}}{\partial t}. \quad (9)$$

The boundary-value problem for these equations has the form of the Cauchy boundary conditions[48]

$$\left.\frac{\partial \psi}{\partial n}\right|_S + \left.\left(\frac{2ei}{c}A_n - b\right)\psi\right|_S = 0. \quad (10)$$

The constant b depends on the situation at the boundary S of the superconductor.

Equation (8) agrees with the nonstationary equations obtained in Refs. 49,50 if the charge of the nonequilibrium carriers is neglected. Of course, this only attests to the applicability of the Lagrangian model (5) in the quasiequilibrium case under consideration, which is characteristic for the motion of the system of Abrikosov vortices in the field of an electromagnetic wave of the rf range in the linear approximation. We note that the description of the dynamics of a quasiequilibrium Cooper condensate by means of Lagrange's equations is close to the idea proposed in the classic paper by Gor'kov and Kopnin,[12] that the rate of change of the order parameter is proportional to the variational derivative of the free energy.

By virtue of of the Maxwell equation

$$\text{curl curl } \mathbf{A} = \frac{4\pi}{c}\mathbf{j}_s + \frac{4\pi}{c}\sigma_n \mathbf{e} + \frac{1}{c}\frac{\partial \mathbf{e}}{\partial t}, \tag{11}$$

Eq. (9) can be written in the form[51]

$$\mathbf{j}_s = \frac{c|\Psi|^2}{4\pi\lambda^2}\left(\frac{\hbar c}{2e}\nabla\theta - \mathbf{A}\right), \tag{12}$$

where

$$\Psi = \psi/\psi_0 - |\Psi|\exp(i\theta), \quad \lambda = \frac{c}{2e}\sqrt{m/\pi n_s}.$$

The imaginary part of Eq. (8) with allowance for relation (12) takes the form of the continuity equation for the superconducting component $\partial|\Psi|^2/\partial t = -(1/en_s)\text{div}\,\mathbf{j}_s$, and the real part is accordingly

$$\frac{\partial\theta}{\partial t} = \frac{\hbar}{4m}\left(\frac{\Delta|\psi|}{|\psi|} - \left|\nabla\theta - \frac{2e}{c\hbar}\mathbf{A}\right|^2\right) - \frac{\alpha}{\hbar}(|\psi|^2 - 1) - \frac{2e}{\hbar}\varphi. \tag{13}$$

If we set $|\Psi| = 1$ outside the vortex core and assume that the core radius is negligible if the field is not too high, then, after taking the curl of Eq. (12) and using formulas (2) and (11), we obtain[47]

$$\mathbf{b} + \lambda^2 \text{curl curl } \mathbf{b} + \frac{4\pi\sigma_n\lambda^2}{c^2}\frac{\partial \mathbf{b}}{\partial t} + \frac{\lambda^2}{c^2}\frac{\partial^2 \mathbf{b}}{\partial t^2} = \mathbf{\Phi}_0\delta(\mathbf{r} - \mathbf{r}_i). \tag{14}$$

Here $\mathbf{r}_i$ are the coordinates of the vortex centers, $\mathbf{\Phi}_0 = \Phi_0\mathbf{1}_i$, where $\mathbf{1}_i$ is a unit vector directed along the axis of the vortex, and $\Phi_0 = \pi\hbar c/e$.

In the stationary case Eq. (14) coincides with the well-known equation of a nonmoving Abrikosov vortex.[51] For a vortex moving with velocity v along the x axis, the fourth term on the right-hand side of Eq. (14) is equal to $(\lambda^2 v^2/c^2)\partial^2\mathbf{b}/\partial x^2$ and describes the deformation of a moving vortex due to the Lorentz contraction. For $v \ll c$ one can neglect it and assume that the moving vortex is undeformed. The third term is due to the normal conduction current. Neglecting the interference of this current with the superconducting component,[37] we can assume that it does not distort the distribution of the supercurrent and the order parameter with respect to the core of the moving vortex.

We average Eq. (14) over a volume V containing many parallel vortices and chosen in the form a cylinder with base S perpendicular to the vortex axes and with generator parallel to the vortex axes:

$$\mathbf{B} + \lambda^2 \text{curl curl } \mathbf{B} + \frac{4\pi\lambda^2\sigma_n}{c^2}\frac{\partial \mathbf{B}}{\partial t} + \frac{\lambda^2}{c^2}\frac{\partial^2 \mathbf{B}}{\partial t^2} = n\mathbf{\Phi}_0, \tag{15}$$

where n is the density of vortices. In the averaging it is assumed that formula (5), which follows from the Ginzburg–Landau equations,[1] is applicable at small values of the order parameter. Then one can assume that the concentration of the normal phase changes insignificantly at the superconducting transition, while the normal conductivity σ_n is almost constant over the whole volume of the superconductor.

It follows from the wave equation (15) that only in a uniform static field can it be assumed that $B = n\Phi_0$. This is because in the averaging according to formula (3) the boundary of the base S divides several vortices into parts, and if the vortices are distributed nonuniformly they will not compensate each other. Equation (15) can be regarded as a nonlocal and nonstationary constitutive relation for the mixed state of a type II superconductor. The field function it it is the vortex density n instead of the magnetic field strength $\mathbf{H}$.

It follows from Eqs. (4) that the boundary condition for the magnetic induction is the total surface current density, which depends on the position of the vortices near the boundary. Thus there arises the problem of the additional boundary conditions that are imposed on the function $n(\mathbf{r})$. As in the case of spin waves,[27] the additional boundary conditions aside from the electrodynamic conditions (4) are determined by the interaction of the magnetic moments, in this case vortices, with the boundary.[52–54] Since the lattice parameters are practically nonvarying near the boundary of a superconductor,[54] the additional boundary conditions for the mixed state can be stated as Cauchy conditions analogous to Eq. (10).

DYNAMICS OF VORTICES IN A PLANE WAVE

The electrodynamics of the mixed state of a superconductor are significantly "richer" than in crystal optics, where the nonlocality is due to the rigid lattice, or in a plasma, where there is no short-range order. When an electromagnetic wave of wavelength comparable to the period of the vortex lattice is propagating in a superconductor, the velocity field of the Abrikosov vortices is nonuniform in space, causing a change of the electric field produced by the moving vortices.

We differentiate Eq. (12) with respect to time, taking Eq. (13) into account:

$$\frac{\partial \mathbf{j}_s}{\partial t} = \frac{c^2|\psi|^2}{4\pi\lambda^2}\mathbf{e} + \frac{\hbar c^2}{8\pi\lambda^2 e}\frac{\partial|\psi|^2}{\partial t}\left(\nabla\theta - \frac{2e}{\hbar c}\mathbf{A}\right) + \nabla f. \tag{16}$$

Here we have used the notation

$$f = \frac{\hbar}{4m}\left(\frac{\Delta|\psi|}{|\psi|} - \left|\nabla\theta - \frac{2e}{c\hbar}\mathbf{A}\right|^2\right) - \frac{\alpha}{\hbar}|\psi|^2.$$

The first term in Eq. (16) coincides with the first London equation,[51] while the second and third terms are the contribution of the moving vortices and are equal to zero for a

nonmoving vortex. For $v \ll c$ it can be assumed that the vortex in its motion is undeformed. Therefore the modulus and phase of the order parameter, the superconducting current density and, hence, the vector potential, are distributed relative to the center $\mathbf{r}_i(t)$ of the moving vortex in the same manner as in the nonmoving vortex.

Let $\boldsymbol{\rho}=\mathbf{r}-\mathbf{r}_i$. Then $\partial|\psi|^2/\partial t=\mathbf{v}\cdot\nabla|\psi|^2$, where $\mathbf{v}(\mathbf{r}_i)=d\mathbf{r}_i/dt$ is the velocity of the center of the vortex, and

$$\nabla\theta=1\times\boldsymbol{\rho}/\rho^2,\ \mathbf{A}=1\times\boldsymbol{\rho}A(\rho)/\rho,$$

$$\nabla|\psi|^2=(d|\psi|^2/d\rho)\boldsymbol{\rho}/\rho,\ \nabla f=(df/d\rho)\boldsymbol{\rho}/\rho.$$

We average Eq. (16) over a physically small volume containing many vortices, the centers $\mathbf{r}_i$ of which are distributed in the superconductor with a density n. It is not hard to see that the third term, by virtue of the symmetry of the vortex, averages to zero. Then

$$\left\langle\frac{\partial\mathbf{j}_s(\mathbf{r})}{\partial t}\right\rangle=\frac{c^2}{4\pi\lambda^2}\mathbf{E}+\frac{\hbar c^2}{8\pi\lambda^2 e}1\times\int_S\int n(\mathbf{r}-\mathbf{c})(\mathbf{v}(\mathbf{r}-\mathbf{c})\cdot\mathbf{c})\frac{\mathbf{c}}{\rho^2}\frac{d|\psi|^2}{d\rho}\left(\frac{1}{\rho}-\frac{2e}{\hbar c}A\right)d^2\rho.$$

Here the integration on the right-hand side is over the whole cross section of the vortex.

We direct the z axis along the axis of the vortex; then the vector $\boldsymbol{\rho}$ in the integrals will have components x and y, while the respective components of $\mathbf{r}$ are x_0 and y_0. Because the region of supercurrents and magnetic fields in the vortex has a size of the order of λ, the functions nv_x and nv_y can be expanded in a Taylor series to second order in x and y.

The integrals obtained are conveniently evaluated in cylindrical coordinates. Integrating by parts with allowance for the facts that the vortex field has a faster than exponential decay field at infinity[51] and that the flux trapped by a vortex is equal to the flux quantum Φ_0, and that $|\psi(0)|=0$ and $|\psi(\infty)|=1$, using the stationary equation (14), and performing some some vector transformations, we obtain

$$\frac{\partial^2\mathcal{P}}{\partial t^2}=\sigma_n\frac{\partial\mathbf{E}}{\partial t}+\frac{c^2}{4\pi\lambda^2}\left[\mathbf{E}+\frac{1}{c}\boldsymbol{\Phi}_0\times(n\mathbf{v}+\lambda^2\Delta(n\mathbf{v}))\right]. \tag{17}$$

In Eq. (17) the total microscopic current consists of the currents of the superconducting and normal components without the interference.[37] The last term in (17), which depends on the vortex velocity, can be regarded as an additional field produced by the moving vortices: $\mathbf{E}_v=\boldsymbol{\Phi}_0\times(n\mathbf{v}+\lambda^2\Delta(n\mathbf{v}))/c$. Taking the curl of the right and left sides of this equation with allowance for the fact that the constant vector $\boldsymbol{\Phi}_0$ is perpendicular to the vectors $\mathbf{v}$ and ∇n and doing some straightforward vector transformations, we obtain

$$\operatorname{curl}\mathbf{E}_v=\boldsymbol{\Phi}_0\{(\mathbf{v}+\lambda^2\Delta(n\mathbf{v})/n)\cdot\nabla n+n\nabla\cdot(\mathbf{v}+\lambda^2\Delta(n\mathbf{v})/n)\}/c=\boldsymbol{\Phi}_0\operatorname{div}(n\mathbf{v}+\lambda^2\Delta(n\mathbf{v}))/c.$$

We differentiate both sides of Eq. (15) with respect to time and take its Laplacian Δ. Taking into account the continuity equation $\partial n/\partial t=-\operatorname{div}(n\mathbf{v})$ and keeping only terms up to the second derivatives, we obtain $\lambda^2\Delta(\partial\mathbf{B}/\partial t)-\partial\mathbf{B}/\partial t=\boldsymbol{\Phi}_0\operatorname{div}(n\mathbf{v})$. Accordingly, $\partial(\Delta\mathbf{B})/\partial t=\boldsymbol{\Phi}_0\partial(\Delta n)/\partial t=-\boldsymbol{\Phi}_0\Delta\times(\operatorname{div}(n\mathbf{v}))=-\boldsymbol{\Phi}_0\operatorname{div}(\Delta(n\mathbf{v}))$. Thus $\operatorname{curl}\mathbf{E}_v=-(1/c)\partial\mathbf{B}/\partial t$, which coincides with the Maxwell equation and confirms the applicability of formulas (15) and (17).

In the motion of a uniform vortex lattice with a velocity constant in time and space in a superconductor in the absence of external fields, Eq. (17) goes over to the well-known formula $\mathbf{E}=\mathbf{V}\times\mathbf{v}/c$ (Refs. 12,55, which can be derived from the Lorentz transformation.[34,43,46] Indeed, in a system tied to a vortex flow uniform in time and space, all of the vortices are at rest, and there is no electric field. If, however, the vortex density and velocity are functions of time and the coordinates, in any inertial reference frame some of the vortices will be moving with variable velocities, and consequently an additional electric field will be present.

For constructing the generalized polarization (1) the generalized friction force[47] on the right-hand side of Eq. (7) should be expressed in terms of the normal conduction current. It is not difficult to show that the magnetic moment $\mathbf{M}$ per unit length of vortex is equal to $\boldsymbol{\Phi}_0/(4\pi)$. Since the superconducting component creating that moment does not exchange energy with the normal component, the field $\mathbf{B}_n$ created by the normal conduction currents can be treated as an external current for that moment. If the superconductor is uniform along the z axis, then the field $\mathbf{B}_n=B_n\mathbf{1}$, and the magnetic moment $\mathbf{M}$ is directed along z. Using the formula for the force exerted on a magnetic dipole in an external field,[34] we obtain

$$\mathbf{f}_f=\operatorname{grad}(\mathbf{M}\cdot\mathbf{B}_n)=M\ \operatorname{grad}B_n=M\mathbf{I}\times\operatorname{curl}\mathbf{B}_n=\Phi_0\times\mathbf{j}_n/c. \tag{18}$$

We note that the force exerted on the vortex by the normal conduction currents is directed oppositely to the force exerted by the superconducting currents.[51] This is natural, since the field formed by the superconducting currents is not external with respect to the vortex.

LINEAR SUSCEPTIBILITY

Suppose that stationary distributions of the vortices $n_0(\mathbf{r})$ and of the corresponding magnetic field $B_0(\mathbf{r})$ are established in the superconductor by an external source, e.g., a transport current. In the analysis of the linear susceptibility we shall assume that the variable parts of the vortex density and field are small compared to the stationary values, and we set $n(\mathbf{r},t)=n_0(\mathbf{r})$ in Eq. (17).

We shall assume that in the stationary state the vortices are pinned at pinning centers and oscillate about them under the influence of the wave without going into the flux flow regime. Then vortices are not created or annihilated inside the superconductor. We use the model of collective pinning of an elastic vortex on distributed defects.[51] Performing the averaging in (3) first with respect to the z axis, along which the unit vector 1 is directed, and then over the cross section S perpendicular to that unit vector, in the first step we obtain linear vortices oriented along the z axis with a uniformly distributed pinning force.

We assume in the linear approximation that the pinning force acting on a unit length of vortex is equal to $\mathbf{f}_p=-a\mathbf{u}$, where $\mathbf{u}$ is the displacement of the vortex from its equilibrium position. Using the known formula[51] for the force exerted on a unit length of vortex by the superconducting cur-

rents $\mathbf{j}_s$ flowing around the vortex cores and taking formula (18) into account, we write the equation of motion of a vortex in the form

$$a\mathbf{u} = (\mathbf{j}_s - \mathbf{j}_n) \times \Phi_0/c. \tag{19}$$

We average this equation over the cross section of a physically small volume:

$$\mathbf{v} = \frac{\partial \mathbf{u}}{\partial t} = \frac{1}{ac}\left(\frac{\partial^2 \mathcal{P}}{\partial t^2} - 2\sigma_n \frac{\partial \mathbf{E}}{\partial t}\right) \times \Phi_{\mathbf{0}}.$$

Substituting this relation into formula (17), we obtain

$$\frac{\partial^2}{\partial t^2}\left[\mathcal{P} - \frac{\Phi_0^2 n_0}{4\pi a\lambda^2}\left(\mathcal{P} - \frac{\lambda^2}{n_0}\Delta(n_0\mathcal{P})\right)\right] = \frac{c^2}{4\pi\lambda^2}\mathbf{E} + \sigma_n \frac{\partial}{\partial t} \times\left[\mathbf{E} - \frac{\Phi_0^2 n_0}{2\pi a\lambda^2}\left(\mathbf{E} - \frac{\lambda^2}{n_0}\Delta(n_0\mathbf{E})\right)\right].$$

Expressing the instantaneous values of the field and polarization in terms of their Fourier transformations (1), we obtain

$$[1 - \gamma(1 + k^2\lambda^2)]n_0\hat{\chi} + \gamma\lambda^2[\Delta(n_0\hat{\chi}) + 2i\mathbf{k}\cdot\nabla(n_0\hat{\chi})] = [1 - 2\gamma(1 + k^2\lambda^2)]n_0 + \frac{ic^2 n_0}{4\pi\lambda^2\omega\sigma_n} + 2\gamma\lambda^2[\Delta n_0 + 2i\mathbf{k}\cdot\nabla n_0], \tag{20}$$

where $\gamma = \Phi_0^2 n_0/(4\pi a\lambda^2)$. For vortices rigidly pinned to pinning centers at $\alpha \to \infty$ we obtain

$$\hat{\chi}(\omega, \mathbf{k}, \mathbf{r}) = \hat{\chi}_0(\omega, \mathbf{r}) = \frac{i\sigma_n}{\omega} - \frac{c^2}{4\pi\lambda^2\omega^2}.$$

The generalized susceptibility

$$\hat{\sigma} = -i\omega\hat{\chi} = \sigma_n + \frac{ic^2}{4\pi\lambda^2\omega}$$

corresponds to the complex conductivity of the superconductor in the framework of the two-fluid model and describes the penetration of the electromagnetic field to a depth $\delta(\omega) \approx \lambda/\sqrt{1 + \omega^2/\omega_s^2}$, where $\omega_s = c^2/(4\pi\lambda^2\sigma_n) = e^2 n_s/(\sigma_n m) \approx 10^{13}\text{s}^{-1}$ is the frequency at which the currents of the superconducting and normal components become equal.[51]

We seek a solution of equation (20) for the case of a low density of strongly coupled vortices at $\gamma \ll 1$ by the method of successive approximations in the small parameter γ: $\hat{\chi}(\omega, \mathbf{k}, \mathbf{r}) = \hat{\chi}_0(\omega, \mathbf{r}) + \gamma\hat{\chi}_1(\omega, \mathbf{k}, \mathbf{r})$, and then

$$\hat{\chi}_1(\omega, \mathbf{k}, \mathbf{r}) = -\left(\frac{i\sigma_n}{\omega} + \frac{c^2}{4\pi\lambda^2\omega^2}\right)[n_0 + \lambda^2(k^2 n_0 - 2i\mathbf{k}\cdot\nabla n_0 - \Delta n_0)].$$

For a metallic superconductor $\lambda^2 k^2 \ll 1$ in the rf range. Superconductors with an appreciable pinning force typically have triangular distributions of the vortex density.[51] The Laplacian of such a distribution is equal to zero everywhere except at an kink, and in the averaging one can set $\lambda^2\Delta n_0 \ll n_0$. Therefore the expression for the generalized susceptibility of a hard superconductor has the form

$$\hat{\varepsilon}(\omega, \mathbf{k}, \mathbf{r}) = 1 + \frac{c^2}{\lambda^2\omega^2}\left(\frac{i\omega}{\omega_s} - 1\right) - \frac{\Phi_0^2}{\lambda^2 a}\frac{c^2}{\lambda^2\omega^2}\left(\frac{i\omega}{\omega_s} + 1\right)(n_0 - 2i\lambda^2\mathbf{k}\cdot\nabla n_0). \tag{21}$$

It is seen from formula (21) that the spatial dispersion is manifested in nonuniformly magnetized superconductors. Here both the real and imaginary parts of the generalized permeability depend on the angle between the wave vector $\mathbf{k}$ and the gradient of the vortex density. The influence of the spatial dispersion on a wave propagating along the vortex density gradient is particularly strong.

By increasing the transport current in a superconducting slab and then decreasing it to zero one can create a vortex distribution in the slab such that the surface density is equal to zero and the gradient is maximal and determined by the critical current.[51] In that case, even in the case of weak pinning, i.e., a large value of Φ_0^2/a, the parameter γ in the boundary region will be small and representation (21) can be used.

To solve rigorously the problem of wave propagation in the direction of the gradient, i.e., in the direction of the change of the parameters of the medium, is rather complicated. For example, in such nonuniform media there can be longitudinal waves, for example, for which $\mathbf{E} = \mathbf{k}E_{\|}$. For a longitudinal plane wave the second of Maxwell's equations (2) takes the form $\text{div}\,\mathcal{D} = \text{div}(\tilde{\varepsilon}(\mathbf{r})\mathbf{E}) = \mathbf{E}\cdot\nabla\tilde{\varepsilon} + \tilde{\varepsilon}\mathbf{k}\cdot\mathbf{E} = 0$, i.e., $\mathbf{k}\cdot\nabla\hat{\varepsilon} = -k^2\tilde{\varepsilon}$. For $\omega \ll \omega_s$ it follows from Eq. (21) that for longitudinal waves $\mathbf{k} = -\Phi_0^2\nabla n_0/(a\lambda^2)$, which is attainable in the boundary region.

In the opposite case of a high density of weakly coupled vortices, Eq. (20) can be solved by the method of successive approximations in the small parameter $1/\gamma$:

$$\tilde{\varepsilon}(\omega, \mathbf{k}, \mathbf{r}) = 1 + \frac{8\pi i\sigma_n}{\omega} + \frac{16\pi^2 a\lambda^2}{\Phi_0^2 n_0(1 + \lambda^2 k^2)} \times\left(\frac{i\sigma_n}{\omega} + \frac{c^2}{4\pi\lambda^2\omega^2}\right). \tag{22}$$

In the limit of free vortices ($a \to 0$) we obtain a purely imaginary susceptibility, i.e., the motion of the superconducting phase in the vortices simply doubles the loss in the normal phase. This is natural, since in an ideal type II superconductor losses arise at arbitrarily low frequencies.[47] For $\omega \ll \omega_s$ the generalized susceptibility (22) is almost real and positive. If $\gamma = 0.1$ and $\lambda = 10^{-5}$ cm, then at a frequency $\omega = 10^6\ \text{s}^{-1}$ one has $\varepsilon \sim 10^{20}$ and a refractive index of the order of 10^{10}, which corresponds to a wave number $k = 10^5\ \text{cm}^{-1} \sim 1/\lambda$.

NONLINEAR SUSCEPTIBILITY

The generation of higher harmonics and combination frequencies in the propagation of an electromagnetic wave in nonlinear media is usually studied by the method of successive approximations after separating the generalized polarization into a linear and a nonlinear part:[34,46,56]

$$\mathcal{P}(\mathbf{r}, t) = \mathcal{P}^{\text{lin}}(\mathbf{r}, t) + \mathcal{P}^{\text{nonlin}}(\mathbf{r}, t), \mathcal{P}^{\text{lin}}(\mathbf{r}, t) = \mathcal{P}^{(1)}(\mathbf{r}, t), \times\mathcal{P}^{\text{nonlin}}(\mathbf{r}, t) = \mathcal{P}^{(2)}(\mathbf{r}, t) + \mathcal{P}^{(3)}(\mathbf{r}, t) + \ldots,$$

$$\mathcal{P}^{(2)}(\mathbf{r},t)=\int_0^\infty\int_0^\infty dt_1dt_2\iint\tilde{\chi}^{(2)}(\mathbf{r},\mathbf{r}_1,\mathbf{r}_2,t_1,t_2)\mathbf{E}(\mathbf{r}-\mathbf{r}_1,t-t_1)\mathbf{E}(\mathbf{r}-\mathbf{r}_2,t-t_2)d^3r_1d^3r_2$$
$$=\int_{-\infty}^\infty\int_{-\infty}^\infty\frac{d\omega_1d\omega_2}{(2\pi)^8}\iint\hat{\chi}^{(2)}\times(\mathbf{r},\mathbf{k}_1,\mathbf{k}_2,\omega_1,\omega_2)\mathcal{E}(\mathbf{k}_1,\omega_1)\mathcal{E}(\mathbf{k}_2,\omega_2)\times\exp[i(\mathbf{k}_1+\mathbf{k}_2)\cdot\mathbf{r}-i(\omega_1+\omega_2)t]d^3k_1d^3k_2,$$

$$\hat{\chi}^{(2)}(\mathbf{r},\mathbf{k}_1,\mathbf{k}_2,\omega_1,\omega_2)=\int_0^\infty\int_0^\infty dt_1dt_2\iint\tilde{\chi}^2(\mathbf{r},\mathbf{r}_1,\mathbf{r}_2,t_1,t_2)\times\exp(i\omega_1t_1+i\omega_2t_2-i\mathbf{k}_1\cdot\mathbf{r}_1-i\mathbf{k}_2\cdot\mathbf{r}_2)d^3r_1d^3r_2. \quad (23)$$

Here the spatial integrals over infinite limits are denoted by the integral sign alone, and condition (1) holds for the polarization $\mathcal{P}^{(1)}$.

A nonlinear (cubic) polarization $\mathcal{P}^{(3)}$ in a superconductor can arise from a nonlinear dependence of the pinning force on the displacement of the vortex, and a quadratic polarization $\mathcal{P}^{(2)}$ from field dependence of the vortex concentration n in Eq. (17) and also from nonlocality, which is manifested when the amplitude of the vibrations of the vortex are comparable to the wavelength of the wave. The latter case is specific to superconductors. Neither in crystals nor in plasmas does the nonlocality give rise to nonlinearity, since it is practically independent of field. In a superconductor, however, the contributions of these components to the nonlinear polarization are approximately equal.

With the nonlocality taken into account, Eq. (19) becomes

$$ca\mathbf{u}(\mathbf{r})=(\mathbf{j}_s(\mathbf{r}+\mathbf{u})-\mathbf{j}_n(\mathbf{r}+\mathbf{u}))\times\mathbf{\Phi}_0=[\mathbf{j}_s(\mathbf{r})-\mathbf{j}_n(\mathbf{r})+(\mathbf{u}\cdot\nabla)(\mathbf{j}_s(\mathbf{r})-\mathbf{j}_n(\mathbf{r}))]\times\mathbf{\Phi}_0.$$

In the framework of the method of successive approximations we restrict consideration to the case of weak dispersion, when $\lambda k\ll 1$, and we set $n=n_0+n^{(1)}$, $\mathbf{u}=\mathbf{u}^{(1)}+\mathbf{u}^{(2)}$, where $|n^{(1)}|\sim\lambda k|n_0|$, $|\mathbf{u}^{(2)}|\sim\lambda k|\mathbf{u}^{(1)}|$, respectively, and $|\mathcal{P}^{(2)}|\sim\lambda k|\mathcal{P}^{(1)}|$. Then from the continuity equation we obtain $n^{(1)}=-\mathrm{div}(n_0\mathbf{u}^{(1)})$, and Eqs. (17) and (19) decompose into the equations of the first and second approximations (with respect to λk):

$$\frac{\partial^2\mathcal{P}^{(1)}}{\partial t^2}=\sigma_n\frac{\partial\mathbf{E}}{\partial t}+\frac{c^2}{4\pi\lambda^2}\left(\mathbf{E}+\frac{1}{c}\mathbf{\Phi}_0\times n_0\frac{\partial\mathbf{u}^{(1)}}{\partial t}\right),$$

$$\mathbf{u}^{(1)}=\frac{1}{ac}\left(\frac{\partial\mathcal{P}^{(1)}}{\partial t}-2\sigma_n\mathbf{E}\right)\times\mathbf{\Phi_0}, \quad (24)$$

$$\mathbf{u}^{(2)}=\frac{1}{ac}\left[(\mathbf{u}^{(1)}\cdot\nabla)\left(\frac{\partial\mathcal{P}^{(1)}}{\partial t}-2\sigma_n\mathbf{E}\right)\right]\times\mathbf{\Phi_0}$$
$$=(\mathbf{u}^{(1)}\cdot\nabla)\mathbf{u}^{(1)}=\frac{1}{2}\nabla(\mathbf{u}^{(1)}\cdot\mathbf{u}^{(1)})-\mathbf{u}^{(1)}\times\nabla\times\mathbf{u}^{(1)}, \quad (25)$$

$$\frac{\partial^2\mathcal{P}^{(2)}}{\partial t^2}=\frac{c}{4\pi\lambda^2}\mathbf{\Phi}_0\times\left(n_0\frac{\partial\mathbf{u}^{(2)}}{\partial t}-n_0\frac{\partial\mathbf{u}^{(1)}}{\partial t}\cdot\nabla\mathbf{u}^{(1)}-\mathbf{u}^{(1)}\cdot\frac{\partial\mathbf{u}^{(1)}}{\partial t}\nabla n_0\right). \quad (26)$$

The effect of nonlocality is substantial in the case of a high density of weakly coupled vortices for $4\pi\lambda^2a\ll\Phi_0^2n_0$. Then the stationary density of vortices $n_0(\mathbf{r})$ can be assumed to be a slowly varying function, and the last term in (26) can be neglected, while from the equations of the zeroth approximation (24) we obtain with the aid of the spectral method

$$\mathbf{u}^{(1)}(\mathbf{r},t)=\frac{1}{(2\pi)^4}\int_{-\infty}^\infty\int_{-\infty}^\infty\frac{4\pi\lambda^2\sigma_n\omega-ic^2}{n_0\Phi_0^2c\omega}[\mathcal{E}(\mathbf{k},\omega)\mathbf{\Phi}_0]\times\exp(i\mathbf{k}\cdot\mathbf{r}-i\omega t)d\omega d^3k,$$

$$\mathbf{u}^2(\mathbf{r},t)=\frac{i}{(2\pi)^8}\int_{-\infty}^\infty\int_{-\infty}^\infty\frac{(4\pi\lambda^2\sigma_n\omega_1-ic^2)(4\pi\lambda^2\sigma_n\omega_2-ic^2)}{2n_0^2\Phi_0^2c^2\omega_1\omega_2}\times\exp(i(\mathbf{k}_1+\mathbf{k}_2)\cdot\mathbf{r}-i(\omega_1+\omega_2)t)d\omega_1d\omega_2$$
$$\times\int_{-\infty}^\infty\int_{-\infty}^\infty[(\mathbf{k}_1+\mathbf{k}_2)(\mathcal{E}(\mathbf{k}_1,\omega_1)\mathcal{E}(\mathbf{k}_2,\omega_2))-\mathcal{E}(\mathbf{k}_1,\omega_1)\mathbf{k}_2\mathcal{E}(\mathbf{k}_2,\omega_2)-\mathcal{E}(\mathbf{k}_2,\omega_2)\times(\mathbf{k}_1\mathcal{E}(\mathbf{k}_1,\omega_1))]d^3k_1d^3k_2.$$

Substituting these expressions into the right-hand side of Eq. (26) and into the left-hand side of expression (23), we obtain for the quadratic polarization

$$-(\omega_1+\omega_2)^2\hat{\chi}(\mathbf{k}_1,\mathbf{k}_2,\omega_1,\omega_2)\mathcal{E}_1\mathcal{E}_2=\frac{(4\pi\lambda^2\sigma_n\omega_1-ic^2)(4\pi\lambda^2\sigma_n\omega_2-ic^2)}{8\pi c\lambda^2B_0\omega_1\omega_2}\{(\omega_1+\omega_2)1\times[(\mathbf{k}_1+\mathbf{k}_2)(\mathcal{E}_1\mathcal{E}_2)-\mathcal{E}_1(\mathbf{k}_2\mathcal{E}_2)-\mathcal{E}_2(\mathbf{k}_1\mathcal{E}_1)]-\omega_1\mathcal{E}_1(\mathbf{k}_2[\mathcal{E}_2\times 1])-\omega_2\mathcal{E}_2(\mathbf{k}_1[\mathcal{E}_1\times 1])\}.$$

Here $\mathcal{E}(\mathbf{k}_1,\omega_1)=\mathcal{E}_1$, $\mathcal{E}(\mathbf{k}_2,\omega_2)=\mathcal{E}_2$. The explicit form of the quadratic susceptibility operator is more conveniently represented in tensor form. If the vectors $\mathcal{E}$, $\mathcal{P}^{(2)}$, and $\mathbf{k}$ lie in the xy plane while the unit vector 1 is directed along the z axis, then

$$\chi_{ijk}^{(2)}(\mathbf{k}_1,\mathbf{k}_2,\omega_1,\omega_2)=\frac{(4\pi\lambda^2\sigma_n\omega_1-ic^2)(4\pi\lambda^2\sigma_n\omega_2-ic^2)}{8\pi c\lambda^2B_0\omega_1\omega_2(\omega_1+\omega_2)^2}g_{ijk}(\mathbf{k}_1,\mathbf{k}_2,\omega_1,\omega_2),$$

$$g_{xxx}=\omega_1k_{1y}+\omega_2k_{2y},\ g_{xxy}=\omega_1k_{2x}-(\omega_1+\omega_2)k_{2x},\ g_{xyx}=\omega_2k_{1x}-(\omega_1+\omega_2)k_{1x},\ g_{xyy}=0,$$

$$g_{yxx}=0,\ g_{yxy}=-\omega_2 k_{1y}+(\omega_1+\omega_2)k_{2y},\ g_{yyx}=-\omega_1 k_{2y}+(\omega_1+\omega_2)k_{1y},\ g_{yyy}=-\omega_1 k_{1x}-\omega_2 k_{2x}. \quad (27)$$

CONCLUSION

Analysis of the electromagnetic processes in type II superconductors by the generalized polarization method allows one, in the averaging of the microscopic fields in a system of vortices moving with a velocity that varies in space and time, to take into account the nonlocality of the interaction of the vortices and the spatial dispersion caused by it. Despite the anisotropy created by the transport current, the generalized permeabilities (21) and (22) are scalars, i.e., the longitudinal and transverse permeabilities are equal. Consequently, the differential magnetic susceptibility of the superconductor is equal to unity.[34] This corresponds to the model considered, in which the vortices vibrate around the pinning centers. In such motion the magnetization does not vary.

The variation of the magnetization and, accordingly, the tensor character of the generalized permeability are manifested in the flux flow regime. Analysis of the spatial dispersion in such motion of the vortices requires the application of kinetic methods.[41] However, the expressions we have obtained for the generalized susceptibility show the possibility of several types of waves—longitudinal, slow—but not to the same degree as follows from formula (22).

The approximate character of formula (22) is due to the fact that the features of the generalized susceptibility are of second-order smallness with respect to λk. Then not only the quadratic polarization $\mathcal{P}^{(2)}$ but also the cubic polarization $\mathcal{P}^{(3)}$ are substantial, and the latter, in turn, influences the dispersion relation of the main wave.[56] Analysis of the cubic polarization, including the pinning due to the nonlinearity, is done in a manner analogous to the derivation of formula (27), although more awkwardly.

The possibility of electric control of the dispersion characteristics of linear and nonlinear waves and of the anisotropy of the medium by using the transport current and external magnetization to obtain the necessary vortex distribution makes it possible to use them like spin waves in functional electronics.[29,31,57] The complex character of the frequency and spatial dispersion relation (27) of nonlinear waves suggests the possibility of a nonlinear resonance interaction, in particular, the generation of echo responses, which can be used to create analog Fourier processors.[57] Such an interaction can be manifested in the rf range in ceramic superconductors, where the nonlocality is related to the Josephson penetration depth.

[a]E-mail: ignatjev@vistcom.ru

[1]V. L. Ginzburg and L. D. Landau, Zh. Eksp. Teor. Fiz. **20**, 1064 (1950).
[2]E. H. Brandt, Z. Phys.: Condens. Matter **80**, 167 (1990).
[3]V. N. Kushnir, C. Coccores, S. L. Prischepa, and N. Salvato, Physica C **275**, 211 (1997).
[4]A. A. Abrikosov, Zh. Eksp. Teor. Fiz. **32**, 1442 (1957) [Sov. Phys. JETP **5**, 1174 (1957)].
[5]E. H. Brandt, Rep. Prog. Phys. **58**, 1465 (1995).
[6]E. H. Brandt, Physica B **165–166**, 1129 (1990).
[7]D. G. Kobzev and A. L. Rakhmanov, Sverkhprovodimost: Fiz., Khim., Tekh. **4**, 2079 (1991) [J. Supercond. **4**, 1987 (1991)].
[8]S. B. Rutkevich, Fiz. Nizk. Temp. **16**, 288 (1990) [Sov. J. Low Temp. Phys. **16**, 157 (1990)].
[9]A. I. Larkin and Yu. N. Ovchinnikov, Zh. Eksp. Teor. Fiz. **73**, 299 (1977) [Sov. Phys. JETP **46**, 155 (1977)].
[10]B. D. Josephson, Phys. Rev. A **152**, 211 (1966).
[11]J. D. Livingston, Rev. Mod. Phys. **36**, 54 (1964).
[12]L. P. Gor'kov and N. B. Kopnin, Usp. Fiz. Nauk **116**, 413 (1975) [Sov. Phys. Usp. **18**, 157 (1975)].
[13]V. N. Krivoruchko and Yu. A. Dimashko, Sverkhprovodimost: Fiz., Khim., Tekh. **5**, 967 (1992) [J. Supercond. **5**, 972 (1992)].
[14]A. M. Campbell and J. E. Evetts, *Critical Currents in Superconductors*, Taylor and Francis, London (1972), Mir, Moscow (1975).
[15]L. M. Fisher, N. V. Il'in, I. F. Voloshin, N. M. Makarov, V. A. Yampol'skii, F. P. Rodriguez, and R. L. Snyder, Physica C **206**, 195 (1993).
[16]A. M. Larkin and Yu. M. Ovchinnikov, Zh. Eksp. Teor. Fiz. **65**, 1704 (1973) [Sov. Phys. JETP **38**, 854 (1974)].
[17]L. P. Gor'kov and N. B. Kopnin, Zh. Eksp. Teor. Fiz. **60**, 2331 (1971) [Sov. Phys. JETP **33**, 1251 (1971)].
[18]I. F. Voloshin, V. S. Gorbachev, S. E. Savel'ev, L. M. Fisher, and V. A. Yampol'skiĭ, JETP Lett. **59**, 55 (1994).
[19]J. R. Clem, J. Appl. Phys. **50**, 3518 (1979).
[20]A. C. Mota, G. Juri, P. Visani, and A. Pollini, Physica C **162–164**, 1152 (1989).
[21]E. B. Sonin and A. K. Tagantsev, Phys. Lett. A **140**, 127 (1989).
[22]J. Carini, L. Drabeck, and G. Gruner, Mod. Phys. Lett. B **3**, 5 (1989).
[23]V. M. Dzugutov and L. M. Fisher, Fiz. Tverd. Tela (Leningrad) **30**, 2148 (1988) [Sov. Phys. Solid State **30**, 1238 (1988)].
[24]V. M. Agranovich and V. L. Ginzburg, *Spatial Dispersion in Crystal Optics and the Theory of Excitons*, Wiley-Interscience, New York (1966), Nauka, Moscow (1965).
[25]K.-H. Muller, Physica C **159**, 717 (1989).
[26]K.-H. Muller, Physica C **168**, 585 (1990).
[27]Z. Y. Zeng, Y. Yu, A. M. Cun, X. N. Xu, S. Y. Ding, and X. X. Yao, Physica C **272**, 101 (1996).
[28]A. I. D'yachenko and V. V. Chabanenko, Fiz. Nizk. Temp. **18**, 826 (1992) [J. Low Temp. Phys. **18**, 581 (1992)].
[29]A. L. Fetter, Phys. Rev. **147**, 153 (1966).
[30]A. I. Akhiezer, V. G. Bar'yakhtar, and S. V. Peletminskii, *Spin Waves*, North-Holland, Amsterdam (1968), Nauka, Moscow (1967).
[31]N. N. Akhmediev and V. V. Yatsyshen, Fiz. Tverd. Tela (Leningrad) **18**, 1679 (1976) [Sov. Phys. Solid State **18**, 975 (1976)].
[32]A. B. Al'tman, B. M. Lebed', A. V. Nikiforov, I. A. Yakovlev, and S. V. Yakovlev, Sverkhprovodimost: Fiz., Khim., Tekh. **3**(10), 73 (1990) [J. Supercond. **3**, 1638 (1990)].
[33]K. K. Likharev, Semicond. Sci. Technol. **3**, 325 (1990).
[34]M. M. Bredov, V. V. Rumyantsev, and I. N. Toptygin, *Classical Electrodynamics* [in Russian], Lan', St. Petersburg (2003).
[35]F. London, *Superfluids*, Vol. 1, New York (1950).
[36]L. P. Gor'kov and G. M. Éliashberg, Zh. Eksp. Teor. Fiz. **54**, 612 (1968) [Sov. Phys. JETP **27**, 328 (1968)].
[37]A. M. Gulyan, G. F. Zharkov, and G. M. Sergoyan, Tr. Fiz. Inst. Akad. Nauk SSSR **204**, 3 (1990).
[38]L. P. Gor'kov and N. B. Kopnin, Zh. Eksp. Teor. Fiz. **64**, 356 (1973) [Sov. Phys. JETP **37**, 183 (1973)].
[39]L. P. Gor'kov and N. B. Kopnin, Zh. Eksp. Teor. Fiz. **65**, 396 (1973) [Sov. Phys. JETP **38**, 195 (1974)].
[40]A. F. Aleksandrov and A. A. Rukhadze, *Lectures on the Electrodynamics of Plasmalike Media* [in Russian], MGU, Moscow (2002).
[41]Yu. L. Klimontovich, *The Kinetic Theory of Electromagnetic Processes*, Springer-Verlag, Berlin (1983), Nauka, Moscow (1980).
[42]A. Schmid, Phys. Condens. Mater. **5**, 302 (1966).
[43]V. V. Batygin and I. N. Toptygin, *Modern Electrodynamics* [in Russian], IKI, Moscow (2003).
[44]L. D. Landau and E. M. Lifshitz, *The Classical Theory of Fields*, 4th English ed., Pergamon Press, Oxford (1975), cited Russ. ed. Fizmatlit, Moscow (2001).
[45]A. I. Larkin and Yu. N. Ovchinnikov, Zh. Eksp. Teor. Fiz. **61**, 1221 (1971)

[Sov. Phys. JETP **34**, 651 (1972)].
[46]V. M. Galitskiĭ and V. M. Ermachenko, *Macroscopic Electrodynamics* [in Russian], Vysshaya Shkola, Moscow (1988).
[47]L. D. Landau and E. M. Lifshitz, *Mechanics*, 3rd ed., Pergamon Press, Oxford (1976), cited Russ. ed. Fizmatlit, Moscow (2001).
[48]V. F. Elesin, V. A. Kashurnikov, and A. V. Kharlamov, Fiz. Nizk. Temp. **12**, 694 (1986) [Sov. J. Low Temp. Phys. **12**, 392 (1986)].
[49]T. J. Rieger, D. J. Scalapino, and J. E. Mercereau, Phys. Rev. B **6**, 1734 (1972).
[50]E. Abrahams and T. Tsuneto, Phys. Rev. **152**, 416 (1966).
[51]V. V. Shmidt, *Introduction to the Physics of Superconductors* [in Russian], MTsNMO, Moscow (2000).
[52]C. P. Bean and J. D. Livingston, Phys. Rev. Lett. **12**, 14 (1964).
[53]G. S. Mkrtchyan, F. R. Shakirzanova, E. A. Shapoval, and V. V. Shmidt, Zh. Eksp. Teor. Fiz. **63**, 667 (1972) [Sov. Phys. JETP **36**, 352 (1973)].
[54]G. S. Mkrtchyan and V. V. Shmidt, Zh. Eksp. Teor. Fiz. **41**, 186 (1975) [Sov. Phys. JETP **41**, 90 (1975)].
[55]Y. B. Kim, C. F. Hempstead, and A. R. Strand, Phys. Rev. **139**, A1163 (1965).
[56]N. M. Ryskin and D. I. Trubetskov, *Nonlinear Waves* [in Russian], Nauka, Moscow (2000).
[57]S. A. Baruzdin, Yu. V. Egorov, V. A. Kalinikos, *et al.*, *Functional Signal-Processing Devices* [in Russian], Radio Svyaz', Moscow (1997).

Translated by Steve Torstveit

Spatial–temporal structure of dissipative magnetic fluxes in type II superconductors

Yu. V. Medvedev[a] and I. B. Krasnyuk

A. A. Galkin Donetsk Physicotechnical Institute, ul. R. Lyuksemburg 72, Donetsk 83114, Ukraine
(Submitted December 10, 2004; resubmitted June 10, 2005)

The nonlinear boundary-value problem of the penetration of a magnetic field b into a superconducting half space with resistivity $\rho_f(b)\sim b^\sigma$ is investigated under the condition that the field amplitude at the boundary increases in time by a power law $(b(0,t)\sim(1+t)^m, m>0)$ or in the peaking regime $(b(0,t)\sim(1-t/t_0)^m, m<0, 0<t<t_0)$. Conditions on the values of the parameters m and σ are given under which different scenarios of magnetic flux penetration can occur. The velocity of the magnetic flux front is calculated in relation to the parameters m and σ. © *2005 American Institute of Physics*. [DOI: 10.1063/1.2144454]

The systematics of magnetic flux penetration into superconducting media have been discussed in many papers (see, e.g., Refs. 1–5. A detailed analysis of these processes in the isothermal case, with a field increasing at a constant rate, was given in Ref. 1 for type II superconductors with different types of current–voltage characteristics. The velocity and structure of the electromagnetic wave with allowance for the nonisothermal dynamics of the flux were investigated in Refs. 3–5. However, in Refs. 3–5 the field at the boundary of the sample was fixed, i.e., the question investigated was that of the stability of the critical state against external perturbations. Such thermodynamic instability leads to anomalies of the nucleation and propagation of the normal phase, depending on the electrodynamic conditions at the surface of the sample.[5]

In the present paper we investigate the dissipative processes of magnetic flux propagation in superconducting media with a model resistivity $\rho_f(b)=\rho_n b^\sigma$, $\sigma>0$ (here ρ_n is the resistivity in the normal state, $b=B/B_{c2}$, where B_{c2} is the second critical field) in the case when the external magnetic field at the boundary of the sample varies by a power law or in a peaking regime. The investigation is based on analysis of the self-similar solutions of the parabolic equations (see Ref. 6 describing the process of penetration of a magnetic flux that is increasing in time into a medium with a finite conductivity.

We consider the standard problem of the magnetic flux penetration into a semi-infinite superconductor in a uniform external magnetic field parallel to its boundary surface: $\mathbf{B}\|\mathbf{z}$, $\mathbf{j}\|\mathbf{y}$, $E=\rho_f(b)(j-j_c)$. Here j_c is the critical current. We shall assume that the temperature of the superconductor is equal to that of the coolant, i.e., we shall neglect the nonisothermicity of the process.

The interrelationship between the magnetic induction, electric field $\mathbf{E}$, and transport current density $\mathbf{j}$ is established by Maxwell's equations:

$$\text{curl}\ \mathbf{E}=-\frac{1}{c}\frac{\partial \mathbf{B}}{\partial t},\quad \text{curl}\ \mathbf{B}=\frac{4\pi}{c}\mathbf{j}, \tag{1}$$

where c is the speed of light.

It follows from system (1) and the definition of the field $\mathbf{E}$ that $\mathbf{B}$ satisfies a generalized Burgers equation. In dimensionless form (upon the change of variables $b=B/B_{c2}$, $x=\lambda x$, $t=t_h t$, where λ is the London penetration depth, $t_h=4\pi\lambda^2/c^2\rho_n$ is the characteristic diffusion time of the magnetic field, and we have dropped the diacritical marks indicating the new variables) this equation becomes

$$b_t-c(b)b_x=\rho_n^{-1}[\rho_f(b)b_x]_x,\quad t>0,\quad x>0,\quad \sigma>0. \tag{2}$$

Here

$$c(b)=\rho_n^{-1}[\alpha\rho_f(b)]_b,\quad \alpha=4\pi j_c(b)\lambda/cB_{c2}.$$

At a sufficiently small rise of the external magnetic field we can write the boundary conditions in the form (the power-law boundary regime)

$$b(0,t)=b_0(1+t)^m,\quad m>0 \tag{3}$$

or, if the rate of increase of the field is large,

$$b(0,t)=b_0(1-t/t_0)^m,\quad m<0,\quad 0<t<t_0, \tag{4}$$

where t_0 is the dimensionless peaking time of the power-law regime. In the latter case for $t\to t_0$ the field $b\to\infty$, and we have the so-called boundary regime with peaking. The initial dimensionless field amplitude b_0 can be taken equal to B_{c1}/B_{c2}, i.e., here $B_0=B_{c1}$.

The second-order parabolic evolutionary Eqs. (2) underlie the mathematical models of diverse physical processes. According to their general properties (for $\alpha=0$), in order for them to have a finite solution $b(x,t)$ of the traveling wave type it is necessary and sufficient to satisfy the inequality (see Ref. 6

$$\int \rho_f(b)b^{-1}db<\infty.$$

The spatial–temporal structure of these solutions is determined by the character of the dependence of the coefficients ρ_f on the quantities b determining the state of the nonlinear media and by the type of boundary conditions. For example, in the theory of thermal processes the function $\rho_f(b)=k(b)$ has the meaning of the thermal conductivity. In boundary-value problems with a thermal influence acting on the boundary of the sample, the explicit form of the temperature dependence of this coefficient determines the law of motion of the thermal wave. In particular, if $k(b)$ is a power law, in the peaking regime, despite the unbounded growth of

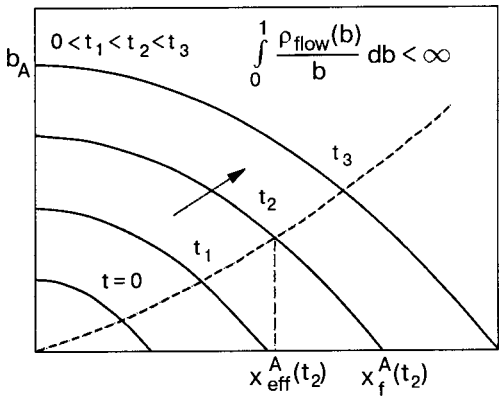

FIG. 1. Evolution of the self-similar solution (5) ($m>0, \sigma>1$).[6]

the temperature at the boundary, the thermal perturbations can be localized at a finite depth. Since the propagation of magnetic field in a medium with a finite conductivity is described by the same differential equation (2), one expects that an analysis of the known spatial–temporal solutions of equation (2) will permit a description of a developing perturbation of the magnetic structures in superconductors.

As we see from Eq. (2), for finding the function $b(x,t)$ it is necessary to know the dependence of the critical current density on b. Taking this into consideration, let us analyze first the case when $j_c=0$ (the coefficient α in Eq. (2) is equal to zero). In this case Eq. (2) takes the simple form

$$b_t = (b^\sigma b_x)_x. \tag{5}$$

We shall show below that taking j_c explicitly into account does not influence the qualitative picture of the spatial–temporal structures of the magnetic flux. Only the velocity of the wave front is affected. Therefore it is useful to start by considering the simplest version of the phenomenon.

LOCALIZATION OF MAGNETIC FLUX IN THE POWER-LAW REGIME OF FIELD VARIATION

Suppose that the rise of the external magnetic field field is determined by the boundary condition (3). Then Eq. (5) has a self-similar solution of the form[6]

$$b(x,t) = b_0(1+t)^m f(\zeta), \quad \zeta = x b_0^{-1/2}(1+t)^{-(1+m\sigma)/2}, \tag{6}$$

where f satisfies the ordinary differential equation

$$(f^\sigma f')' + [(1+m\sigma)/2]\zeta f' - mf = 0, \quad \zeta > 0, \tag{7}$$

and, as following from the statement of the initial problem and the spatial–temporal structure of solution (6), the following boundary conditions should hold:

$$f(0) = 1, \quad f(\infty) = 0. \tag{8}$$

A generalized solution of problem (7) and (8) exists, is unique, and is a finite function.[6] A qualitative graphical representation of the solution at different points in time is given in Fig. 1. The dashed curve denotes the trajectory of the half-width (the point $x_{\text{eff}}(t)$ at which the magnetic induction is equal to one-half the value of b at the boundary) of the magnetic inhomogeneity, and $x_{\text{eff}}(t)$ is the point at which the function $b(x,t)$ goes to zero (the wave front). Here the time dependence of the half-width of the magnetic wave is given by the relation

$$x_{\text{eff}} = \zeta_{\text{eff}} b_o^{1/2}(1+t)^{(1+m\sigma)/2}; \quad f(\zeta_{\text{eff}}) = 1/2. \tag{9}$$

The solution (see Fig. 1) determines the spatial profile of a magnetic wave moving in the superconducting sample with a velocity

$$v = \zeta_{\text{eff}} b_0^{1/2} \frac{(1+m\sigma)}{2}(1+t)^{(m\sigma-t)/2}. \tag{10}$$

In the particular case $m=1/\sigma$ the problem (6)–(8) has the generalized solution

$$b(x,t) = b_0(1+t)^{1/\sigma}[(1-\sigma^{1/2}\zeta)_+]^{1/\sigma},$$

$$\zeta = x b_0^{-1/2}(1+t)^{-1}. \tag{11}$$

Here we have introduced the notation $(k)_-=k$ if $k\geqslant 0$ and $(k)_+=0$ if $k<0$.

For such a special choice of conditions of pumping by the external field we obtain a constant velocity of the wave front,

$$v = \zeta_{\text{eff}} b_0^{1/2} = [1-(1/2)^\sigma]\sigma^{-1/2} b_0^{1/2}, \tag{12}$$

which for $\sigma=1$ gives $v=b_0^{1/2}/2$.

PEAKING REGIME. EFFECTIVE LOCALIZATION OF THE MAGNETIC FLUX

In the peaking regime (4) the self-similar solution of Eq. (5) has the form

$$b(x,t) = b_0(1-t/t_0)^m f(\zeta),$$

$$\zeta = x(b_0 t_0)^{-1/2}(1-t/t_0)^{-(1+m\sigma)/2} \geqslant 0, \tag{13}$$

where $f(\zeta)$ is determined from the equation

$$(f^\sigma f')' - [(1+m\sigma)/2]\zeta f' + mf = 0, \quad \zeta > 0 \tag{14}$$

with the boundary conditions (8).

For the self-similar solution (13) the half-width and the magnetic wave front have the time dependence

$$x_{\text{eff}} = \zeta_{\text{eff}}(b_0 t_0)^{1/2}(1-t/t_0)^{(1+m\sigma)/2}, \tag{15}$$

$$x_f = \zeta_f(b_0 t_0)^{1/2}(1-t/t_0)^{(1+m\sigma)/2}, \tag{16}$$

where ζ_f is the value of the self-similar coordinate at which $f(\zeta)=0$.

For a graphical illustration in Fig. 2 we present the results of a numerical solution[6] of problem (14) for $1+m\sigma>0$ and $1+m\sigma<0$.

For $1+m\sigma<0$ the solution is characterized by the following properties: the coordinate of the wave front is found at a finite point and together with x_{eff} increases without bound as the time of the peaking is approached.

For $1+m\sigma>0$ the wave front is bound at an infinitely remote point, and $x_{\text{eff}}(t)$ decreases at $t\to t_0$. The solutions of this type can be called (by analogy with thermal waves in the peaking regime) magnetic waves with contracting effective sizes. The magnetic field penetrating the medium in this case will be concentrated in a spatial region that decreases with

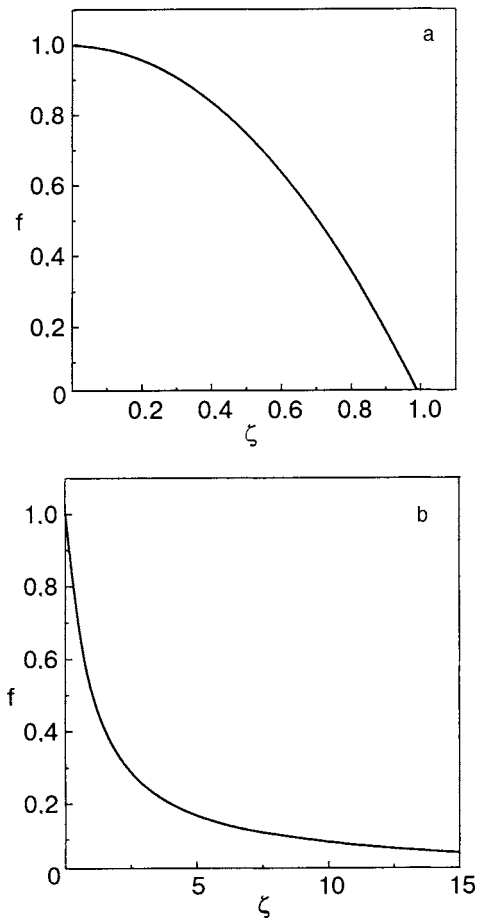

FIG. 2. Variation of the magnetic field as a function of the self-similar variable ζ for $1+m\sigma<0$ (a) and $1+m\sigma>0$ (b).

time. Of course, in the real situation the rise of $b(x,t)$ corresponding to this process will be bounded above by the value of the upper critical field.

We note that the boundary regime for the special choice $m=-1/\sigma$ corresponds to a self-similar solution of unusual form—a stationary magnetic wave:

$$b(x,t)=b_0(1-t/t_0)^{-1/\sigma}[(1-x/x_0)_+]^{2/\sigma}, \tag{17}$$

where $x_0=[2(\sigma+2)/\sigma]^{1/2}$. The position of the front of this wave, $x_f(t)=x_0$, does not change during the entire peaking time—magnetic disturbances do not propagate into the sample, despite the fact that in the region $(0,x_0)$ the magnetic field increases at $t\to t_0$.

TAKING THE CRITICAL CURRENT INTO ACCOUNT

For superconductors with high critical currents the solutions of Eq. (2) must be analyzed taking into account not only the value of j_c itself but also the relation of the critical current to the induction, which is reflected in the function $c(b)$ of the initial diffusion equation (2), describing the dependence of the field propagation velocity c on the value of the local quantity b. In seeking the solution of such a nonlinear diffusion equation for the magnetic flux one should transform to the "stretched" coordinates $\eta=x-x_s(t)$, where $x_s(t)$ is a certain function specified by the equation

$$dx_s/dt=-c[b(\eta(t),t)]. \tag{18}$$

In this case Eq. (2) reduces to Eq. (5):

$$b_t=[b^\sigma b_\eta]_\eta, \tag{19}$$

and for the boundary regime of greatest interest, with peaking, Eq. (19) has the same form (13) and (14) but with the self-similar variable

$$\zeta=\{x+\int_0^{t/t_0}c[b(\eta,t)]dt\}(b_0t_0)^{-1/2}(1-t/t_0)^{-(1+m\sigma)/2}\geqslant 0 \tag{20}$$

for the function $f(\zeta)$, which must satisfy the boundary conditions (8).

Taking relations (13) and (20) into account, one can easily note that for the initial function $b(x,t)$ the boundary condition (4) at $x=0$ is satisfied asymptotically at $t\to t_0$ and only when $1+m\sigma<0$. Therefore the solution of the corresponding boundary-value problem can be considered to be defined only in the limit $t\to t_0$ under the additional condition $1+m\sigma<0$ on the exponent σ of the dissipative medium and the exponent m of the rate of change of the external magnetic field. In this case the position of the front of the magnetic wave is specified by the integral of the function $c[b(\eta,t)]$,

$$x_f=-\int_0^{t/t_0}c[b(\eta,t)]dt+\eta_f(b_0t_0)^{1/2}(1-t/t_0)^{(1+m\sigma)/2}, \tag{21}$$

and, consequently, the magnetic wave front propagation velocity is equal to

$$v_f=-c[b(\eta,t)]-\frac{(1+m\sigma)}{2}\eta_f(b_0)^{1/2}(1-t/t_0)^{(m\sigma-1)/2},$$

$$1+m\sigma<0. \tag{22}$$

It follows from the definition of $c[b(\eta,t)]$ [see Eq. (2)] that this function is specified by the functions $\rho_f(b)$ and $j_c(b)$. In the Bean model for $\rho_f(b)\sim b$ it degenerates into a constant $c=\alpha=4\pi j_c/cB_{c2}$, and result (22) becomes obvious: the velocity of the wave front (contrary to the case considered above) decreases by an amount α.

The critical current density, as a rule, falls off monotonically with increasing b. At low fields ($b\ll 1$) a good approximation for $j_c(b)$ is the Kim–Andersen model $j_c(b)=j_c(0)(b+b_1)^{-1}$, where b_1 is an experimentally determined constant. In the limiting case of high magnetic fields one has $j_c(b)=j_c(0)(1-b)$. However, even for such a simple dependence of the current on b it is difficult to obtain information about the evolution of the spatial–temporal properties of the field penetrating into the sample. Nevertheless, for $b\gg b_1$ one can make certain interesting observations. For example, at $\sigma=2$ Eq. (2) is completely identical to the equation for $j_c=$const (the Bean model) and $\sigma=1$. Therefore, the conclusions reached above in the analysis of the solutions of the correspond equation for $j_c=$const are also valid for a more complex process of vortex penetration into the sample.

Thus the dissipative magnetic fluxes propagating in nonideal superconductors can have diverse spatial–temporal structure. The diversity is directly correlated with the ratio of

the exponent m of the rate of imposition of the magnetic field and the exponent σ of the increase of the resistivity of the sample with respect to magnetic field. Here one observes the natural relationship—the higher the intensity of the boundary regime, the higher the penetration velocity of the magnetic wave front. However, there is an exception—for $m=-1/\sigma$ in the peaking regime the wave can be localized and the position of its front will not vary with time.

In conclusion we note several important aspects of the studies reported above. By assuming that the temperature of the superconductor is the same as that of the coolant, we have neglected the nonisothermicity of the process. Of course, in the general case the density of vortices (or the field b) penetrating into the sample is determined not only by the value of the induced current but also by the local temperature. Therefore, Maxwell's equations should be supplemented by the equation of heat balance. The energy of dissipation due to the viscous due to the viscous flow of vortex lines acts as a heat source in the samples. Such an approach is usually used in studying the critical state of a superconductor with a random distribution of pinning centers. Here one investigates the flux jumps caused by the a propagating thermal wave large enough to overcome the pinning. In the present paper we consider either clean superconductors (for which the density of defects is insubstantial) or the above-critical state. A thermal wave exists in either case. Following behind the magnetic flux front, it does not affect the qualitative picture of its distribution but only shifts the position of the front on account of an increase in the size of the vortex. On the other hand, when the motion of the flux lines is delayed by the pinning centers, the temperature coefficient of diffusion can bring about a rapid equilibration of the local temperature gradient, and one can then neglect the nonisothermicity of the process. Such an effective cooling is a known[2] characteristic of of composite superconductor.

When one chooses the unknown profile $b(x,0)=b_0F(x)$ in the form of a self-similar function $F(x)$ at $t=0$, then the numerical solution obviously coincides with the self-similar solution for the diffusion equation (5). It is proved in the monograph[7] that for monotonically decreasing unknown functions the solution of the initial equation (5) converges to the self-similar solutions at $t\to t_0$. At intermediate t the number solutions can differ from the self-similar ones. In other words, arbitrary (numerical) solutions are drawn toward the self-similar solution at $t\to t_0$. It is said that the self-similar solutions form an attractor of the problem.

As to the asymptotic stability of the solutions, for regimes with resistivity $\rho_f(b)$ close to a power law, the asymptotic stability is proved in the aforementioned monograph,[7] and, in a particular case (for a power-law resistivity) in the book[6] (see also Ref. 8. For a stationary wave front the stability of the solutions was proved numerically by Barenblatt and Vishik[9] back in 1956. The theoretical proof of this result can also be found in Ref. 7, where the fundamental S theorem for the stability of self-similar solutions was proved for a wide class of equations of the diffusion type.

[a)]medvedev@kinetc.ac.donetsk.ua

[1]V. R. Romanovskiĭ, Zh. Tekh. Fiz. **70**(12), 47 (2000) [Tech. Phys. **45**, 1557 (2000)].
[2]A. V. Gurevich, R. G. Mints, and A. L. Rakhmanov, *The Physics of Composite Superconductors*, Begell House, New York (1997), Nauka, Moscow (1987).
[3]I. L. Maksimov, Yu. N. Mastakov, and N. A. Taĭlanov, Fiz. Tverd. Tela (Leningrad) **28**, 2323 (1986) [Sov. Phys. Solid State **28**, 1300 (1986)].
[4]N. A. Taĭlanov and U. T. Yakhshiev, Pis'ma Zh. Tekh. Fiz. **26**, 8 (2000) [Tech. Phys. Lett. **26**, 897 (2000)].
[5]N. A. Buznikov, A. A. Pukhov, and A. L. Rakhmanov, Cryogenics **34**, 761 (1994).
[6]A. A. Samarskiĭ, V. A. Galaktionov, S. P. Kurdyumov, and A. P. Mikhaĭlov, *Regimes with Peaking in Problems for Quasilinear Parabolic Equations* [in Russian], Nauka, Moscow (1987).
[7]V. A. Galaktionov and J. L. Vazquez, *A Stability Technique for Evolution Partial Differential Equations, A Dynamical Systems Approach*, Birkhauser, Boston–Basel–Berlin (2004).
[8]V. A. Galaktionov and A. A. Samarskiĭ, Mat. Sb. **120**, 3 (1983).
[9]G. I. Barenblatt and M. I. Vishik, Prikl. Mat. Mekh. **20**, 411 (1956).

Translated by Steve Torstveit

Underdoped cuprate antiferromagnet as a two-dimensional antiferromagnetic metal

G. G. Sergeeva[a)]

National Science Center "Kharkov Physicotechnical Institute" of the National Academy of Sciences of Ukraine, yl. Akademicheskaya 1, Kharkov 61108, Ukraine
(Submitted May 17, 2005)

An approach to describing the pseudogap state as a two-dimensional antiferromagnetic metal with non-Fermi charge carriers is developed for quasi-two-dimensional underdoped HTSC cuprates with one CuO_2 plane. The model of local closed Varma currents is extended to holes of the ion Cu^{3+} surrounded by four ionic complexes $Cu^{2+}_{\uparrow}O^{2-}_4$ (or $Cu^{2+}_{\downarrow}O^{2-}_4$). It is shown that taking account of the electron-vibrational interactions results in vibronic transitions from a nondegenerate state of the Cu^{3+} ion into doubly degenerate $Cu^{2+}_{\uparrow}$ (or $Cu^{2+}_{\downarrow}$) with splitting of the energy band for two types of quasilocal states of a "copper-oxygen" hole (vortex or antivortex), each of which moves in its own magnetic sublattice. The transfer of the vortex current from the "molecule" $Cu^{3+}O^{2-}_4$ to the complex $Cu^{2+}_{\downarrow}O^{2-}_4$ with the copper ion from the same magnetic sublattice creates the dynamical effect of a displacement of a Cu^{3+} ion to the site of a $Cu^{2+}_{\downarrow}$ ion and a transition of the "molecule" $Cu^{3+}O^{2-}_4$ into the complex $Cu^{2+}_{\downarrow}O^{2-}_4$. © *2005 American Institute of Physics*. [DOI: 10.1063/1.2144455]

For underdoped (UD) cuprate HTSCs it can now be regarded as an established fact that on the (T,p) phase diagram, where p is the doping concentration, the temperature $T^*(p)$ of the transition into the pseudogap (PG) state separates the regions where for $p>p_{cr}$ the normal state is the Fermi-liquid state and for $p<p_{cr}$ the normal state is a state with non-Fermi charge carriers. For almost all UD HTSCs, to adequate accuracy,

$$T^*(p) \approx 1250(1-p/p_{cr})\mathrm{K}, \quad p_{cr} \sim 0{,}22, \quad p \neq 0. \qquad (1)$$

As shown in Ref. 1 the PG and superconducting states coexist. In the present paper an approach to the PG state as a two-dimensional ($2D$) antiferromagnetic (AFM) state, perturbed by charge carrier motion, i.e. a $2D$ AFM metal with non-Fermi charge carriers, is developed for quasi-two-dimensional UD HTSCs with one CuO_2 plane.[2–4] Starting from the assumption that in the CuO_2 plane the hole concentration equals the concentration of Cu^{3+} ions randomly distributed in it, the model of local closed (LC) Varma currents[5,6] is extended to a hole of a Cu^{3+} ion surrounded by four ionic complexes—$Cu^{2+}_{\downarrow}O^{2-}_4$ "squares" (or $Cu^{2+}_{\uparrow}O^{2-}_4$, where the arrow denotes the spin direction of copper, see Fig. 1). The energy of the nondegenerate state of the Cu^{3+} ion is higher than the energy of the doubly degenerate state of the Cu^{2+} ion, and the normal electron-vibrational (EV) modes of oxygen ions in the complexes $Cu^{2+}_{\downarrow}O^{2-}_4$ or $Cu^{2+}_{\uparrow}O^{2-}_4$ result in vibronic transitions from a nondegenerate state of the Cu^{3+} ion into a doubly degenerate state (to $A\rightarrow E$ singlet-doublet transitions). Such vibronic transistions of the "molecules" $Cu^{3+}O^{2-}_4 \rightarrow Cu^{2+}_{\downarrow}O^{2-}_4$ or $Cu^{3+}O^{2-}_4 \rightarrow Cu^{2+}_{\uparrow}O^{2-}_4$ with excitation of a quasilocal hole state can be called the "inverse" Jahn–Teller (JT) effect, which results in a transition of an UD antiferromagnet (AF) into a $2D$ AFM metal state.

INVERSE JAHN–TELLER EFFECT

The selection rules for vibronic transitions in a molecule have been discussed in reviews.[7,8] In their classic work Longuet–Higgins *et al.* show convincingly that the allowed transitions $A\rightarrow E$ with splitting of the energy band, whose magnitude is all the greater the stronger the JT interaction, do indeed exist.[9] Experimental investigations of such transitions in the absorption spectra of Fe^{2+} ions in crystals with trigonal and cubic symmetry are discussed in Ref. 7.

Let a d hole of a Cu^{3+} impurity ion interact only with the EV JT modes Q_k of the nearest oxygen ions, which are shared with the neighboring complexes $Cu^{2+}_{\uparrow}O^{2-}_4$ (Fig. 1). For example, a hole of the Cu^{3+} ion, substituting for a $Cu^{2+}_{\downarrow}$ ion, transforms into a collectivized, by the "molecule" $Cu^{3+}O^{2-}_4$, state with four LC currents, i.e. into a state with "mixed" symmetry $d_{x^2-y^2}\pm i(p_x\pm p_y)$ ($d_{x^2-y^2}$ is a state of the "copper" hole; p_x and p_y are states of the "oxygen" hole).[6] Taking account of the compensation of the currents $Cu^{2+}_{\downarrow}-O^{2-}$ in neighboring quadrants of the molecule such LC currents form a circular current around the complex $Cu^{2+}_{\downarrow}O^{2-}_4$, which can be regarded as a quasilocal state of a "copper-oxygen" hole,[1)] i.e. a vortex-like state—$2D$ antivortex $v_{\uparrow}$ (or $2D$ vortex $v_{\downarrow}$ around the complex $Cu^{2+}_{\uparrow}O^{2-}_4$). Depending on the magnetic sublattice containing the Cu^{3+} ion the condition for conservation of the magnetic moment in the "molecule"

$$m_{Cu^{3+}} = m_{Cu^{2+}_{\downarrow}} + m_{v_{\uparrow}} = m_{Cu^{2+}_{\uparrow}} + m_{v_{\downarrow}} = 0$$

determines the direction of the LC currents:[2)] $v_{\downarrow}$—clockwise, $v_{\uparrow}$—counterclockwise, for example ($m_{v_{\uparrow}}=-m_{Cu^{2+}_{\downarrow}}$ and $m_{v_{\downarrow}}=m_{Cu^{2+}_{\uparrow}}$ are the magnetic moments of the circular current around the complex $Cu^{2+}_{\downarrow}O^{2-}_4$ or $Cu^{2+}_{\uparrow}O^{2-}_4$, which determine the direction of the circular currents). The vortices $v_{\downarrow}$ and $v_{\uparrow}$ with weak damping can move into the CuO_2 plane along the magnetic sublattice of the $Cu^{2+}_{\uparrow}$ (or $Cu^{2+}_{\downarrow}$) ion whose site was occupied by the Cu^{3+} ion; this creates the dynamical effect of the movement of a Cu^{3+} ion to the site of a $Cu^{2+}_{\downarrow}$ ion and a transition of the "molecule" $Cu^{3+}O^{2-}_4$ into the complex $Cu^{2+}_{\downarrow}O^{2-}_4$. Thus, the vibronic transitions $A\rightarrow E$ with splitting of the energy band result in an inverse JT effect with a transition of the UD AF into a state which can be called a $2D$

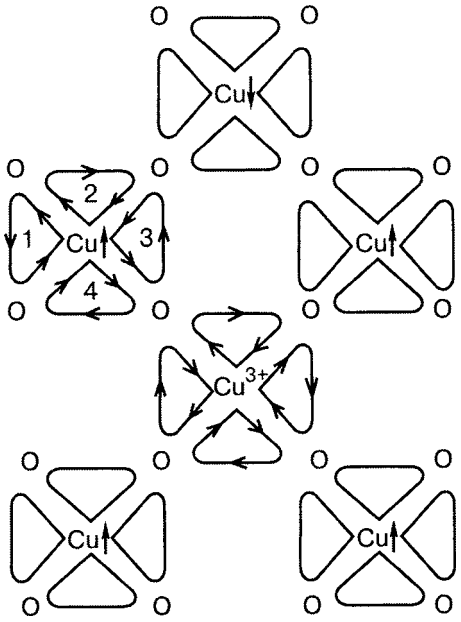

FIG. 1. Local currents v_i (closed lines) in the quadrants of ionic complexes CuO_4 in the copper-oxygen plane: Varma currents in four complexes $Cu^{2+}_{\uparrow}O^{2-}_4$ and the complex $Cu^{2+}_{\downarrow}O^{2-}_4$ with magnetic moments m_{v_i} of the currents v_i in four quadrants $\Sigma^4_{i=1}m_{v_i}=0$ (1), (3); vortex current $v_\uparrow$ in the "molecule" $Cu^{3+}O^{2-}_4 \rightarrow Cu^{2+}_{\downarrow}O^{2-}_4+v_\uparrow$ with magnetic moment $m_{v_\uparrow}=\Sigma^4_{i=1}m_{v_i}=-m_{Cu^{2+}_{\downarrow}}$ (2), (4). The arrows on the closed lines, indicating the direction of the currents, are drawn only in the two complexes; the Cu^{3+} ion occupies a position in the magnetic sublattice of $Cu^{2+}_{\downarrow}$. The transition of the vortex current $v_\uparrow$ from the "molecule" $Cu^{3+}O^{2-}_4$ to the complex $Cu^{2+}_{\downarrow}O^{2-}_4$ with a copper ion from the same magnetic sublattice creates the dynamical effect of a Cu^{3+} ion moving into the site of a $Cu^{2+}_{\downarrow}$ ion and a transition of the "molecule" $Cu^{3+}O^{2-}_4$ into the complex $Cu^{2+}_{\downarrow}O^{2-}_4$.

AFM metal with two types of quasilocal charge carriers (two-dimensional vortices $v_\downarrow$ and antivortices $v_\uparrow$) with non-Fermi statistics.

The following two conditions must be satisfied in order for such a state to exist.

1. The sample must be quasi-two-dimensional.

2. A transition $A \rightarrow E$ of a copper ion from a nondegenerate into a degenerate state $Cu^{3+}O^{2-}_4 \rightarrow Cu^{2+}_{\downarrow}O^{2-}_4+v_\uparrow$ (if Cu^{3+} occupied the site of the $Cu^{2+}_{\downarrow}$ ion) and $Cu^{3+}O^{2-}_4 \rightarrow Cu^{2+}_{\uparrow}O^{2-}_4+v_\downarrow$ (if Cu^{3+} occupied the $Cu^{2+}_{\uparrow}$ site), which results in consistent ordering of the magnetic moments of the copper holes and ions in the CuO_2 plane at $T \leqslant T_f(p)$. Consequently, the region of existence of a 2*D* AFM metal in the phase diagram is bounded by the lines $T^*(p)$, $T_f(p)$, and $T_g(p)$, where $T_g(p)$ is the temperature of the transition of a 2*D* AFM metal into a 3*D* cluster glass state.[3)]

POSSIBILITY OF EXPERIMENTAL CONFIRMATION OF THE EXISTENCE OF A 2*D* AFM METAL

The model of the PG state as a 2*D* AFM metal with splitting into two energy bands of charge carriers—2*D* vortices and antivortices—which satisfy non-Fermi statistics, just as the structure of the LC Varma currents,[5,6] results in breaking of time-reversal symmetry for which spontaneous ordering occurs without breaking of translational symmetry. The experiment proposed in Refs. 5 and 6 for observing LC currents consisted in measuring the intensity of the photoemission spectrum (ARPES) with right- and left-circular polarization of light and analyzing the relative difference between the circular dichroism spectra obtained. Two groups performed these measurements: on thin UD Bi2212 films[10] and on UD Y–Pb–Bi2212 single-crystals (T_c=80K) and overdoped Pb–Bi2212 (T_c=72K).[11] The results show that dichroism was observed in the UD[10] and overdoped[11] samples, which can be explained by the bilayer splitting of the unit cell of these compounds into two CuO_2 planes.

To confirm the hypothesis advanced in Refs. 5 and 6 that LC currents exist in UD HTSCs it is necessary to perform measurements on samples with one CuO_2 plane in a unit cell. An ideal object for such investigations could be $Bi_2Sr_{2-x}La_xCuO_{6+\delta}$ single crystals, for which nuclear magnetic resonance measurements[1] have made it possible to establish the region of the PG state and have shown that the Fermi-liquid state is characteristic only of overdoped samples. The study of photoemission spectra could also answer the question, which is important for UD HTSCs, of the role of the interactions along the *c* axis. This requires measurements similar to those performed on Bi2212 (see Fig. 4 in Ref. 12) for energies equal to $\varepsilon_F \pm 30$ meV and two values of the temperature $T^*(p) \pm \Delta$ close to $T^*(p)$. An appreciable difference in the broadening of the spectral lines for $T^*(p)-\Delta$ and $T^*(p)+\Delta$ would make it possible to judge the dimension of the PG state. For the same samples with doping concentration $p_2 < p < p_{cr}$, it would be interesting to perform measurements of the resistance in magnetic fields $H > H_{c2}$ (p_2 is determined by the equality $T_f(p_2)=T^*(p_2)$). This would make it possible to observe with decreasing temperature in the normal state of the sample two transitions with a change in the dimension of the state: 1) a transition from a 3*D* Fermi metal to a 2*D* AFM metal at $T^*(p)$; 2) at lower temperatures $T_g(p)$—a transition of a 2*D* AFM metal into a 3*D* cluster glass state. The observation of a narrow EPR line at $T < 150$ K is convincing evidence of the existence of metallic regions in weakly doped $La_{2-x}Sr_xCuO_4$, $0.01 \leqslant x \leqslant 0.06$.[13]

In closing, we present the words of D. Pines concerning the mechanism of high-temperature superconductivity: "It is electronic and magnetic origin."[4] These words could be the answer to the question of the nature of the pseudogap state: this is a two-dimensional AFM metal with two types of quasilocal states of a copper-oxygen hole—vortices and antivortices, each of which moves in its own magnetic sublattice.

a)E-mail: gsergeeva@kipt.kharkov.ua

1)The "mixed" symmetry of the hole state shows that the transition of a hole into a quasilocal state cannot be regarded as ionization of a Cu^{3+} ion.

2)It should be noted that the sum of the magnetic moments m_{v_i} of LC Varma currents v_i in the quadrants of the complexes $Cu^{2+}O^{2-}_4$ is zero.

3)The assumption that the line $T^*(p)$ bounds the region of existence of a 2*D* AFM metal results in the obvious equality $T^*(p_{cr})=T_g(p_{cr})$.

[1]G.-Q. Zheng, P. L. Kuhns, A. P. Reyes, B. Liang, and C. T. Lin, Phys. Rev. Lett. **94**, 047006 (2005).

[2]V. G. Bar'yakhtar and V. M. Loktev, Ukr. Fiz. Zh. (Russ. Ed.) **36**, 850 (1991).

[3]V. M. Loktev, Fiz. Nizk. Temp. **31**, 645 (2005) [Low Temp. Phys. **31**, 490 (2005)].

[4]D. Pines, *Pseudogap Behavior in Underdoped Cuprates*, cond-mat/0404151.

[5]Tai-Kai Ng and C. M. Varma, Phys. Rev. B **70**, 054514 (2004).

[6]M. E. Simon and C. M. Varma, Phys. Rev. Lett. **89**, 247003 (2002).
[7]M. D. Sturge, Solid State Phys. **20**, 91 (1967).
[8]H. Sponer and E. Teller, Rev. Mod. Phys. **13**, 75 (1941).
[9]H. C. Longuet-Higgins, U. Opik, M. H. Pryce, and H. Sack, Proc. R. Soc. London, Ser. A **244**, 1 (1958).
[10]A. Kaminski, S. Rozenkranz, H. M. Fretwell, J. C. Campuzano, Z. Li, H. Raffy, W. G. Gullen, H. You, C. G. Olson, C. M. Varma, and H. Hochst, Nature (London) **416**, 610 (2002); cond-mat/0204106.
[11]S. V. Borisenko, A. Kordyuk, S. Legner, M. S. Golden, M. Sing, R. Claessen, A. Yaresko, H. Berger, C. Graziolo, and S. Turchini, cond-mat/0313036.
[12]A. Banzil, M. Lindroos, S. Sahrakorpi, and R. S. Markievicz, Phys. Rev. B **71**, 012503 (2005).
[13]A. Shengelaya, M. Bruun, B. I. Kochelaev, A. Safina, K. Konder, and K. A. Muller, Phys. Rev. Lett. **93**, 017001 (2004).

Translated by M. E. Alferieff

Pinning in nomagnetic borocarbides

A. N. Zholobenko, G. P. Mikitik, and V. D. Fil'[a)]

B. I. Verkin Institute for Low Temperature Physics and Engineering of the National Academy of Sciences of Ukraine, pr. Lenina 47, Kharkov 61103, Ukraine

D. V. Fil'

Institute of Single Crystals of the National Academy of Sciences of Ukraine, pr. Lenina 60, Kharkov 61001, Ukraine

J. D. Kim and E. M. Choi

Pohang University of Science and Technology, Pohang 794-784, Republic of Korea

S. I. Lee

Korea Basic Science Institute, Daejeon 305-333, Republic of Korea
(Submitted June 8, 2005; resubmitted July 1, 2005)

The field dependences of the Labush parameter in nonmagnetic borocarbides are measured by a method that does not require achieving a critical state. The expected values of the critical current are estimated. The values obtained are two orders of magnitude greater than the results of "direct" measurements performed on the basis of transport (magnetic) experiments. A giant peak effect, which the collective pinning model describes quantitatively well, is observed in the field dependences of the Labush parameter in Y-containing borocarbides. © *2005 American Institute of Physics*. [DOI: 10.1063/1.2144457]

The dynamics of vortex matter in type-II superconductors is determined by the ratios of the elasticity of the fluxoid lattice, the viscosity, and the pinning. The study of such dynamics still attracts a great deal of attention even though it has been pursued for the past 40 years. This refers to, first and foremost, the characteristics of pinning because of the practical importance of understanding its physical nature in detail.

At the present time the intensity of pinning is ordinarily characterized, primarily, by the current density j_c, corresponding to the achievement of a critical state, i.e. a transition from a regime of dissipation-free current flow to a regime of free motion of vortices. Pinning can also be characterized by the "spring" Labush parameter $\alpha_L = d^2W_p/dx^2$, which determines the average curvature of the pinning potential W_p. A transition into the critical state corresponds to the Lorentz force being equal to the effective pinning force:

$$\alpha_L \xi \approx \frac{1}{c} j_c B, \tag{1}$$

where ξ is the coherence length and B is the induction in the sample.

Using the relation (1) it is easy to estimate the value of j_c to be expected for known a_L and compare it with "direct" measurements.

In the present communication the results of measurements of α_L in nonmagnetic borocarbides (YNi_2B_2C, $Y_{0.95}Tb_{0.05}Ni_2B_2C$, and $LuNi_2B_2C$), obtained by a method that does not require reaching a critical state, are presented. It was found that our estimates of j_c are two orders of magnitude higher than the critical currents obtained in transport or magnetic measurements. In addition, a giant peak effect was found in the field dependences of α_L for Y-containing samples. It can be described quantitatively well on the basis of a collective pinning model.[1] In leutecium borocarbide, pinning on defects, whose range is greater than the core size, is also found to be substantial.

The method is based on analysis of the amplitude and phase of the electromagnetic field emitted from a conducting medium under the action of a transverse sound wave propagating along the magnetic field H. For a uniform half-space and an elastic free interface the induction (Hall) component of the field is described by the simple expression:[2,3 1)]

$$E_{\text{ind}} = \frac{[\dot{u}B]}{c} \cdot \frac{k^2}{q^2 + k^2} \equiv \frac{[\dot{u}B]}{c} \cdot X(B), \tag{2}$$

where u is the amplitude of the displacements in the elastic wave at the interface, q is the wave number of the sound, and k is the skin wave number of the experimental medium. In the normal state $k^2 = k_n^2 = (4\pi i\omega\sigma_0)/c^2$ and $\sigma_0 = (ne^2\tau)/m$ is the static conductivity.

In the mixed phase $k^2 = k_m^2 = 4\pi(i\omega\eta + \alpha_L)/B^2$, where η and α_L are, respectively, the viscosity and Labush parameter per unit volume.

Since η is approximately proportional to B ($i\omega\eta \approx k_n^2 B H_{C2}/4\pi$, the Bardeen-Stephen relation[4]), in sufficiently weak field $|k_m^2| \gg q^2$ and $X(B)$ is close in amplitude to 1 and its phase is close to zero.

For $\kappa \gg 1$ (κ is the Ginzburg-Landau parameter), in the actual region of the fields we need not distinguish between the induction in the sample and the applied field. Normalizing the measured value of E/H so that for $H \sim (5-10)H_{C1}$ its modulus is close to 1, and taking the phase Φ in these fields as the point of reference, we obtain the field dependence of the complex quantity $X(H)$.

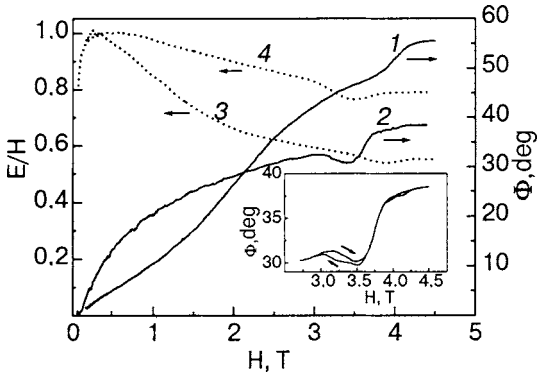

FIG. 1. Typical field dependence of the amplitude and phase of $X(H)$. The scale on the left-hand side is normalized as explained in the text: Φ (1), (2); E/H (3), (4); $LuNi_2B_2C$ (T=6 K) (1), (3); $Y_{0.95}Tb_{0.05}Ni_2B_2C$ (T=1.7K) (2), (4). Inset—hysteresis of the phase near the peak effect in $Y_{0.95}Tb_{0.05}Ni_2B_2C$ (T=1.7 K).

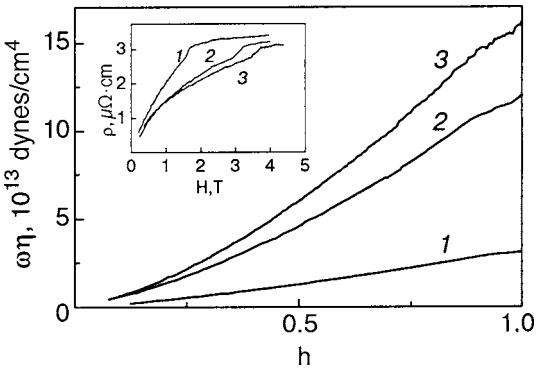

FIG. 2. Field dependences of $\omega\eta$ in $Y_{0.95}Tb_{0.05}Ni_2B_2C$: T=8 K, H_{C2} =1.7 T (1); T=4K, H_{C2}=3.3 T (2); T=1.7K, H_{C2}=3.8 T (3). Inset—expected variation of the resistivity. The labeling is the same as in the main figure.

The values of the viscosity and the Labush parameter are determined by the relations

$$\alpha_L = \mathrm{Re}\left(\frac{X(H)}{1-X(H)}\right)\cdot\frac{q^2H^2}{4\pi}, \tag{3}$$

$$\omega\eta = \mathrm{Im}\left(\frac{X(H)}{1-X(H)}\right)\cdot\frac{q^2H^2}{4\pi}. \tag{4}$$

It should be remembered that the information obtained in this experiment refers to a thin ($\sim q^{-1}$) layer near the surface. If this layer is nonuniform, the simple relations (2)–(4) break down. This question is studied in detailed in Ref. 5. It is shown that the nonuniformity of σ_0 (the decrease of the conductivity of a layer near the surface) increases the phase angle, fixed in the normal state. However, the nonuniformity of pinning results in an apparent nonmonotonic variation of the parameter η, if the relation (4) is used to reconstruct η, right up to the appearance of nonphysical negative values of the viscosity.

We shall indicate a simple test for revealing at least the nonuniformity of σ_0: in the normal state the modulus and phase of $X(H)$ in a uniform material should be related as

$$|X(H)| = (1+\tan^2\Phi(H))^{-0,5}.$$

In the experiments described below this condition always holds to within ~5%.

The samples were grown by the standard technology used for compounds of this class.[6] They were in the form of thin ~0.5 mm thick flakes with transverse size ~3 mm. The C_4 axis was always orthogonal to the plane of the platelet. A quite perfect face of natural growth was used as the emitting surface. The opposite face was polished to create a reliable acoustic contact with a germanium delay line, making it possible to separate the exciting and analyzed signals in time. The excitation frequencies were 54–55 MHz. The details of the measurement procedure are described in Ref. 5.

Examples of typical experimental dependences of the modulus and phase of $X(H)$ are presented in Fig. 1. All experimental samples, irrespective of composition, had close values of k_n^2 and, correspondingly, the residual resistivity $\rho_{\mathrm{res}}\sim 3\ \mu\Omega\cdot$cm and London penetration depth $\lambda(0)$ $\sim 10^{-5}$ cm. The values of the velocities, required for these estimates, of the C_{44} modes are presented in Ref. 7.

The field dependences of the viscosity, which also turned out to be similar for identical values of H_{C2}, were found, using Eq. (4), from data similar to those presented in Fig. 4. An example is presented in Fig. 2. Their behavior is close to that predicted by the Bardeen-Stephen phenomenological model,[4] although the deviations from a linear dependence are quite large. The inset in Fig. 2 shows the behavior of the resistivity expected in the resistive regime from the measured values of the viscosity. The field dependences $\eta(H)$ do not show sufficiently strong nonmonotonic behavior, which in accordance with the results of Ref. 5 indicates that there is no significant nonuniformity in the characteristics of pinning. We also call attention to the fact that the presence of substantial nonmonotonic behavior near H_{C2} in the primary data (Fig. 1, curve 2) has essentially no effect on $\eta(H)$.

Examples of the field dependences of the Labush parameter are presented in Fig. 3. One notices first and foremost the giant peak effect in the Y-containing samples near H_{C2}. Traces of its existence are also seen in $LuNi_2B_2C$. We also note that the solution (3) gives negative values of α_L for $Y_{0.95}Tb_{0.05}Ni_2B_2C$ in intermediate-value fields. We shall assume that for very weak pinning the accuracy of the procedure used to reconstruct the Labush parameter using Eq. (2) is inadequate because factors such as the nonuniformity of the near-surface layer or thermal fluctuations are neglected, and the result $\alpha_L<0$ is a kind of artifact.

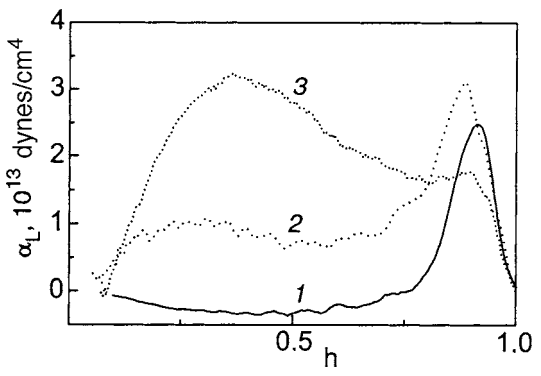

FIG. 3. Field dependences of α_L: $Y_{0.95}Tb_{0.05}Ni_2B_2C$ (T=1.7K, H_{C2}=3.8 T) (1); YNi_2B_2C (T=4K, H_{C2}=3.8 T) (2); $LuNi_2B_2C$ (T=6 K, H_{C2}=4.2 T) (3).

Pippard has proposed a qualitative explanation for the nature of the peak effect.[8] The structure of the mixed phase is determined by the competition between the pinning and the intervortex interaction force. When the latter predominates the fluxoids form a nearly translationally ordered lattice and the details of the relief of the pinning potential are largely ignored. As H_{C2} is approached the elasticity of the vortex lattice decreases more rapidly than the pinning intensity, which results in more efficient adjustment of the structure to the relief of the pinning potential and, correspondingly, to an increase of α_L and j_c.

The theory of collective pinning (CP) of vortex structures by point defects (i.e. defects whose range is shorter than the coherence length) made it possible to convert these qualitative considerations into a quantitative foundation.[1] In the CP theory a single free parameter characterizing the pinning force is introduced. It is convenient to take as this free parameter the dimensionless magnetic field $h_{SV} \equiv H_{SV}/H_{C2}$, determining the boundary of the so-called *bundle vortex pinning* (BVP) regime $h_{SV} < h < 1 - h_{SV}$, where $h = H/H_{C2}$ and the transverse size R_c of Larkin's correlation region is greater than the vortex lattice parameter $a = \sqrt{\Phi_0/H}$ (Φ_0 is the flux quantum). In the BVP regime α_L is determined from the condition that the pinning energy ($\sim \alpha_L \xi^2 V_c$) is equal to the elastic energy ($\sim C_{66}(\xi/R_c)^2 V_C$) of the vortex lattice in the correlation volume V_C. This gives

$$\alpha L \approx \frac{C_{66}}{R_c(H)^2}. \tag{5}$$

The shear modulus is defined by the relation[9]

$$C_{66} \cong \frac{\Phi_0 H_{C2}}{(8\pi\lambda)^2} h(1-h)^2. \tag{6}$$

The equation for finding R_c (with $a \ll \lambda$) has the form

$$\left[\frac{h(1-h)}{h_{SV}(1-h_{SV})}\right]^{3/2} \approx 1 + 2\ln\frac{R_c}{a} + \frac{R_c}{\lambda}(1-h)^{1/2}. \tag{7}$$

Actually, Eq. (7) is Eq. (4.17) from Ref. 10, where the possibility that H approaches H_{C2} is taken into account (see Eq. (8) in Ref. 11 and the accompanying explanation). The Labush parameter in the *single vortex pinning* (SVP) regime, in the lower region with respect to the magnetic field ($h < h_{SV}$), is linear in the magnetic field with the coefficient of proportionality determined from the condition of matching with Eq. (5). In the upper SVP region ($1 - h_{SV} < h < 1$) the estimate $\alpha_L \approx C_{66}(h)/\beta a^2(h)$ can be used, where β is a correction factor close to 1, which also provides matching with Eq. (5) for $h = 1 - h_{SV}$.

The computed values of $\alpha_L(h)$, constructed for $H_{C2} = 4$ T and $\lambda = 10^{-5}$ cm, characteristic for the experimental samples, for various values of the parameter h_{SV} are presented in Fig. 4. A remarkable property of these dependences is the single-valued relation between the form of the field dependence and the scale of the variations of $\alpha_L(h)$. In other words if $\alpha_L(h)$ is bell-shaped without a distinct peak effect, then the maximum value of $\alpha_L(h)$ must be at the level 10^{15} dynes/cm^4. Conversely, if the peak effect is pronounced, the observed values of $\alpha_L(h)$ should not exceed $10^{13}-10^{14}$ dynes/cm^4. Turning to Fig. 3 we immediately

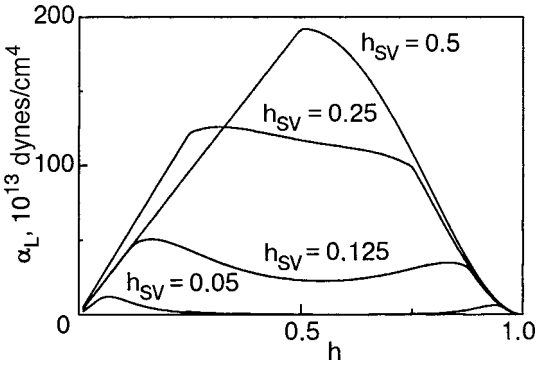

FIG. 4. Computed dependence $\alpha_L(h)$ ($H_{C2}=4$ T, $\lambda = 10^{-5}$ cm) for various values of the parameter h_{SV}.

conclude that the behavior of $\alpha_L(h)$ in Y-containing samples can be analyzed from the standpoint of the CP theory, which cannot be said of leutecium borocarbide.

The CP theory predicts a nearly symmetric function $\alpha_L(h)$ with respect to $h = 0.5$, i.e. if a peak effect is observed near H_{C2}, then a rise of $\alpha_L(h)$ of the same type should also occur in weak fields. In our experiments we never observed such a dependence. However, we note that a low-field peak effect should occur in the field range where it is no longer possible to neglect the difference between B and H and Eqs. (3) and (4) become invalid. In addition, in these fields $X(H)$ is close to 1, and the relation (3), as already mentioned earlier, is very sensitive to the possible corrections which were neglected, including also to thermal fluctuations, which decrease the effective magnitude of pinning.[5]

Figure 5 demonstrates the "quality" of the description of the amplitude of the peak effect near H_{C2} by the CP theory at various temperatures. This description is fully acceptable. The figure was constructed using the only adjustable parameter $h_{SV}(0) = 0.033$ and the temperature dependences $\lambda(t) = \lambda(0)(1-t^2)^{-1/2}$ and $h_{SV}(t) = h_{SV}(0)(1-t^2)^{1/2}$. The latter dependence corresponds to δl pinning.[11]

The point of view that a transition into the peak-effect regime corresponds to a first-order phase transformation from a vortex lattice state into a disordered amorphous state is currently very popular (see Ref. 11 in the references cited there). It is shown in Ref. 11 that the position of this transition is correlated with the boundary of the upper region of

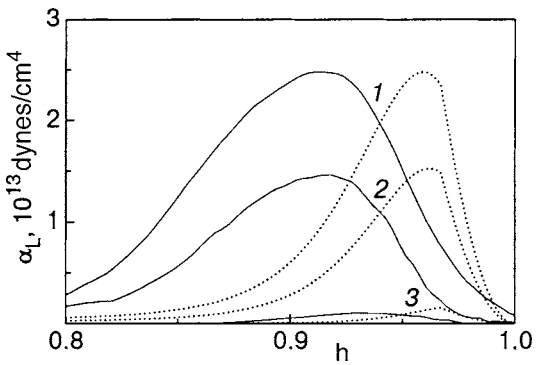

FIG. 5. Comparing the values of α_L measured in $Y_{0.95}Tb_{0.05}Ni_2B_2C$ (solid lines) and the computed values ($h_{SV}=0.033$, points) under different conditions: $T=1.7$ K, $H_{C2}=3.8$ T (1); $T=4$ K, $H_{C2}=3.3$ T (2); $T=8$ K, $H_{C2}=1.7$ T (3).

the SVP regime. In other words, this point of view relates the peak effect not simply to a smooth transition from the BVP into the SVP regime but to a true phase transition. The inset in Fig. 1 demonstrates the hysteresis observed in our experiment. This hysteresis is characteristic for extended phase transformations, such as of the martensite type, and confirms this point of view.

As already mentioned above, the scale and form of $\alpha_L(h)$ in $LuNi_2B_2C$ do not permit describing the field dependence of the Labush parameter on the basis of only the CP model. Since an indistinct peak for the same values of h as in the Y-containing borocarbides is present on the right-hand wing of $\alpha_L(h)$, it is evident that weak pinning centers described by the CP model are also present in leutecium borocarbide. The main maximum at $h \sim 0.4$ is probably due to sparse but stronger pinning centers, whose range r is greater than the coherence length.[1] The maximum value of $\alpha_L(h)$ is then described by the relation

$$\alpha_{L\,\max} \approx \frac{nr^2}{\xi}\frac{H_{C2}^2}{\pi^3\kappa^2},$$

where n is the density of "strong" pinning centers. For $\kappa \sim 10$ and $r \sim 10^{-6}$ the approximate density $n \sim 10^{14}$ is indeed low.

It is of interest to compare our estimates of the critical currents with the values obtained in the transport (magnetic) measurements. We shall use Eq. (1) to calculate the critical current expected from the measured values of α_L. For all experimental samples (with $H \sim 4$ T) we obtain $j_c \sim 10^4$ A/cm^2. In Ref. 12 the transport measurements in a $LuNi_2B_2C$ crystal with $H \| c$ near H_{C2} and $T = 2.2$ K gave $j_c \sim 10^2$ A/cm^2. The same value is obtained in measurements of the irreversible magnetization in a YNi_2B_2C single crystal at $T = 5$ K.[13] It is important to note that the single crystals studied in the works cited were grown, just as in the present investigation, using completely identical technologies. These samples should also have close pinning characteristics, and the two orders of magnitude difference in the measured values of the critical currents from our estimates is hardly due to the individual characteristics of concrete samples.

On the one hand, we note that in the works cited above it is most likely the current j_t established in the sample over the measurement time in the thermally activated vortex flow regime is measured rather than j_c. The quantity j_t can be estimated from the expression[10]

$$j_t \approx j_c\left[1 + \frac{\mu T}{U_c}\ln\left(1 + \frac{t}{t_0}\right)\right]^{-1/\mu}, \qquad (8)$$

where t ($\sim 10^2$–10^3 s) is the characteristic measurement time in the experiments of Refs. 12 and 13, t_0 ($\sim 10^{-5}$ s) is a constant which depends on the conductivity and the size of sample,[10] and U_c is an energy barrier which prevents free motion of a fluxoid. For the parameter μ at the boundary of the BVP and SVP regimes the estimate given by the CP theory is quite indefinite ($\mu \sim 1/7$–$5/2$). The pinning energy in the correlation volume V_c ($U_c \approx \alpha_L \xi^2 V_c$) should be used as U_c. Near the peak effect $V_c \sim a^3$, $U_c \sim 1$ K, and $j_t/j_c \sim 10^{-2}$ is comparable to (8) for $\mu \sim 0.7$–1. Unfortunately, the lack of the required data in Refs. 12 and 13 (the current-voltage characteristics and the time evolution of the irreversible magnetization) precludes a quantitative check of the explanation presented.

The difference of the values of j_t measured in Refs. 12 and 13 from our estimates of j_c could have another reason, at least partially. The relation (1) in some sense should be understood as a condition for attaining the theoretical limit of elasticity in a vortex lattice. However, it is well known that in ordinary crystal lattices, as a rule, because of the presence of defects (dislocations), irreversible plastic deformations appear long before the moment of brittle fracture. A similar scenario can also be expected in vortex lattices with defects. We shall underscore the fact that it is precisely in borocarbides that vortex structures are characterized by a high density of defects,[12] which is due to the phase transformations, occurring in them, from a low-field hexagonal fluxoid lattice into a square high-field lattice. In such a case the estimates of the critical field on the basis of the CP theory must be modified, since they neglect the possibility of the existence of dislocations in the vortex lattice. Specifically, the relation (1), which presumes that the parameter α_L remains unchanged with small and large ($\sim \xi$) deformations, becomes invalid. In other words, fluxoid motion in defective vortex lattices with small supercriticality also start as plastic flow.

In closing, we shall formulate the basic results of this work. The field dependences of the Labush parameter were measured in single crystals of nonmagnetic borocarbides by a method that does not require reaching a regime of free flow of vortices. An estimate of the critical current based on these dependences gives values which are two orders of magnitude higher than the values obtained in transport (magnetic) measurements. This is the main result of the present work. In Y-containing samples, a giant peak effect was found in the field dependences of α_L near H_{C2}. Its magnitude (and temperature variations) are described well on the basis of the collective pinning model. In leutecium borocarbide, pinning on defects with range longer than the coherence length makes the main contribution to α_L.

This work was performed under partial support by the CRDF Foundation (grant No. UP1-2566-KH-03) and INTAS (grant No. 03-51-3036).

[a]E-mail: fil@ilt.kharkov.ua

[1)]Strictly speaking, a receiving antenna reacts to the high-frequency magnetic component $\tilde{H}$. Near an interface the emitted field is a plane wave, so that $\tilde{H} = \tilde{E}$. The component $\tilde{E}$, because of continuity, equals to within $\delta/\lambda_{EM} \sim 10^{-5}$ (δ is the skin depth and λ_{EM} is the wavelength of the electromagnetic wave in vacuum) the field E_{ind} generated by the elastic wave in the conductor.[2]

[1]A. I. Larkin and Yu. N. Ovchinnikov, J. Low Temp. Phys. **34**, 409 (1979).
[2]V. D. Fil', Fiz. Nizk. Temp. **27**, 1347 (2001) [Low Temp. Phys. **27**, 993 (2001)].
[3]T. V. Ignatova, G. A. Zvyagina, I. G. Kolobov, E. A. Masalitin, V. D. Fil', Yu. B. Paderno, A. N. Bykov, V. N. Paderno, and V. I. Lyashenko, Fiz. Nizk. Temp. **28**, 270 (2002) [Low Temp. Phys. **28**, 190 (2002)].
[4]J. Bardeen and M. J. Stephen, Phys. Rev. A **140**, 1197 (1965).
[5]V. D. Fil, D. V. Fil, Yu. A. Avramenko, A. L. Gaiduk, and W. L. Johnson, Phys. Rev. B **71**, 092504 (2005).
[6]M. O. Mun, S. I. Lee, W. C. Lee, P. C. Canfield, B. K. Cho, and D. C. Johnson, Phys. Rev. Lett. **76**, 2790 (1996).
[7]E. A. Masalitin, V. D. Fil', K. R. Zhekov, A. N. Zholobenko, T. V. Ignatova, and S. I. Lee, Fiz. Nizk. Temp. **29**, 93 (2003) [Low Temp. Phys. **29**,

72 (2003)].
[8]A. B. Pippard, Philos. Mag. **19**, 217 (1969).
[9]E. H. Brandt, J. Low Temp. Phys. **26**, 709 (1977).
[10]G. Blatter, M. V. Feigel'man, V. B. Geshkenbein, A. I. Larkin, and V. M. Vinokur, Rev. Mod. Phys. **66**, 1125 (1994).
[11]G. P. Mikitik and E. H. Brandt, Phys. Rev. B **64**, 184514 (2001).
[12]V. M. R. Eskildsen, P. L. Gammel, B. P. Barber, A. P. Ramirez, D. J. Bishop, N. H. Andersen, K. Mortensen, C. A. Bolle, C. M. Lieber, and P. S. Canfield, Phys. Rev. Lett. **79**, 487 (1997).
[13]V. Silhanek, J. R. Thompson, L. Civale, D. McK. Paul, and C. V. Tomy, Phys. Rev. B **64**, 012512 (2001).

Translated by M. E. Alferieff

ELECTRONIC PROPERTIES OF METALS AND ALLOYS

Influence of the character of electron reflection from a surface on the electric properties of a cylindrical particle

É. V. Zavitaev[a)] and A. A. Yushkanov

Moscow State Forestry University, Mytishchi-5, Moscow oblast 141004, Russia
(Submitted April 5, 2004; resubmitted June 20, 2005)

The cross section for the absorption of electromagnetic radiation in a cylindrical metallic particle is calculated. Specular-diffuse reflection of electrons from the inner surface of the particle is taken as the boundary condition for the problem. Limiting cases are studied, and the results obtained are discussed. © *2005 American Institute of Physics*. [DOI: 10.1063/1.2144458]

I. INTRODUCTION

The electromagnetic properties of small metallic particles have a host of special features.[1] These features are due to the fact that the electron mean free path length in such particles is of the same order of magnitude as the linear dimensions of the particles (this effect is most pronounced at low temperatures, when the electron mean free path length is long). Nonlocal effects start to play a substantial role here. The classical theory of the interaction of electromagnetic radiation with metallic particles (Mie's theory),[2] based on the local equations of macroscopic electrodynamics, is inapplicable in this case.

The question of the magnetic dipole absorption of infrared radiation by cylindrical particles is examined in Refs. 3 and 4. The standard kinetic theory of a degenerate Fermi gas of conduction electrons in metals was used to describe the electromagnetic response of a particle.[5] In Ref. 3 the analysis was limited to the case of purely diffuse reflection of conduction electrons from the inner surface of a particle, and in Ref. 4 a detailed analysis of the magnetic dipole absorption by a cylindrical particle was performed under the condition that the reflection of electrons from the particle surface is of a mixed (specular-diffuse) character.[5]

The idea that the specular reflection of electrons from the surface could influence the electromagnetic properties of small metallic particles was first advanced in Refs. 6–8.

In the present article the theory of the interaction of an ac electromagnetic field with a cylindrical particle of metal is constructed taking account of the mixed (specular-diffuse) character of the reflection of electrons inside the particle.

II. FORMULATION OF THE PROBLEM

A metallic cylinder of length L and radius R, placed in the field of an electromagnetic plane wave with frequency ω, which in order of magnitude is much lower than the plasma resonance frequency ω_p in metals ($\omega_p \sim 10^{16}$ s^{-1}), is the subject of study. The particle is assumed to be small, meaning that $R \ll 2\pi c/\omega$ (c is the speed of light in vacuum). The nonuniformity of the external field of the wave and the skin effect are neglected (R is assumed to be less than the skin-layer depth δ).

We shall study the general case of the interaction of linearly polarized electromagnetic radiation with a cylindrical particle, when the symmetry axis of the particle is orthogonal to the propagation direction of the radiation.

Let the direction of the electric field vector **E** of the wave make an angle γ with the axis of the cylindrical particle. Then the magnitude of the projection of the electric field vector in the direction of the cylinder axis is $E_l = E\cos\gamma$, and the magnitude of the projection of the electric field vector in a direction perpendicular to the axis is $E_n = E\sin\gamma$.

The absorption cross section of the particle can be represented as

$$\sigma = \sigma_l \cos^2\gamma + \sigma_n \sin^2\gamma.$$

The quantities σ_l and σ_n are due to the projections of the electric field vector E_l and E_n, respectively.

In the present work σ_l (the index l is dropped in what follows) is calculated. When the electric field vector **E** of the wave is perpendicular to the cylinder axis, the magnetic field vector **H** of the wave is directed along the axis of the cylinder. In this case the magnetic dipole absorption of the particle, which is due to eddy currents, makes the dominant contribution to the absorption cross section. This absorption is analyzed in Refs. 3 and 4.

For a sufficiently long cylinder the electric field of the wave remains unscreened in most of the cylinder. To estimate the parameters for which this regime occurs we shall examine the well-known solution for a prolate ellipsoid in an electric field.[9] We start with the fact that a sufficiently long cylinder can be approximated by a prolate ellipsoid. The desired limiting ratio between the radius and length of the particle ($\Gamma = R/L$) follows from the condition that the local field of a prolate ellipsoid goes to the unscreened field of an infinite cylinder:

$$\Gamma \ll \sqrt{\frac{\omega}{2\pi\Sigma(0)}} \Bigg/ \sqrt{\ln\frac{4\pi\Sigma(0)}{\omega}}.$$

Here $\Sigma(0) = e^2 n\tau/m$ is the static conductivity of the metal (e and m are the charge and effective mass of an electron in the metal, n is the concentration of conduction electrons, and τ is the electronic relaxation time).

An estimate using this formula for an external field with frequency, for example, 10^{12} s^{-1} shows that in this case the particle length should be approximately four times longer than the radius of the particle (for higher frequencies of the external field there is virtually no screening).

The electric absorption of such a uniform particle is due to the appearance of high-frequency currents inside it. The electric field giving rise to these currents has the form

$$\mathbf{E} = \mathbf{E}_0 \exp(-i\omega t). \tag{1}$$

The average dissipated power $\bar{Q}$ in the particle is given by[9]

$$\bar{Q} = \int \overline{(\mathrm{Re}\,\mathbf{E})(\mathrm{Re}\,\mathbf{j})} d^3r = \frac{1}{2}\,\mathrm{Re}\int \mathbf{j}\mathbf{E}^* d^3r, \tag{2}$$

where the overbar denotes time averaging, the asterisk denotes complex conjugation, $\mathbf{j}$ is the high-frequency current, and $\mathbf{r}$ is the radius vector (the coordinate origin is placed on the axis of the particle).

The relation between $\mathbf{E}$ and $\mathbf{j}$ in the case where the particle radius R is comparable to the electron mean free path length Λ in the metal (or less than Λ) is strongly nonlocal. To describe this relation we shall apply the kinetic equation (in the relaxation time approximation) to a degenerate Fermi gas of the conduction electrons inside the particle.

For sufficiently weak external fields this equation can be linearized with respect to the external field $\mathbf{E}$ and with respect to small deviations $f_1(\mathbf{r},\mathbf{v})$ from the equilibrium Fermi distribution function f_0:

$$-\omega f_1 + \mathbf{v}\frac{\partial f_1}{\partial \mathbf{r}} + e(\mathbf{v}\mathbf{E})\frac{\partial f_0}{\partial \varepsilon} = -\frac{f_1}{\tau}, \tag{3}$$

where $\mathbf{v}$ is the velocity of the conduction electrons.

In what follows we consider a quadratic velocity dependence of the energy of the electrons $\varepsilon = mv^2/2$, and we use a step-function approximation for the equilibrium electron energy distribution function $f_0(\varepsilon)$:[10]

$$f_0(\varepsilon) = \theta(\varepsilon_F - \varepsilon) = \begin{cases} 1, & 0 \leqslant \varepsilon \leqslant \varepsilon_F \\ 0, & \varepsilon_F < \varepsilon \end{cases},$$

where $\varepsilon_F = mv_F^2/2$ is the Fermi energy (v_F is the Fermi velocity) (the Fermi surface is assumed to be spherical).

The electron distribution function is

$$f(\mathbf{r},\mathbf{v}) = f_0(\varepsilon) + f_1(\mathbf{r},\mathbf{v}), \quad \varepsilon = \frac{m\mathbf{v}^2}{2}.$$

The deviation $f_1(\mathbf{r},\mathbf{v})$, arising under the action of an electric field, of the electron distribution function $f(\mathbf{r},\mathbf{v})$ from the equilibrium value $f_0(\varepsilon)$ results in the appearance of a high-frequency current inside the particle

$$\mathbf{j} = en\langle\mathbf{v}\rangle = en\left[\int f_0 d^3v\right]^{-1}\int f_1 \mathbf{v} d^3v. \tag{4}$$

The electron density n in the particle is determined using the standard formula, according to which

$$\pi = 2\left(\frac{m}{h}\right)^3 \int f_0 d^3v = 2\left(\frac{m}{h}\right)^3 \frac{4\pi v_F^3}{3}, \tag{5}$$

where h is Planck's constant.

Taking in Eq. (3) the field $\mathbf{E}$ in the form (1) we find $f_1(\mathbf{r},\mathbf{v})$ as the solution of this equation. Then, using the expressions (4) and (2), we determine for the particle the current and the cross section for the absorption of energy from the external electric field:

$$\sigma = \frac{8\pi\bar{Q}}{cE_0^2}. \tag{6}$$

A unique solution of this problem can be obtained by choosing a boundary condition for the unknown function $f_1(\mathbf{r},\mathbf{v})$ on the cylindrical surface of the metallic particle. For this boundary condition we take the condition of specular-diffuse reflection of electrons from the surface:[4]

$$f_1(\mathbf{r}_\perp,\mathbf{v}_\perp,\mathbf{v}_z) = qf_1(\mathbf{r}_\perp,\mathbf{v}'_\perp,\mathbf{v}_z) \text{ for } \begin{cases} |\mathbf{r}_\perp| = R \\ \mathbf{r}_\perp\mathbf{v}_\perp < 0 \end{cases}, \tag{7}$$

where $\mathbf{v}_\perp$ and $\mathbf{r}_\perp$ are, respectively, the components of the electron radius vector $\mathbf{r}$ and velocity vector $\mathbf{v}$ in a plane perpendicular to the axis of a uniform cylinder;

$$\mathbf{v}'_\perp = \mathbf{v}_\perp - \frac{2\mathbf{r}_\perp(\mathbf{r}_\perp\mathbf{v}_\perp)}{R^2}$$

is the velocity vector, which on specular reflection from the inner surface of the particle at the point $\mathbf{r}_\perp$ ($|\mathbf{r}_\perp| = R$) transforms into the vector $\mathbf{v}_\perp$; $\mathbf{v}_z$ is the component of the electron velocity along the axis of the particle; and, q is the specularity coefficient (the probability of specular reflection): $0 \leqslant q \leqslant 1$.

For $q=0$ we obtain the condition for diffuse reflection of conduction electrons from the inner surface of a metallic particle, and for $q=1$ we obtain the condition of purely specular reflection. For $q \neq 0$ and $q \neq 1$ we obtain different variants of mixed (specular-diffuse) reflection of electrons.

III. DISTRIBUTION FUNCTION

The kinetic Eq. (3) is solved by the method of characteristics.[11] The change f_1 along a trajectory (characteristic)

$$d\mathbf{r} = \mathbf{v}dt$$

is determined by the equation

$$df_1 = -\left[\nu f_1 + e(\mathbf{v}\mathbf{E})\frac{\partial f_0}{\partial \varepsilon}\right]dt, \tag{8}$$

where $\nu = (1/\tau) - i\omega$ is the complex scattering frequency.

The boundary condition (7) makes it possible to follow the change in the function $f_1(\mathbf{r}_\perp,\mathbf{v}_\perp,\mathbf{v}_z)$ along the specularly reflecting trajectory. At the reflection point $t=t_n$ the function $f_1(t)$ undergoes a jump:

$$f_1(t_n + 0) = qf_1(t_n - 0). \tag{9}$$

Here the $+/-$ signs denote the limits of the function $f_1(\mathbf{r}_\perp,\mathbf{v}_\perp,\mathbf{v}_z)$ at the reflection point t_n to the right or left with respect to the time of flight.

For specular reflection, the projection of the electron velocity on the Z axis is conserved (see below). Consequently, the quantity $\mathbf{v}\cdot\mathbf{E} = v_z E$ is constant along a trajectory.

The difference $t_n - t_{n-1}$ is independent of the number n of the reflection point:

$$t_n = nT + \text{const}, \quad n \ni Z,$$

where T is the transit time of an electron with velocity $\mathbf{v}_\perp$ from the point $\mathbf{r}_{n-1,\perp}$ to the point $\mathbf{r}_{n\perp}$:

$$T = -\frac{2(\mathbf{v}_{n\perp}\mathbf{r}_{n\perp})}{v_\perp^2}.$$

The solution of Eq. (8) is the function

$$f_1 = C\exp(-\upsilon t) + A, \tag{10}$$

where $A = e(\mathbf{v}\cdot\mathbf{E})/\nu\,\partial f_0/\partial\varepsilon$.

The parameter t in the expression (10) is the time required for an electron to move along a trajectory from the boundary where reflection occurs to the point $\mathbf{r}_\perp$ with velocity $\mathbf{v}_\perp$.

We present the solution of this equation on the interval (t_{n-1}, t_n) for the case of specular reflection of electrons from the inner surface of the particle.

At the time origin ($t=0$)

$$f_1(t_{n-1}+0) = C + A,$$

where we find the value of the constant C:

$$C = f_1(t_{n-1}+0) - A.$$

Now we obtain a relation between the initial value of the function f_1 on two neighboring links of the trajectory. Since $t_n - 0 = t_{n-1} + T$,

$$f_1(t_n - 0) = [f_1(t_{n-1}+0) - A]\exp(-\upsilon T) + A$$
$$= A[1 - \exp(-\upsilon T)] + f_1(t_{n-1}+0)\exp(-\upsilon T).$$

Using the condition (9) we obtain

$$f_1(t_n + 0) = q\{A[1 - \exp(-\upsilon T)] + f_1(t_{n-1}+0)\exp(-\upsilon T)\}.$$

Next, using this recurrence relation, expressing $f_1(t_{n-1}+0)$ in terms of $f_1(t_{n-2}+0)$, and so on, we arrive at an expression for $f_1(t_n+0)$ in terms of the sum of an infinite geometric progression with the denominator $q_2\exp(-\nu T)$. Summing the progression we have

$$f_1(t_n + 0) = \frac{qA[1 - \exp(-\upsilon T)]}{1 - q\exp(-\upsilon T)}. \tag{11}$$

To find the specific form of the solution of Eq. (8) we employ the relation (10) and the initial condition (11). At $t = 0$,

$$\frac{qA[1 - \exp(-\upsilon T)]}{1 - q\exp(-\upsilon T)} = C + A,$$

where

$$C = A\left\{\frac{q[1 - \exp(-\upsilon T)]}{1 - q\exp(-\upsilon T)} - 1\right\} = A\left\{\frac{q-1}{1 - q\exp(-\upsilon T)}\right\}.$$

Consequently,

$$f_1(t) = A\left\{\frac{q-1}{1 - q\exp(-\upsilon T)}\right\}\exp(-\upsilon T) + A$$
$$= A\left\{\frac{(q-1)\exp(-\upsilon T)}{1 - q\exp(-\upsilon T)} + 1\right\}. \tag{12}$$

The parameters t and T can be related with the coordinates of the point $(\mathbf{r}_\perp, \mathbf{v}_\perp)$ in phase space (for $n=0$, $\mathbf{v}_{0\perp} = \mathbf{v}_\perp$) by the conditions

$$\mathbf{r}_\perp = \mathbf{r}_{0\perp} + \mathbf{v}_\perp t; \quad \mathbf{v}_\perp\mathbf{r}_{0\perp} < 0; \quad r_{0\perp}^2 = R^2;$$

$$T = -\frac{2(\mathbf{v}_\perp\mathbf{r}_{0\perp})}{v_\perp^2},$$

where $\mathbf{r}_{0\perp}$ are the components of the electron radius vector in a plane perpendicular to the axis of the cylinder at the moment of reflection from the cylindrical boundary of the particle.

Eliminating $\mathbf{r}_{0\perp}$ we obtain

$$t = \frac{1}{v_\perp^2}\{\mathbf{r}_\perp\mathbf{v}_\perp + [(\mathbf{r}_\perp\mathbf{v}_\perp)^2 + (R^2 - r_\perp^2)v_\perp^2]^{1/2}\}, \tag{13}$$

$$T = \frac{2}{v_\perp^2}[(\mathbf{r}_\perp\mathbf{v}_\perp)^2 + (R^2 - r_\perp^2)v_\perp^2]^{1/2}. \tag{14}$$

The relations (12)–(14) completely determine the function $f_1(\mathbf{r}_\perp, \mathbf{v}_\perp, \mathbf{v}_z)$ for specular-diffuse reflection of electrons from the inner surface of a cylindrical particle.

IV. ABSORPTION CROSS SECTION

The distribution function found above makes it possible to calculate the current (4), the average dissipated power (2), and the cross section (6) for the absorption of energy from the external electromagnetic field.

To calculate the integrals (4) and (2) it is convenient to switch to cylindrical coordinates in coordinate space ($\mathbf{r}_\perp$, φ, z; polar axis—Z axis; the vector $\mathbf{E}_0$ is parallel to the Z axis) and in velocity space ($\mathbf{v}_\perp$, α, v_z; polar axis—v_z axis). The cylinder axis is also the Z axis.

The field (1) in cylindrical coordinates possesses only a z component:

$$\mathbf{E} = E_z\mathbf{e}_z; \quad E_z = E_0\exp(-i\omega t). \tag{15}$$

Correspondingly, the current (4) possesses only a z component (the current lines are straight lines parallel to the Z axis) and can be calculated from the formula

$$j_z = E_z 2e^2\left(\frac{m}{h}\right)^3\frac{1}{v}\int v_z^2\delta(\varepsilon - \varepsilon_F)\left\{\frac{(q-1)\exp(-\upsilon t)}{1 - q\exp(-\upsilon T)} + 1\right\}d^3v.$$

Using the properties of the δ function we have

$$\delta(\varepsilon - \varepsilon_F) = \frac{2}{m}\delta(\mathbf{v}_z^2 + \mathbf{v}_\perp^2 - \mathbf{v}_F^2) = \frac{2}{m}\delta[\mathbf{v}_z^2 - (\mathbf{v}_F^2 - \mathbf{v}_\perp^2)]$$
$$= \frac{2}{m}\delta[(\mathbf{v}_z - \sqrt{\mathbf{v}_F^2 - \mathbf{v}_\perp^2})(\mathbf{v}_z + \sqrt{\mathbf{v}_F^2 - \mathbf{v}_\perp^2})]$$
$$= \frac{1}{m\sqrt{\mathbf{v}_F^2 - \mathbf{v}_\perp^2}}[\delta(\mathbf{v}_z - \sqrt{\mathbf{v}_F^2 - \mathbf{v}_\perp^2}) + \delta(\mathbf{v}_z + \sqrt{\mathbf{v}_F^2 - \mathbf{v}_\perp^2})].$$

On account of the symmetry of the problem the integration over the entire range of velocities v_z can be replaced by integration over a positive region. This doubles the result. Substituting the integration limits we arrive at the expression

$$j_z = E_z 2e^2\left(\frac{m}{h}\right)^3 \frac{2}{v}\frac{2}{m}\int_0^{v_F}\int_0^{\pi}\int_0^{\infty} v_z^2 \frac{\delta(v_z-\sqrt{v_F^2-v_z^2})}{\sqrt{v_F^2-v_z^2}} \times\left\{\frac{(q-1)\exp(-vt)}{1-q\exp(-vT)}+1\right\} v_\perp dv_\perp d\alpha dv_z$$

(the motion of the electrons is symmetric with respect to any diametric plane which contains the point of the position of the electrons on a trajectory, so that the angle α in velocity space can be assumed to vary from 0 to π, and the result of integrating over this variable can be doubled).

Integrating with respect to the variable v_z we have

$$j_z = \frac{3nE_z e^2}{\pi v_F^3 m v}\int_0^{v_F}\int_0^{\pi}\sqrt{v_F^2-v_\perp^2} \times\left\{\frac{(q-1)\exp(-vt)}{1-q\exp(-vT)}+1\right\} v_\perp dv_\perp d\alpha. \tag{16}$$

Here we have taken account of the fact that the concentration of conduction electrons in metals is given by the relation (5).

The cross section for the absorption of electromagnetic radiation by a nonuniform particle is

$$\sigma = \frac{1}{2}\frac{8\pi}{cE_0^2}\,\mathrm{Re}\left\{\int j_z E_z^* d^3 r\right\},$$

or, taking account of (15) and (16), simple transformations yield

$$\sigma = \frac{24ne^2\pi L}{v_F^3 mc}\,\mathrm{Re}\left\{\int_0^R r_\perp dr_\perp \int_0^{v_F}\int_0^{\pi}\sqrt{v_F^2-v_\perp^2} \times\left[\frac{(q-1)\exp(-vt)}{v(1-q\exp(-vT))}+\frac{1}{v}\right]\right\} v_\perp dv_\perp d\alpha. \tag{17}$$

For further calculations and analysis of the results we introduce the new variables

$$\xi = \frac{\mathbf{r}_\perp}{R}, \quad \rho = \frac{v_\perp}{v_F},$$

$$z = v\frac{R}{v_F} = \left(\frac{1}{\tau}-i\omega\right)\frac{R}{v_F} = x - iy \tag{18}$$

and transform the expressions (13) and (14):

$$t = \frac{R}{v_\perp}(\xi\cos\alpha + \sqrt{1-\xi^2\sin^2\alpha}) = \frac{R}{v_\perp}\eta,$$

$$T = \frac{R}{v_\perp}2\sqrt{1-\xi^2\sin^2\alpha} = \frac{R}{v_\perp}\eta_0.$$

Here we have taken into account the fact that $\mathbf{r}_\perp\cdot\mathbf{v}_\perp = r_\perp v_\perp\cos\alpha$ (all electrons on the Fermi surface inside the particle move with velocity v_F).

It is convenient to represent the absorption cross section (17) in the following form using Eq. (18):

$$\sigma = \sigma_0 F(x,y,q),$$

where

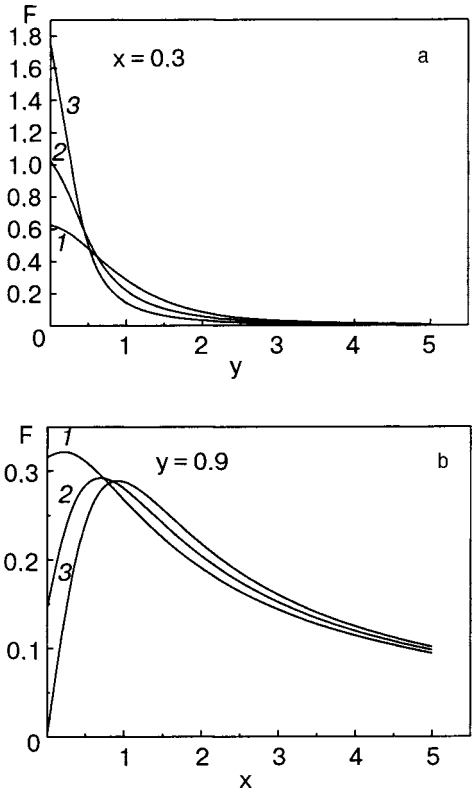

FIG. 1. Dimensionless absorption cross section F versus the dimensionless frequency $y=R\omega/v$ (a) and the reciprocal of the electron mean free path length $x=R/v\tau$ (b) for different values of the reflection coefficient q: 0 (1), 0.5 (2), 1 (3).

$$\sigma_0 = \frac{24\pi ne^2R^3L}{mcv_F}, \tag{19}$$

$$F(x,y,q) = \mathrm{Re}\left\{\frac{1}{z}\int_0^1 \xi d\xi\int_0^1\int_0^{\pi}\rho\sqrt{1-\rho^2} \times\left[\frac{(q-1)\exp(-z\eta/\rho)}{1-q\exp(-z\eta_0/\rho)}+1\right] d\rho d\alpha\right\}. \tag{20}$$

For $q=0$ (diffuse reflection of electrons) it follows from Eq. (20) that the dimensionless absorption cross section of the particle is

$$F(x,y) = \mathrm{Re}\left\{\frac{1}{z}\int_0^1 \xi d\xi \times \int_0^1\int_0^{\pi}\rho\sqrt{1-\rho^2} \times[1-\exp(-z\eta/\rho)] d\rho d\alpha\right\}. \tag{21}$$

Figures 1 and 2 show the numerical calculations of $F(x,y,q)$.

V. DISCUSSION

In the limit of purely specular reflection of electrons at the boundary of the particle ($q=1$) we obtain the following expression for the dimensionless absorption cross section $F(x,y)$:

$$F(x,y) = \mathrm{Re}\left\{\frac{\pi}{6}\frac{1}{z(x,y)}\right\}.$$

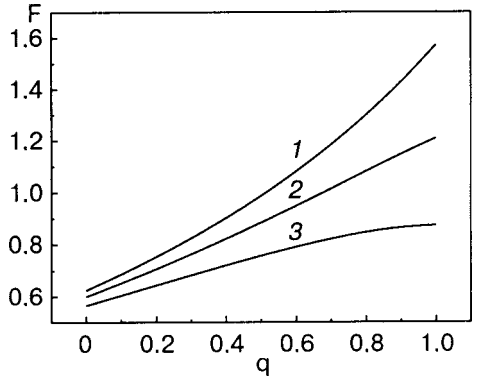

FIG. 2. Dimensionless absorption cross section F versus the electron reflection coefficient q for $x=0.3$ and different values of y: 0.1 (1), 0.2 (2), 0.3 (3).

As a result, the absorption cross section of a cylinder becomes

$$\sigma(x,y)=\sigma_0\,\mathrm{Re}\left\{\frac{\pi}{6}\frac{1}{z(x,y)}\right\}=\sigma_0\frac{\pi}{6}\frac{x}{x^2+y^2}. \tag{22}$$

The expression (22) corresponds to the classical result for a cylindrical particle (i.e. the result which is obtained using the classical Drude formula for the conductivity of a metal).[10] This is because for $q=1$ the particle boundary has no effect on the electron distribution function $f_1(\mathbf{r}_\perp,\mathbf{v}_\perp,\mathbf{v}_z)$. The high-frequency current inside a specularly reflecting metallic cylinder (see Eq. (16)) satisfies the local Ohm's law with any ratio between the cylinder radius R and the electron mean free path length Λ. Thus, for specular reflection there are no nonlocal (surface) effects.

Irrespective of the character of the electron reflection at the boundary (for any q), as particle size increases (for $x\gg 1$; in this case the term with the exponentials in Eq. (20) can be neglected because they decay rapidly) the macroscopic asymptotic behavior (22) also obtains.

In Ref. 12 the electric absorption of a prolate ellipsoid of revolution (actually an infinite cylinder) was studied with a diffuse boundary condition for reflection of electrons from the inner surface of an ellipsoid. For low-frequency surface scattering of electrons, when $x\ll 1$ and $y\ll 1$ (free electron regime), the expression found for the absorption cross section using Eq. (21) (in this case the exponential appearing in the expression (21) can be expanded in a Taylor series up to the second term) is identical to the result

$$\sigma_{\mathrm{el}}=\frac{8\pi ne^2R}{mc\upsilon_F}V$$

(V is the volume of an ellipsoid) obtained in Ref. 12, if the specific (per unit volume) absorption cross sections of a cylinder and ellipsoid are calculated. However, if the surface scattering of electrons is high-frequency scattering ($x<1, y\gg 1, x\ll y$), then the result obtained in Ref. 12

$$\sigma_{\mathrm{el}}=\frac{9}{16}\frac{\pi^2ne^2R}{16mc\upsilon_F y^2}V \tag{23}$$

differs appreciably from the exact kinetic calculation.

To compare the results for high-frequency surface scattering we shall find the macroscopic asymptotic cross section for the absorption by an infinite cylinder, using the expression (21) and the technique proposed in Ref. 3. The required calculations yield

$$\sigma(z)=\sigma_0\frac{\pi}{6}\,\mathrm{Re}\left[\frac{1}{z}-\frac{3}{8z^2}\right]=\sigma_0\frac{\pi}{6}\left[\frac{x}{x^2+y^2}-\frac{3(x^2-y^2)}{8(x^2+y^2)^2}\right]. \tag{24}$$

We shall now find the ratio of the specific (per unit volume) absorption cross sections (23) and (24) in the high-frequency limit (under the conditions indicated above the second term in Eq. (24), proportional to $-1/y^2$, dominates): $\sigma_{\mathrm{el}}/\sigma(z)=9/4=2.25$.

Thus the result obtained in Ref. 12 for high-frequency surface scattering is much greater than the result of the exact kinetic calculation for electric absorption by an elongated cylindrical particle.

Figure 1a shows the dependence of the dimensionless absorption cross section F on the dimensionless frequency y of the external field. The figure was constructed for particles with a small (compared with the electron mean free path length Λ) radius, which is the same for all curves. Each curve was constructed for different values of the reflection coefficient q. As one can see in the figure, for low dimensionless frequencies y ($y<0.5$) the dimensionless absorption cross section F is greater for particles where purely specular reflection of conduction electrons occurs. In the other region of dimensionless frequencies ($y>0.5$) the dimensionless absorption cross section is greater for particles where the reflection of conduction electrons at the particle surface is purely diffuse.

Figure 1b shows the dimensionless absorption cross section F versus the dimensionless reciprocal x of the mean free path length. The figure was constructed for a prescribed dimensionless frequency y and different values of the reflection coefficient q. Each curve has a maximum, whose magnitude depends on the dimensionless frequency y of the external field. In addition, the curves 1 and 2 do not start from the coordinate origin, because surface effects influence the dimensionless absorption cross section F. These effects are strongest when the particle radius is small compared with the electron mean free path length Λ. As the particle radius increases, all curves merge and the result becomes the classical result, which corresponds to curve 3 (for specular reflection of electrons there are no surface effects).

Figure 2 elucidates the effect of the electron reflection coefficient q on the dimensionless absorption cross section F. For any values of the reflection coefficient q the absorption cross section is larger for particles which are in a field with lower frequency (the particle radius is the same and small compared with the electron mean free path length Λ).

a)E-mail: zav.mgul@rambler.ru

[1]Yu. I. Petrov, *The Physics of Small Particles*, Nauka, Moscow (1984).
[2]M. Born and E. Wolf, *Principles of Optics*, 4th edition, Pergamon, Oxford, 1969; Nauka, Moscow, 1973.
[3]É. V. Zavitaev, A. A. Yushkanov, and Yu. I. Yalamov, Opt. Spektrosk. **92**, 851 (2002).
[4]É. V. Zavitaev, A. A. Yushkanov, and Yu. I. Yalamov, Zh. Tekh. Fiz. **73**,

16 (2003) [Tech. Phys. **48**, 290 (2003)].
[5]J. M. Ziman, *Electrons and Phonons*, Clarendon, Oxford, 1960; IL Moscow, 1962.
[6]R. B. Dingle, Proc. R. Soc. London, Ser. A **201**, 545 (1950).
[7]A. G. Mal'shukov, Solid State Commun. **44**, 1257 (1982).
[8]A. G. Mal'shukov, Zh. Éksp. Teor. Fiz. **85**, 700 (1983) [JETP **58**, 409 (1983)].
[9]L. D. Landau and E. M. Lifshitz, *Course of Theoretical Physics*, Vol. 8: *Electrodynamics of Continuous Media*, Nauka, Moscow, 1996; Pergamon, New York, 1984.
[10]W. Harrison, *Solid State Theory*, McGraw-Hill, New York, 1984; Mir, Moscow (1972).
[11]R. Courant, and D. Hilbert, *Methods of Mathematical Physics*, Vol. 2: *Partial Differential Equations*, Interscience, New York, 1962; Mir, Moscow (1964).

Translated by M. E. Alferieff

LOW-DIMENSIONAL AND DISORDERED SYSTEMS

Investigation of the single-particle Green's function in a bipartite Hubbard model in the static-fluctuations approximation

G. I. Mironov[a)]

Mariĭskiĭ State Pedogogical Institute, Ioshkar-Ola 424002, Russia
(Submitted July 20, 2004; resubmitted July 15, 2005)

The single-particle anticommutator Green's function of a two-sublattice two-dimensional Hubbard model is calculated in the static-fluctuations approximation taking account of electron transfer to the nearest and second-nearest neighboring sites of the crystal lattice. The behavior of the bipartite Hubbard model for strong and weak coupling is investigated. © *2005 American Institute of Physics*. [DOI: 10.1063/1.2144459]

After the discovery of high-temperature superconductors (HTSCs) it was stated[1,2] that their unusual properties can be described in a unified manner using the concept of a Luttinger liquid.[3–10] The study of these liquids showed that the single-particle Green's function has no poles describing individual elementary excitations. For example, the elementary excitations in the one-dimensional Hubbard model[11] are neutral spinons and spinless holons.[2,10,12] The exact solution of the one-dimensional Hubbard model[13] illustrates the phenomenon of the separation of spin and charge degrees of freedom, which is an integral property of a Luttinger liquid.

According to Anderson,[1,2] if the two-dimensional Hubbard model is considered for any magnitude of the repulsive interaction of the electrons at one lattice site, two Hubbard subbands necessary appear and the existence of the upper Hubbard subband must, in Anderson's opinion, definitely lead to a Luttinger liquid for a gas of strongly interacting electrons and not to a Fermi liquid (see, for example, Ref. 14).

There also exists a different point of view according to which the two-dimensional Hubbard model is a normal Fermi liquid, at least in the case of weak coupling. The development of a new renormalization-group method[15,16] made it possible to obtain a correct numerical solution for the renormalization-group equations for the two-dimensional Hubbard model with weak correlations. These solutions showed that the Hubbard model in the case of weak interaction is described as a Fermi liquid.[17–22]

A method for solving the Hubbard model[11] in the static-fluctuations approximation has been developed in Refs. 23–26, and the energy of the ground state of a two-dimensional bipartite Hubbard model[27] is calculated and investigated in Ref. 26. Comparing the results obtained in Ref. 26 with the exact solution of the one-dimensional model[13] showed that the static-fluctuations approximation describes quite adequately the behavior of the Hubbard model with weak and strong correlations. In the limits $U=0$ and $U=\infty$ the ground-state energy of the one-dimensional Hubbard model in the static-fluctuations approximation[26] is identical to that in the case of the exact solution,[23] and for intermediate values of U there is good agreement with the exact solution. For example, for $U/2B=1$ the difference of the exact and approximate solutions is 2%. This shows that the static-fluctuations approximation works well for weak, intermediate, and strong correlations. This is especially important for layered cuprates.[27]

The objective of the present paper is to investigate the single-particle Green's function in the Hubbard model in the static-fluctuations approximation. We write the Hamiltonian for the Hubbard model in the form proposed in Ref. 27, including a term describing electron hopping to the second-nearest neighbors of the sites:

$$H = H_0 + V, \tag{1}$$

$$H_0 = \sum_{\sigma,f\in A} \varepsilon_1 n_{f\sigma} + \sum_{\sigma,l\in C} \varepsilon_2 n_{l\sigma} + \sum_{\sigma,f,l} B_{fl}(a^+_{f\sigma}a_{l\sigma} + a^+_{l\sigma}a_{f\sigma}) + \sum_{\sigma,l',l} B_{l'l}a^+_{l'\sigma}a_{l,\sigma}, \tag{2}$$

$$V = \frac{U_1}{2}\sum_{\sigma,f\in A} n_{f\sigma}n_{f\bar{\sigma}} + \frac{U_2}{2}\sum_{\sigma,l\in C} n_{l\sigma}n_{l\bar{\sigma}}, \tag{3}$$

where $a^+_{j\sigma}$ and $a_{j\sigma}$ are the Fermi operators creating and annihilating electrons with spin σ at the lattice site j $(j=f,l)$; $n_{f\sigma}=a^+_{f\sigma}a_{f\sigma}$ is the particle number operator; ε_1 and ε_2 are the characteristic energies of an electron at the sites of the sublattices A and C, respectively; $B_{fl}=B(f-l)$ and $B_{l'l}=B(l'-l)$ are transfer integrals describing electron hopping, from atom to atom, as a result of the kinetic energy and crystal field, to the nearest neighbor site and to the second-nearest neighbor site along the diagonal of a square, respectively; and, $\bar{\sigma}=-\sigma$. It is assumed that the electrons of only one sublattice (by analogy to oxygen on CuO_2 planes) can be transported along the diagonal of a square to the sites of the same sublattice (to simplify the discussions we consider a hypothetical square lattice).

The equations of motion for the electron creation operators in the Heisenberg representation $(j=f,l)$ are

$$\frac{d}{d\tau}a_{j\sigma}^{+}(\tau)=\varepsilon_j a_{j\sigma}^{+}(\tau)+\sum_i B_{ij}a_{i\sigma}^{+}(\tau)+\sum_{j'} B_{jj'}a_{j'\sigma}^{+}(\tau)+U_j n_{j\bar{\sigma}}a_{j\sigma}^{+}(\tau), \quad (4)$$

where

$$\varepsilon_j=\begin{cases}\varepsilon_1', & j=f\\ \varepsilon_2', & j=l\end{cases}, \quad U=\begin{cases}U_1, & j=f\\ U_2, & j=l\end{cases},$$

$$B_{jj'}=\begin{cases}0, & j=f,\ j'=f'\\ B_{ll'}, & j=l,\ j'=l'\end{cases}, \quad B_{ij}=B_{fl}=B_{lf}.$$

We shall solve the system of differential equations (4) in the static-fluctuations approximation. The computational method is described in detail in Refs. 23–25. We note in connection with the calculations to be performed that, according to previously obtained results, the computational error in the static-fluctuations approximation goes to zero for $\langle n_{j\bar{\sigma}}\rangle=1/2$, $\langle n_{j\bar{\sigma}}\rangle=0$, and $\langle n_{j\bar{\sigma}}\rangle=1$ and should be minimum in the regions $\langle n_{j\bar{\sigma}}\rangle\approx 1/2$, $\langle n_{j\bar{\sigma}}\rangle\approx 0$, and $\langle n_{j\bar{\sigma}}\rangle\approx 1$ (see Ref. 24). The computational results obtained in the static-fluctuations approximation are identical to the exact results in the limits $U=0$, $B=$const and $U=$const, $B=0$ (see Ref. 26).

We are interested, first and foremost, in the energy spectrum and character of the elementary excitations. To this end we shall calculate, using the results obtained in Refs. 23–25, the Fourier transforms of the anticommutator Green's functions $\langle a_{k\sigma}^{+}|a_{k\sigma}\rangle_E$ and $\langle b_{k\sigma}^{+}|b_{k\sigma}\rangle_E$:

$$\langle a_{k\sigma}^{+}|a_{k\sigma}\rangle_E=\frac{i}{2\pi}\frac{1}{4}\left\{\frac{1+(\varepsilon_{1\sigma}'-\varepsilon_{2k\sigma}')/2t_k}{E-U_1\Phi-t_k-(\varepsilon_{1\sigma}'+\varepsilon_{2k\sigma}')/2}+\frac{1+(\varepsilon_{1\sigma}'-\varepsilon_{2k\sigma}')/2t_k}{E+U_1\Phi-t_k-(\varepsilon_{1\sigma}'+\varepsilon_{2k\sigma}')/2}+\frac{1-(\varepsilon_{1\sigma}'-\varepsilon_{2k\sigma}')/2t_k}{E-U_1\Phi+t_k-(\varepsilon_{1\sigma}'+\varepsilon_{2k\sigma}')/2}+\frac{1-(\varepsilon_{1\sigma}'-\varepsilon_{2k\sigma}')/2t_k}{E+U_1\Phi+t_k-(\varepsilon_{1\sigma}'+\varepsilon_{2k\sigma}')/2}\right\}; \quad (5)$$

$$\langle b_{k\sigma}^{+}|b_{k\sigma}\rangle_E=\frac{i}{2\pi}\frac{1}{4}\left\{\frac{1-(\varepsilon_{1\sigma}'-\varepsilon_{2k\sigma}')/2t_k}{E-U_2\Phi-t_k-(\varepsilon_{1\sigma}'+\varepsilon_{2k\sigma}')/2}+\frac{1-(\varepsilon_{1\sigma}'-\varepsilon_{2k\sigma}')/2t_k}{E+U_2\Phi-t_k-(\varepsilon_{1\sigma}'+\varepsilon_{2k\sigma}')/2}+\frac{1+(\varepsilon_{1\sigma}'-\varepsilon_{2k\sigma}')/2t_k}{E-U_2\Phi+t_k-(\varepsilon_{1\sigma}'+\varepsilon_{2k\sigma}')/2}+\frac{1+(\varepsilon_{1\sigma}'-\varepsilon_{2k\sigma}')/2t_k}{E+U_2\Phi+t_k-(\varepsilon_{1\sigma}'+\varepsilon_{2k\sigma}')/2}\right\}, \quad (6)$$

where

$$\varepsilon_{1\sigma}'+\varepsilon_{2k\sigma}'=\varepsilon_1+\varepsilon_2+(U_1+U_2)/2+\sigma S(U_1-U_2)-4B'\cos(k_xa)\cos(k_ya),$$

$$\varepsilon_{1\sigma}'-\varepsilon_{2k\sigma}'=\varepsilon_1-\varepsilon_2+(U_1-U_2)/2+\sigma S(U_1+U_2)+4B'\cos(k_xa)\cos(k_ya),$$

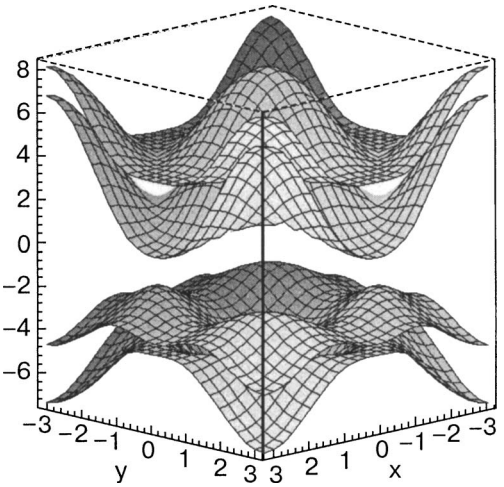

FIG. 1. Energy spectrum of the Hubbard model with $\varepsilon_1=-4$ eV, $\varepsilon_2=-2$ eV, $U_1=8$ eV, $U_2=4$ eV, $B=1.5$ eV, $B'=-0.25B$, $S=1/2$, and $n=1$.

$$\varepsilon_{2k\sigma}'=\varepsilon_2+U_2/2-\sigma SU_2+B_k',$$

$$B_k'=-4B'\cos(k_xa)\cos(k_ya), \quad \Phi=\sqrt{1/4-S^2},$$

$$B_k=-2B[\cos(k_xa)+\cos(k_ya)],$$

$$t_k=t_{k\sigma}=\sqrt{((\varepsilon_{2k\sigma}'-\varepsilon_{1\sigma}')/2)^2+B_k^2},$$

and S is the average value of the electron spin projection. The following Fourier transforms were performed in the derivation of Eqs. (5) and (6):

$$a_{f\sigma}^{+}=\sqrt{\frac{2}{N}}\sum_k a_{k\sigma}^{+}e^{-ikr_f}, \quad a_{l\sigma}^{+}=\sqrt{\frac{2}{N}}\sum_k b_{k\sigma}^{+}e^{-ik\eta},$$

where $b_{k\sigma}^{+}$ and $b_{k\sigma}$ are operators which create and annihilate an electron, belonging to the sublattice C, with wave vector k and spin projection σ.

Given the Green's functions (5) and (6), an equation can be obtained for the chemical potential, whence it follows in the case of an exactly half-filled band ($n=1$) and $T=0$ that the following condition is satisfied:

$$\varepsilon_1+U_1/2=\varepsilon_2+U_2/2=0. \quad (7)$$

Using Eqs. (5) and (6) a matching equation can also be obtained for the spin S, whence follows that $S=1/2$ in the strong-correlations regime.[25] We are interested first and foremost in the case of strong correlations in high-temperature superconductors.

Let us examine the properties of the Hubbard model in the strong-coupling region at low temperatures. Once the ground-state energy has been calculated[26] it can be shown that the ground state of a system with an exactly half-filled band is antiferromagnetic, which agrees with the results obtained by other authors (see, for example, Ref. 28).

The poles of the Green's functions (5) and (6) characterize the spectrum of elementary excitations of the system. Figure 1 shows the energy spectrum of the Hubbard model in the strong-coupling region ($S=1/2, n=1$). Analysis of Fig. 1 shows that the energy band consists of two subbands, and each subband consists of two intersecting branches. We note that as the absolute value of B' increases with the sign re-

maining unchanged the bottom subband separates into two nonintersecting subbands, which in the ground state are filled with electrons. The Fermi surface is a collection of such points in k space at which the energy of elementary excitations, taking account of the shift by the chemical potential, is zero.[29] In Fig. 1 the "Fermi surface," in contrast to the Fermi surface of a noninteracting system, is a collection of four points $(\pi/2,\pi/2)$, $(\pi/2,-\pi/2)$, $(-\pi/2,\pi/2)$, and $(-\pi/2,-\pi/2)$. For lattice parameter $a=1$ these points correspond to the maxima of the top branch of the bottom subband (compare with the result for the Fermi surface for a one-dimensional model in the Luttinger theory[4–10]). This form of the Fermi surface is due to electron transfer along the diagonals of a square. If electron transfer to the second-nearest neighbors of the crystal lattice site is neglected, then the Fermi surface is identical to the unperturbed Fermi surface.

An investigation of the Green's function (6) reveals two electron subsystems whose behavior is different. For electrons in one subsystem the following expressions can be obtained for the anticommutator Green's functions:

$$\langle a^+_{k\uparrow}|a_{k\uparrow}\rangle_E=\frac{i}{2\pi}\frac{1}{2}\left\{\frac{1+(\varepsilon'_{1\uparrow}-\varepsilon'_{2k\uparrow})/2t_{k\uparrow}}{E-t_{k\uparrow}-(\varepsilon'_{1\uparrow}+\varepsilon'_{2k\uparrow})/2}+\frac{1-(\varepsilon'_{1\uparrow}-\varepsilon'_{2k\uparrow})/2t_{k\uparrow}}{E+t_{k\uparrow}-(\varepsilon'_{1\uparrow}+\varepsilon'_{2k\uparrow})/2}\right\},$$

$$\langle b^+_{k\downarrow}|b_{k\downarrow}\rangle_E=\frac{i}{2\pi}\frac{1}{2}\left\{\frac{1-(\varepsilon'_{1\downarrow}-\varepsilon'_{2k\downarrow})/2t_{k\downarrow}}{E-t_{k\downarrow}-(\varepsilon'_{1\downarrow}+\varepsilon'_{2k\downarrow})/2}+\frac{1+(\varepsilon'_{1\downarrow}-\varepsilon'_{2k\downarrow})/2t_{k\downarrow}}{E+t_{k\downarrow}-(\varepsilon'_{1\downarrow}+\varepsilon'_{2k\downarrow})/2}\right\}. \quad (8)$$

Let us examine the behavior of Green's functions at the boundary of the Brillouin zone (Fermi level). The Green's functions (8) can have the following singularities:

$$E_{1,2}=(\varepsilon'_{1\uparrow}+\varepsilon'_{2k\uparrow})/2\pm t_{k\uparrow},$$

$$E_{3,4}=(\varepsilon'_{1\downarrow}+\varepsilon'_{2k\downarrow})/2\pm t_{k\downarrow}, \quad (9)$$

which is characteristic for antiferromagnetic ordering in the system.[28] For an exactly half-filled band $(n=1)$ and $n<1$ (in the case $(1-n)\ll 1$) the electrons in the ground state fill the energy levels corresponding to the roots E_2 and E_4 (minus sign in front of t_k in Eq. (9)). Let us separate in Eq. (8) the Green's functions cooresponding to the energy levels E_2 and E_4 filled in the ground state by electrons:

$$\langle a^+_{k\uparrow}|a_{k\uparrow}\rangle_{E+}=\frac{i}{2\pi}\frac{(1-(\varepsilon'_{1\uparrow}-\varepsilon'_{2k\uparrow})/2t_{k\uparrow})/2}{E+t_{k\uparrow}-(\varepsilon'_{1\uparrow}+\varepsilon'_{2k\uparrow})/2},$$

$$\langle b^+_{k\downarrow}|b_{k\downarrow}\rangle_{E+}=\frac{i}{2\pi}\frac{(1+(\varepsilon'_{1\downarrow}-\varepsilon'_{2k\downarrow})/2t_{k\downarrow})/2}{E+t_{k\downarrow}-(\varepsilon'_{1\downarrow}+\varepsilon'_{2k\downarrow})/2}. \quad (10)$$

The numerators in the Green's functions (10) are the probabilities of finding electrons in the corresponding energy levels (the capacities of these energy levels). Figure 2 shows plots of the numerator of the Green's functions $\langle a^+_{k\uparrow}|a_{k\uparrow}\rangle_{E^+}$ and the top branch of the bottom subband of the Hubbard model in the strong-coupling regime (the plots for the numerator and the spectrum of elementary excitations for the Green's function $\langle b^+_{k\downarrow}|b_{k\downarrow}\rangle_{E^+}$ have a similar form). Analysis of the figure shows that the minimum of the function corresponding to the numerator of the Green's function (10), equal to zero, lies on the boundary of the first Brillouin zone. A zero probability of filling with an up-spin electron corresponds to the Fermi energy, i.e. an up-spin electron of sublattice A and a down-spin electron of sublattice C cannot be found at the Fermi level.

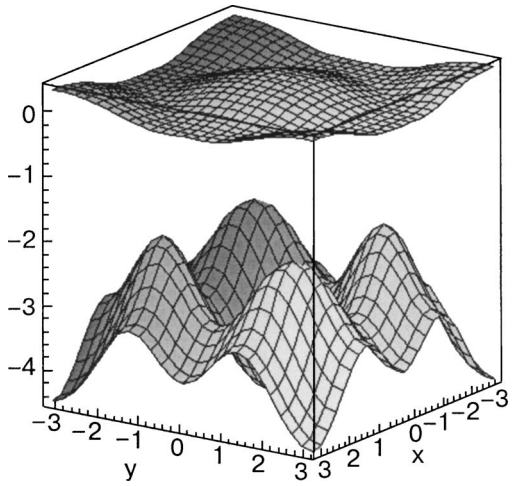

FIG. 2. Capacity of the energy levels (top plot) and energy spectrum (bottom plot) for up-spin electrons of sublattice A for $\varepsilon_1=-4$ eV, $\varepsilon_2=-2$ eV, $U_1=8$ eV, $U_2=4$ eV, $B=1.5$ eV, $B'=-0.30B$, $S=1/2$, and $n=1$.

Let us consider electrons of a different subsystem, which are described by the Green's functions $\langle b^+_{k\downarrow}|b_{k\downarrow}\rangle_E$ and $\langle b^+_{k\uparrow}|b_{k\uparrow}\rangle_E$. The capacities of the energy levels and the energy surfaces corresponding to filling of the sublattice C with electrons in the ground state are shown in Fig. 3. Analysis of Fig. 3 shows that the capacities of the points corresponding to the Fermi energy equal 1—an up-spin electron with probability equal to the probability of an authentic event fills the

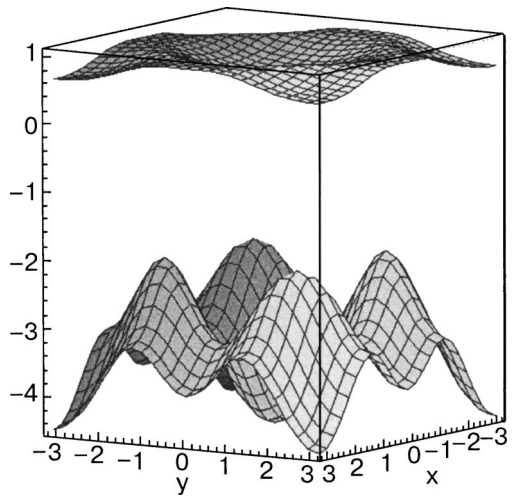

FIG. 3. Capacity of the energy levels (top plot) and energy spectrum (bottom plot) for up-spin electrons of sublattice C for $\varepsilon_1=-4$ eV, $\varepsilon_2=-2$ eV, $U_1=8$ eV, $U_2=4$ eV, $B=1.5$ eV, $B'=-0.30B$, $S=1/2$, and $n=1$.

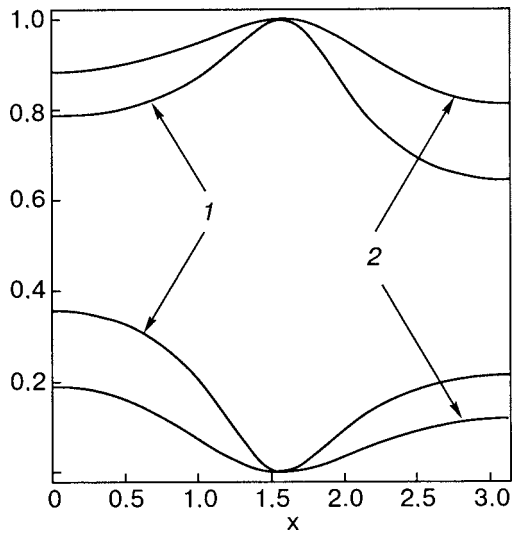

FIG. 4. Distribution function $\langle n_{k\sigma}\rangle$ versus k (lattice constant $a=1$) in the limit of a one-dimensional model taking account of hopping to nearest-neighbor sites of the crystal lattice with $B=1.5$ eV, $B'=-0.20B$, $S=1/2$, $n=1$, $\beta=1/kT=5$ eV^{-1}. Plot 1 corresponds to $\varepsilon_1=-4$ eV, $\varepsilon_2=-2$ eV, $U_1=8$ eV, $U_2=4$ eV; plot 2—$\varepsilon_1=-2$ eV, $\varepsilon_2=-1$ eV, $U_1=4$ eV, $U_2=2$ eV. The top plot in 1 and 2 corresponds to $\langle n_{k\downarrow}\rangle$ and the bottom plot to $\langle n_{k\uparrow}\rangle$.

Fermi level in a site of the C sublattice (in the ground state). For down-spin electrons of sublattice A a down-spin electron with probability 1 occupies a state on the boundary of the Brillouin zone (Fermi level).

Analyzing Figs. 2 and 3 it can be concluded that, apparently, the ground state of the Hubbard model studied here is an antiferromagnetic ground state.

The fluctuation-dissipation theorem and Eq. (10) can be used to obtain the following expression for the distribution function $\langle n_{k\sigma}\rangle$ at temperature T:

$$\langle n_{k\sigma}\rangle = \frac{1}{2}\left\{\left(1+\frac{\varepsilon'_{1\sigma}-\varepsilon'_{2k\sigma}}{2t_{k\sigma}}\right)f^{+}\left(\frac{\varepsilon'_{1\sigma}+\varepsilon'_{2k\sigma}}{2}+t_{k\sigma}\right)+\left(1-\frac{\varepsilon'_{1\sigma}-\varepsilon'_{2k\sigma}}{2t_{k\sigma}}\right)f^{+}\left(\frac{\varepsilon'_{1\sigma}+\varepsilon'_{2k\sigma}}{2}-t_{k\sigma}\right)\right\},$$

where $f^{+}(x)=1/(1+\exp(\beta x))$ and $\beta=1/kT$.

It follows from the exact solution[30] and also, for example, Ref. 4 that the distribution function is a continuous function and has no discontinuities on the "Fermi surface" (at the boundary of the Brillouin zone). Figure 4 shows plots of the distribution function in the right-hand half of the Brillouin zone for two values of the Coulomb potentials. It follows from the figure that the behavior of the distribution function depends on the magnitude of the Coulomb potential: as the Coulomb repulsion energy decreases, the form of the distribution function starts to depend less sharply on the magnitude of the vector **k** (we note that as the magnitude of the Coulomb potential decreases, the decrease in the value of the spin projection S must be taken into account in a self-consistent solution[25]).

In summary, the investigation of the single-particle Green's function shows that in the case of two dimensions with an exactly half-filled band the Hubbard model with strong interaction within the chosen approximation near the boundary of the Brillouin zone, apparently, starts to lose the properties of a Fermi liquid, but it cannot be reduced to a Luttinger liquid.

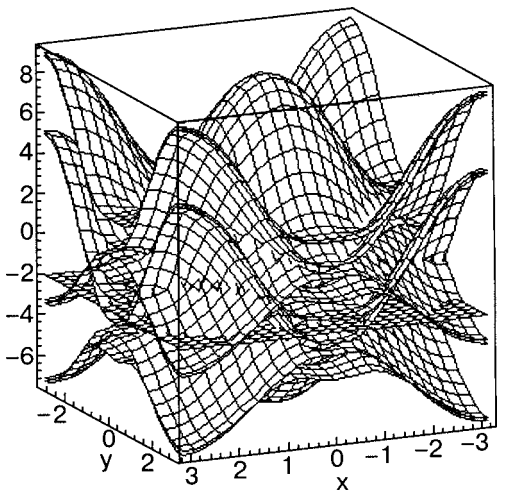

FIG. 5. Energy spectrum of the Hubbard model for weak interaction with $\varepsilon_1=\varepsilon_2=-2$ eV, $U_1=U_2=4$ eV, $B=1.5$ eV, $B'=-0.3B$, $S=0.15$.

It is of interest to study the case of weak coupling, since many works devoted to the investigation of the two-dimensional Hubbard model with weak interaction have appeared recently. Salmhofer recently developed a new method of renormalization for Fermi systems,[15,16] which can be used to solve the two-dimensional Hubbard model with weak interaction. Having solved the renormalization-group equations the authors of Refs. 17–22 showed that the Fermi-liquid picture is characteristic for the two-dimensional Hubbard model, and when the interaction energy is taken into account the Fermi surface becomes deformed compared with the case $U=0$.

It is shown in Ref. 25 that weak coupling corresponds to spin $0<S\ll 1/2$ (see Fig. 4 in Ref. 25). Consequently, in the weak-coupling limit there is no predominant orientation of the spin S (magnetization) within the sublattices. In this case the energy spectrum is a single band, obtained by the intersection of many branches (energy surfaces). Analysis of the energy spectrum and capacities of the corresponding energy

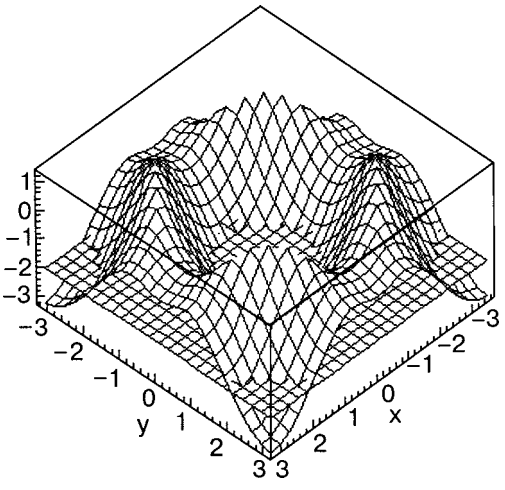

FIG. 6. Fermi surface obtained by the intersection of the energy surface and the plane corresponding to the Fermi level.

levels using Eqs. (5) and (6) shows that the Fermi surface is deformed compared with the case of a noninteracting system. Now, it is not the electrons near the boundary of the first Brillouin, as in the strong-coupling case, but rather the electrons near the Fermi surface, subjected to deformation when the finite value of the Coulomb potential is taken into account, that play the determining role in the system. Figure 5 shows the spectrum of elementary excitations together with the plane corresponding to the Fermi level. For clarity, Fig. 6 shows the energy surface from Fig. 5 near the Fermi level and the plane corresponding to the Fermi level, whose intersection gives the Fermi surface. It follows from Fig. 6 that the Fermi surface does indeed become deformed, in agreement with the results obtained previously using the renormalization-group analysis (see, for example, Refs. 20 and 21), and electrons fill the energy levels near the Fermi surface with a finite probability. This means that the anticommutator single-particle Green's functions have a pole near the Fermi surface, and therefore in the weak-correlation limit the Hubbard model is described within the framework of a normal Fermi liquid.

For the particular case of the one-dimensional model it can be shown[31] that in the static-fluctuations approximation spin and charge excitations characteristic for the exact solution of the one-dimensional Hubbard model[13] arise (we are talking about the calculation of the Green's functions and the correlation functions in terms of even excitations of the one-dimensional Hubbard model).

In conclusion, it can be noted that a linear chain of atoms in the Hubbard model is described within the framework of a Luttinger liquid, while the two-dimensional Hubbard model in the case of strong correlations near the boundary of the Brillouin zone apparently acquires features of a non-Fermi liquid system but cannot be reduced to a Luttinger liquid, and in the case of weak correlations it is described within the framework of a normal Fermi liquid. The preliminary results of this work were presented at the Winter School of Theoretical Physicists "Kourovka-2004."[31]

I thank R. O. Zaĭtsev and V. V. Val'kov for their interest in this work and for a discussion of the results, and R. R. Nigmatullin for his interest in this work and helpful suggestions.

[a)]E-mail: mir@mgpi.mari.ru

[1]P. W. Anderson, Phys. Rev. B **42**, 2624 (1992).
[2]P. W. Anderson and D. Kveshchenko, Preprint cond-mat/9506110 (1995).
[3]I. E. Dzyaloshinskiĭ and A. I. Larkin, Zh. Eksp. Teor. Fiz. **65**, 411 (1973) [JETP Lett. **38**, 202 (1974)].
[4]J. Solyom, Adv. Phys. **28**, 201 (1979).
[5]F. D. M. Haldane, J. Phys. C **14**, 2585 (1981).
[6]A. Luther, Phys. Rev. B **19**, 320 (1979).
[7]J. Carmelo and A. A. Ovchinnikov, J. Phys. C **3**, 757 (1991).
[8]H. J. Shulz, Phys. Rev. Lett. **64**, 2831 (1990).
[9]G. Benfatto and G. Gallavotti, Phys. Rev. B **42**, 9967 (1990).
[10]H. Frahm and V. E. Korepin, Phys. Rev. B **43**, 5653 (1991).
[11]J. Hubbard, Proc. R. Soc. London, Ser. A **276**, 1365 (1963); *ibid.*, p. 238 (1963).
[12]K. B. Blagoev and K. S. Bedell, Preprint cond-mat/9611240 (1996).
[13]H. Lieb and F. Wu, Phys. Rev. Lett. **20**, 1445 (1968).
[14]Yu. A. Izyumov, M. I. Katsnel'son, and Yu. N. Skryabin, *Magnetism of Itinerant Electrons*, Nauka, Moscow (1994).
[15]M. Salmhofer, Commun. Math. Phys. **194**, 249 (1998).
[16]M. Salmhofer, *Renormalization*, Springer-Verlag (1998).
[17]C. J. Halboth and W. Metzner, Phys. Rev. Lett. **85**, 5162 (2000).
[18]D. Zanchi and H. J. Schulz, Europhys. Lett. **44**, 235 (1998).
[19]C. J. Halboth and W. Metzner, Phys. Rev. B **61**, 4364 (2000).
[20]K. Louis, J. L. Alvares, and C. Gros, Preprint cond-mat/0103009 (2001).
[21]W. Metzner, C. Castellani, and C. D. Castro, Adv. Phys. **47**, 5 (1998).
[22]C. J. Halboth and W. Metzner, Preprint cond-mat/9908471 (1999).
[23]V. V. Loskutov, G. I. Mironov, and R. R. Nigmatullin, Fiz. Nizk. Temp. **22**, 282 (1996) [Low Temp. Phys. **22**, 220 (1996)].
[24]G. I. Mironov, Fiz. Tver. Tela (St. Petersburg) **39**, 1594 (1997) [Phys. Solid State **39**, 1420 (1997)].
[25]G. I. Mironov, Fiz. Tver. Tela (St. Petersburg) **41**, 951 (1999) [Phys. Solid State **41**, 864 (1999)].
[26]G. I. Mironov, Fiz. Tver. Tela (St. Petersburg) **44**, 209 (2002) [Phys. Solid State **44**, 216 (2002)].
[27]V. J. Emery, Phys. Rev. Lett. **58**, 2794 (1987).
[28]S. L. Malyshev and V. N. Popov, Theor. Math. Phys. **105**, 149 (1995).
[29]A. A. Abrikosov, L. P. Gor'kov, and I. E. Dzyaloshinskiĭ, *Methods of Quantum Field Theory in Statistical Physics*, Nauka, Moscow (1962); Prentice-Hall, Englewood Cliffs, New Jersey (1963).
[30]D. C. Mattis and E. H. Lieb, J. Math. Phys. **6**, 304 (1965).
[31]G. I. Mironov, in *Abstracts of Reports at the 30th International Winter School of Theoretical Physicists "Kourovka-2004,"* Ekaterinburg-Chelyabinsk (2004), p. 191-D.

Translated by M. E. Alferieff

Detection of fluctuation effects near the phase separation temperature of concentrated ^{3}He–^{4}He solid solutions

T. N. Antsygina, V. N. Grigor'ev, V. A. Maidanov, A. A. Penzev, S. P. Rubets, E. Ya. Rudavskii,[a)]
A. S. Rybalko, E. V. Syrnikov, and K. A. Chishko

B. Verkin Institute for Low Temperature Physics and Engineering, National Academy of Sciences of Ukraine, pr. Lenina 47, Kharkov 61103, Ukraine
(Submitted April 22, 2005)

A precision barometric study has revealed unusual behavior of the pressure of ^{3}He–^{4}He solid solutions with a concentration of around 30% ^{3}He: in the pre-separation region the pressure increases with decreasing temperature long before the start of the phase transition. It is established that such an anomaly is due to correlation effects in the impurity subsystem which give rise to large-scale fluctuations of the impurity concentration, and the fluctuation contribution to the pressure is much greater than the phonon contribution. Quantitative agreement between the experimental data and the proposed theory is obtained, and it is shown that the observed temperature dependence of the pressure in the pre-separation and metastable regions can be explained only when the long-range character of the interaction between impurities is taken into account.
 [DOI: 10.1063/1.2144456]

I. INTRODUCTION

The thermodynamic and kinetic properties of decomposing ^{3}He–^{4}He solid solutions have been the subject of many experimental and theoretical studies.[1–12] The primary focus of attention in those studies has been the details of the phase separation process, the evolution of the heterophase structure, and the anomalies of the thermodynamic quantities near the phase separation temperature T_s. At present it can be considered reliably established that for $T<T_s$ the thermodynamics of ^{3}He–^{4}He solid solutions is adequately described by the self-consistent field approximation (SCFA),[13] which in application to solid mixtures is usually called the regular solution model.[14] That approach has given good agreement of the theory with the experimental data on the jumps of the heat capacity[1] and pressure[2,3] upon phase separation, described the phase diagram of solid solutions of helium isotopes,[4] and yielded reliable information about the kinetics of separation.

As to the single-phase region in the immediate vicinity of the separation temperature, it remains little studied. It it known that the temperature dependence of the heat capacity observed experimentally in that region differs substantially from the predictions of the theory of regular solutions. In Refs. 10,11 it was pointed out that a fundamental role is played by fluctuation effects in the impurity subsystem of ^{3}He–^{4}He solid solutions, and the behavior of their heat capacity near the separation temperature was explained on the basis of these ideas. In those papers a consistent thermodynamic theory of decomposing mixtures of helium isotopes was constructed that can describe the properties of the system from a unified point of view across the entire range of temperatures and concentrations.

Comparatively recent advances in measurement technology have permitted registration of small pressure variations ($\leqslant 10^{-3}$ bar) to high accuracy against the background of the appreciable initial pressure ($P_i \simeq 35$-38 bar) necessary for crystallization of a ^{3}He–^{4}He solid solution.[7] Our present precision barometry experiments show that over a rather wide temperature interval in the pre-separation region and also in the metastable region a nontrivial temperature dependence of the pressure is observed which cannot be explained in the framework of the regular solution model. We believe that the cause of this behavior of the pressure in homogeneous mixtures of helium isotopes is the fluctuation contribution, which grows as the phase separation temperature T_s is approached.

The goal of the present study is to investigate experimental the behavior of $P(T)$ in solid solutions of helium isotopes in the pre-separation region and to interpret the observed effects on the basis of a consistent thermodynamic theory.

II. FEATURES OF THE EXPERIMENTAL TECHNIQUE

We investigated decomposing concentrated ^{3}He–^{4}He solid solutions by the technique used previously for studying dilute solutions of ^{3}He in ^{4}He (Ref. 7 and dilute solutions of ^{4}He in ^{3}He (Ref. 9. Precision measurements of the pressure at constant volume of the sample were made in the vicinity of the phase transition (both for $T>T_s$ in the homogeneous solution and for $T<T_s$ in the two-phase region). The samples were prepared from a gaseous mixture of pure helium isotopes containing approximately 30% ^{3}He, and the crystals were grown by the capillary blocking method. The samples were in a metal cell and were in the form of disks 9 mm in diameter and 1.5 mm in height. The cell was found in constant thermal contact with the mixing chamber, and its temperature was monitored by a ^{3}He melting curve thermometer and a resistance thermometer.

The sample solid solutions were annealed at a temperature of the order of 0.9 times the melting temperature for 24 hours and then, to improve the quality of the crystal and to permit obtaining reproducible results, they were subjected to a special thermocycling between the two-phase region and the homogeneous solution with almost total completion of the separation and homogenization processes within each

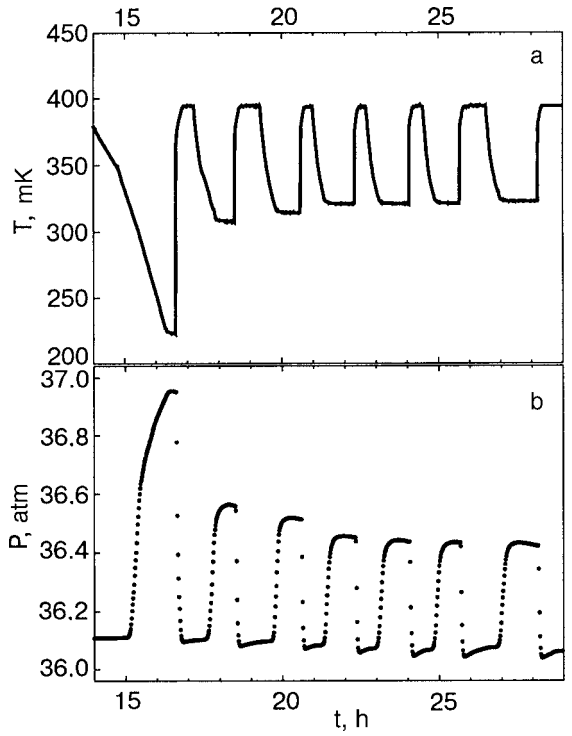

FIG. 1. Time dependence of the variations of the temperature (a) and pressure (b) during thermocycling of the sample with an initial concentration x_0=29.6% ^{3}He.

cycle. In the experiment we measured the time dependence of the variation of the pressure P in the process of cooling the solid solution from an initial temperature $T_i \simeq 440$ mK to different final temperatures $T_f < T_s$, which were held constant during the subsequent measurements.

Figure 1 shows a typical thermogram and the character of the pressure variation during the thermocycling. The rate of cooling of the sample, ~3 mK/min, was determined by the rate of cooling of the dilution refrigerator. As is seen in Fig. 1b, as the number of the cycle increases, the pressure in the homogeneous solution decreases somewhat in comparison with the initial cycle, apparently attesting to an improvement in the quality of the crystals due to annealing of defects and the healing of pores. Starting with the fourth cycle the pressure in the sample remained practically constant on further cycling. Analogous effects have been observed previously in the thermocycling of dilute solid solutions of helium isotopes.[7]

In the present study we did fifteen experiments on two samples. The characteristics of the samples and processes are presented in Tables I and II (P_i is the pressure in the homogeneous solution at temperature T_i, V is the molar volume of the solution, and x_0 is the initial ^{3}He concentration in the solution). Besides the experiments listed in Table II on the cooling of the solutions from an initial temperature T_i in the homogeneous region to a final temperature T_f in the separation region, we also did several experiments with stepwise cooling, during which the temperature was changed by small (8–10 mK) steps in the interval between T_i and T_f.

TABLE I. Initial characteristics of the samples studied.

Sample	x_0, % ^{3}He	V, cm^3 / mole	T_s, mK
A	29.6	21.22	358
B	32.3	21.84	374

TABLE II. Parameters illustrating the course of the experiments.

Exper. No.	P_i, bar	T_i, mK	T_f, mK
Sample A			
1	36.0998	384	346
2	36.1003	443	343
3	36.0954	437	344
4	36.1806	444	346
5	36.0982	442	344
6	36.0915	442	338
7	36.0907	442	337
8	36.0920	444	335
9	36.0898	444	333
10	36.4953	442	316
11	36.0940	443	348
12	36.1060	444	347
Sample B			
13	30.0222	442	382
14	30.0264	444	358
15	30.0164	442	442

III. DETERMINATION OF THE CONCENTRATION OF THE SOLID SOLUTION *IN SITU*

In working with ^{3}He–^{4}He solid solutions particular attention was paid to correct determination of the initial concentration of the isotopes in the mixture, since, owing to isotopic fractionation effects, upon creation of an elevated pressure with the aid of adsorbents and during crystal growth the concentrations of the components in the solid sample can differ noticeably from their concentrations in the initial gas mixture. Thus it is extremely important to have additional independent methods of estimating the concentration of the components in the solution.

Previously for dilute solutions of ^{3}He in ^{4}He and of ^{4}He in ^{3}He the initial concentration x_0 in the crystal was refined directly during the experiment from data on the change of pressure upon phase separation. Here we have made use of the circumstance that ^{3}He–^{4}He solid mixtures are described rather well by the regular solution theory,[4] according to which for a binary solution with a concentration x_0 of one of the components the addition Φ^E to the Gibbs thermodynamic potential due to the energy of mixing has the form

$$\Phi^E = Ax_0(1-x_0), \tag{1}$$

where $A=2T_c$, and T_c is the critical temperature, which is a function of only the pressure in the system (here and below we assume that Boltzmann's constant k_B is equal to unity, i.e., all of the quantities with dimensions of energy are measured in kelvin). For the pressure dependence of the parameter A the authors of Ref. 4 found the following empirical relation:

$$A = 0.76 - 4.38 \cdot 10^{-3}(P - 35.1), \tag{2}$$

where the pressure P is expressed in bar. Upon the isothermal formation of a homogeneous solution the change of the volume V^E of the system in comparison with the volumes of the pure components (the "excess" volume) is given by

$$V^E(x_0) = \left(\frac{\partial \Phi^E}{\partial P}\right)_T = x_0(1-x_0)\frac{\partial A}{\partial P}. \tag{3}$$

Since $\partial T_c/\partial P<0$, the excess volume $V^E(x_0)<0$. Below the separation temperature

$$V^E(x) = x(1-x)\frac{\partial A}{\partial P} > V^E(x_0), \tag{4}$$

because $x=x(T)<x_0$ is the concentration of the "dilute" phase (the local concentration of the impurity) in the solution, and it is clear that $|V^E(x)|<|V^E(x_0)|$. Thus on cooling below the separation temperature T_s the solution should have increased in volume by

$$\Delta V = [x(1-x) - x_0(1-x_0)]\frac{\partial A}{\partial P} > 0. \tag{5}$$

However, because in our experiments the separation occurs at a constant total volume V of the system, the pressure in it increases by the amount

$$\Delta P = \frac{\Delta V}{\beta_T V}, \tag{6}$$

where β_T is the isothermal compressibility,

$$\beta_T = -\frac{1}{V}\left(\frac{\partial V}{\partial P}\right)_T.$$

For a decomposing solution consisting of concentrated and dilute phases, it is necessary to use in the denominator of (6) the averaged quantity, which can be written as

$$\frac{1}{\beta_T V} = \frac{k}{\beta_c V_c} + \frac{(1-k)}{\beta_d V_d}. \tag{7}$$

Here

$$k = \frac{x_0 - x}{1-2x}$$

is the concentrated-phase fraction of the decomposing solution, and $V_{d(c)}$ and $\beta_{d(c)}$ are, respectively, the molar volume and compressibility of the dilute (concentrated) phase of the decomposing solution of ^{3}He in ^{4}He. Taking into account the symmetry of the separation diagram for concentrated solutions, we write

$$V_{d(c)} = V_{3(4)}x + V_{4(3)}(1-x) + V^E(x), \tag{8}$$

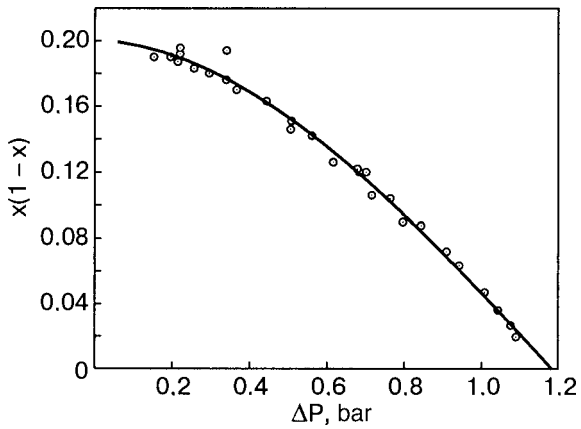

FIG. 2. Graphic representation of the technique of determining the initial concentration of the solution (see text).

$$\beta_{d(c)} = \beta_{3(4)}x + \beta_{4(3)}(1-x) - \alpha x(1-x), \tag{9}$$

where $V_{3(4)}$ and $\beta_{3(4)}$ are the molar volume and compressibility of pure ^{3}He(^{4}He). The term proportional to α is introduced to take into account the nonadditivity of the compressibility, which was noted in Ref. 12. Substituting (7) into (6), we finally get

$$\Delta P = \Delta V\left(\frac{k}{\beta_c V_c} + \frac{1-k}{\beta_d V_d}\right). \tag{10}$$

Figure 2 shows a plot of $x(1-x)$ versus ΔP from the experimental data for sample B. For dilute solutions, when the compressibility could be considered approximately constant, this dependence was linear[12] and could be used to find the initial concentration and compressibility. In the case under discussion this dependence is clearly nonlinear, but it can nevertheless be extrapolated to the value $\Delta P=0$ in order to estimate x_0. However, if relation (10) is used and the experimental data are processed by the least-squares method, then one can obtain a more accurate value for x_0 and can also find the value of α. As a result of such a processing we have found $x_0=(29.6\pm0.4)\%$ for sample A and $x_0=(32.3\pm0.5)\%$ for sample B, and a mean value $\alpha=(8.1\pm10^{-3})$. We note that if the value of $\partial A/\partial P$ is treated as an additional fitting parameter, then its mean value within the limits of error is -0.364 cm^3/mole, in agreement with the value that was found in Ref. 4 in the processing of a large number of experimental data.

IV. PRESSURE ANOMALY NEAR T_s

Our measured curves of the time dependence of the temperature $T(t)$ and pressure $P(t)$ in a concentrated ^{3}He–^{4}He solid solution on cooling from a temperature $T_i>T_s$ to a temperature $T_f<T_s$ are presented in Fig. 3. If it is assumed that in the homogeneous solution the pressure is due to the presence of phonons, then as the temperature decreases toward T_s, where the jumplike growth due to separation begins, the pressure should decrease ($\propto T^4$) in comparison with the initial pressure P_i. As is seen in Fig. 3b, in our case the behavior of the pressure is different: its growth as the separation temperature is approached begins long before T_s (the temperature T_s is indicated by an arrow in Fig. 3), and the dependence $P(t)-P_i$ is nonmonotonic in the vicinity of the

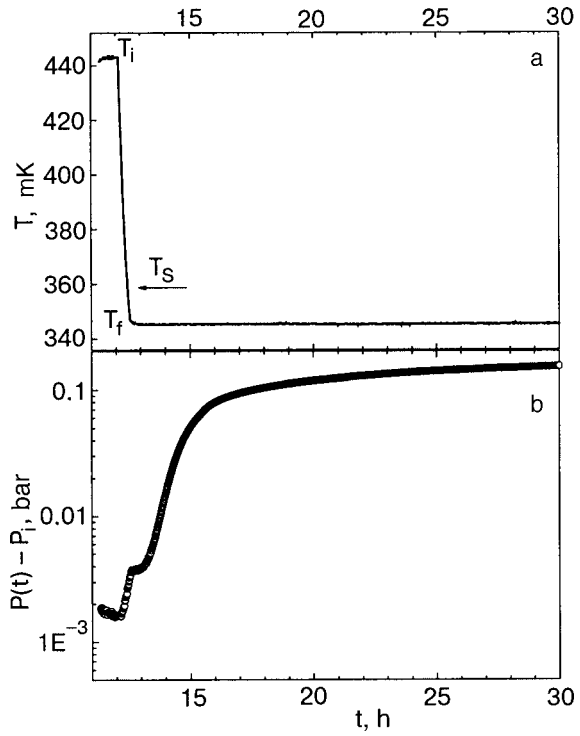

FIG. 3. Typical thermogram of the cooling of the sample with x_0 =29.6% ^{3}He, V=21.22 cm^3/mole in the phase separation region (a) and the corresponding pressure variation (b).

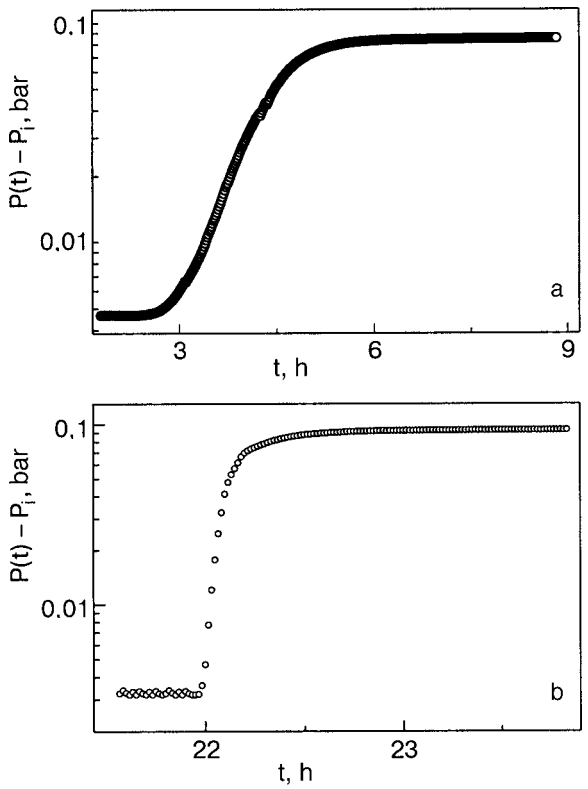

FIG. 4. Typical variation of the pressure upon phase separation of dilute ^{3}He–^{4}He solid solutions: solution of ^{3}He in ^{4}He($x_0 \simeq 2\%$ ^{3}He) (a), solution of ^{4}He in ^{3}He($x_0 \simeq 2\%$ ^{4}He) (b).

separation temperature. And, although the pressure growth in the pre-separation region is less than 1% of the total pressure jump at the phase transition (separation), this effect is plainly seen and well reproduced in experiment. That is the behavior we are calling anomalous and whose mechanism we shall discuss in this paper.

For comparison, in Fig. 4 we show the curves of $P(t) - P_i$ in dilute solutions of ^{3}He in ^{4}He (Fig. 4a) and ^{4}He in ^{3}He (Fig. 4b).[7,9] In both cases the aforementioned anomalous behavior of the pressure upon separation of concentrated solutions (Fig. 3b) was absent within the limits of experimental error. As was established in Refs. 1,2, for dilute solutions the variation of the pressure with time during separation is approximated by the function

$$P(t) = P_f - (P_f - P_i)\exp\left(-\frac{t}{\tau}\right), \tag{11}$$

where τ is the phase separation time constant. Relation (11) gives a good description of the experimental data from the time when the size of the new-phase inclusions can be regarded as practically independent of time.

Usually the time constant τ characterizing the relaxation of the pressure upon phase separation amounts to tens of minutes and sometimes hours, depending on the degree of supersaturation (supercooling).[7–9] The kinetics of the pressure change in the pre-separation region is of a completely different character, as is illustrated in Fig. 5, where the pressure variation upon a stepped temperature decrease is shown on a large scale. It is seen from the plots that the pressure follows the temperature change almost immediately.

The temperature dependence of the pressure in the pre-separation region (Fig. 6) shows that the pressure of a homogeneous solution found in a constant volume begins to grow with decreasing temperature long before the separation temperature is reached and continues into the metastable region $T < T_s$. This means that a nonphononic mechanism operates in that region. Keeping in mind the arguments made in Refs.

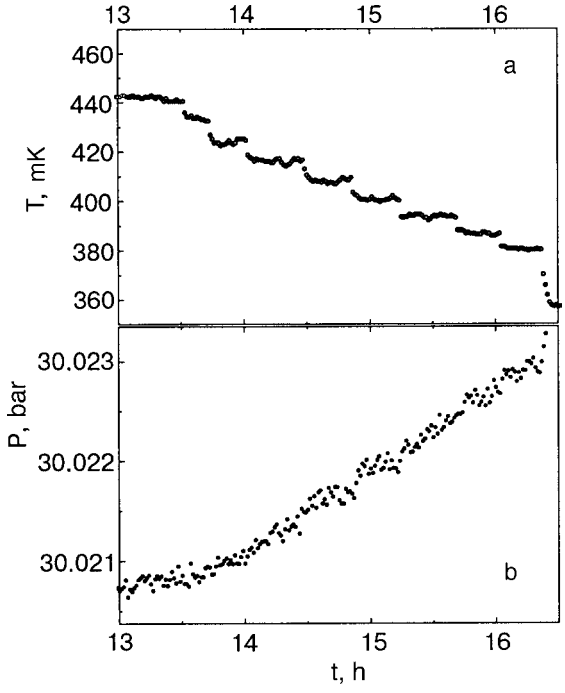

FIG. 5. Kinetics of the pressure variation in the separation region (b) upon a stepped decrease in temperature (a), x_0=32.3% ^{3}He, V=21.84 cm^3/mole.

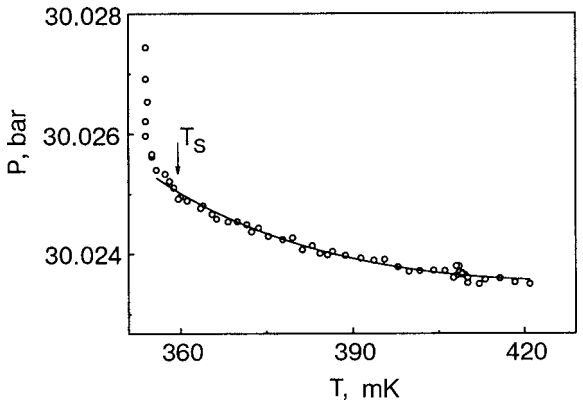

FIG. 6. Temperature dependence of the pressure in the separation region for samples with an initial concentration of 32.3% ^{3}He. The arrow indicates the phase separation temperature. The solid curve is a calculation according to Eq. (26).

10,11, one can naturally attribute the unusual temperature dependence of the pressure of a homogeneous ^{3}He–^{4}He solid solution to a manifestation of fluctuation effects.

V. INCORPORATION OF FLUCTUATION EFFECTS

As we have said, in the two-phase region the SCFA is entirely adequate for interpreting the behavior of the thermodynamic characteristics of solutions of helium isotopes, but in the single-phase region near the separation temperature, where the role of fluctuations becomes important, that approximation dies not permit a qualitatively correct description of the observed effects.

The fluctuation contribution to the thermodynamics of a decomposing solution can be taken into account as a correction to the corresponding thermodynamic quantities calculated in the SCFA.[10,11] Below we shall use a rather simple and well-known model for the energy of interaction between impurities, which essentially reduces to the following. The interaction of an atom located at a site $\mathbf{f}$ with the other impurities is assumed constant (equal to U_0) up to a certain coordination sphere of radius R_0, within which are found z atoms interacting with the given atom. The interaction with the atoms found outside that sphere is assumed equal to zero. Thus the energy of the pair interaction of the impurity atoms, $U_{\mathbf{ff}'}=U(|\mathbf{f}-\mathbf{f}'|)$, has the form

$$U\mathbf{ff}'=\begin{cases} U_0 & |\mathbf{f}-\mathbf{f}'|\leqslant R_0, \\ 0 & |\mathbf{f}-\mathbf{f}'|>R_0. \end{cases} \tag{12}$$

The radius R_0 and the parameter z, which we shall refer to below as the effective coordination number, are related by

$$z=\frac{4\pi R_0^3}{3\omega_0}, \tag{13}$$

where ω_0 is the volume per site. Thus the parameter z serves to characterize the interaction radius and is treated as an adjustable parameter in the comparison of theory with experiment.

In the SCFA one has for the free energy[10]

$$F=\frac{T_c}{2}\sigma^2-T\ln\left(2\cosh\frac{T_c}{T}\sigma\right), \tag{14}$$

where σ is the order parameter, which is related to the concentration x in the separated phases as

$$\sigma=1-2x. \tag{15}$$

The critical temperature T_c is expressed in terms of the interaction energy U_0 as follows:

$$T_c=U_0\frac{z}{4}. \tag{16}$$

The order parameter satisfies the equation of self-consistency

$$\sigma=\tanh T_c\frac{\sigma}{T} \tag{17}$$

and should be found as a solution of Eq. (17) up until the it has reached the limiting value $\sigma_0=1-2x_0$ corresponding to a homogeneous solution with the mean concentration x_0. The temperature at which σ becomes equal to σ_0 is just the separation temperature T_s:

$$T_s^{-1}=\frac{1}{2T_c\sigma_0}\ln\left(\frac{1+\sigma_0}{1-\sigma_0}\right). \tag{18}$$

Upon the transition to the single-phase region ($T>T_s$) the order parameter become independent of temperature and maintains a constant value σ_0.

The pressure is related to the free energy F of the system by the well-known relation

$$P=-\left(\frac{\partial F}{\partial V}\right)_T. \tag{19}$$

As a result, using Eq. (14) we obtain for the excess pressure due to phase separation

$$\Delta P=\frac{\sigma^2-\sigma_0^2}{2}\frac{\partial T_c}{\partial V}. \tag{20}$$

One is readily convinced that Eq. (20) agrees with expression (6).

Relation (20), obtained in the framework of the SCFA, gives a good quantitative description of the behavior of the pressure of a solution only in the two-phase region. Since the SCFA completely ignores the presence of fluctuations in the system, for a correct description of a homogeneous solution it is necessary to calculate the fluctuation contribution to the pressure, ΔP_{fl}. For this purpose we use the expression for the fluctuation correction ΔF_{fl} to the free energy found in Refs. 10,11:

$$\Delta F_{\mathrm{fl}}=\frac{T}{2N}\sum_{\mathbf{q}}\ln\left[1-\frac{u(\mathbf{q})}{4T_c\lambda_0}\right], \tag{21}$$

where

$$\lambda_0^{-1}=\frac{T_c}{T}(1-\sigma^2), \tag{22}$$

$u(\mathbf{q})$ is the Fourier transform of the function $U_{\mathbf{ff}'}$, and n is the total number of sites. Since the impurity–impurity interaction radius is of the order of $z^{1/3}$, the main contribution to the sum

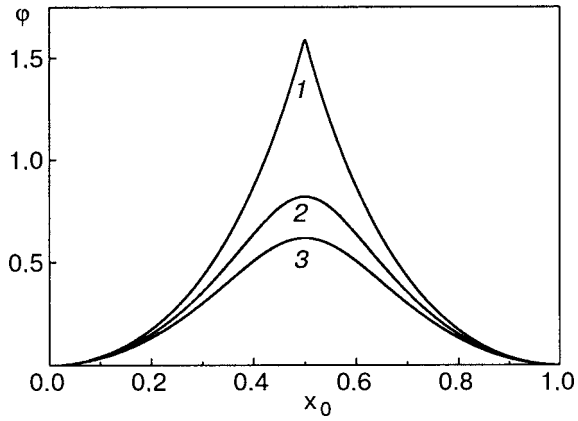

FIG. 7. Concentration dependence of the function $\varphi(\lambda_0(x_0))$ determining the fluctuation contribution to the pressure: *1*—$T/T_c=1.0$, *2*—$T/T_c=1.05$, *3*—$T/T_c=1.1$.

(21) is given by terms with $0<q\leqslant q_0\sim z^{-1/3}$. For the model of the interaction potential used in this study, Eq. (12), the Fourier transform $u(\mathbf{q})$ has the form

$$u(\mathbf{q})=U_0 z f(qR_0), \quad f(y)=\frac{3}{y^3}(\sin y - y\cos y). \tag{23}$$

The function $f(y)$ in the interval from the origin of coordinates to its first zero can be approximated to good accuracy by a parabola of the form

$$f(y)\simeq 1-\left(\frac{y}{4}\right)^2,$$

having set $f(y_0)=0$ for $y>4$. As a result

$$u(\mathbf{q})=\begin{cases} U_0 z[1-(-q/q_0)^2] & q\leqslant q_0, \\ 0 & q>q_0. \end{cases} \tag{24}$$

The value of q_0 is related to the effective coordination number z by the relation

$$q_0=\frac{4}{R_0}=4\left(\frac{4\pi}{3z\omega_0}\right)^{1/3}. \tag{25}$$

Using Eq. (19) and changing from a sum to an integral in the expressions for $\Delta P_{\rm fl}$, we find that the fluctuation contribution to the pressure in the homogeneous phase and in the metastable region has the form

$$\Delta P_{\rm fl}=-\frac{32T}{9\pi z T_c V_0 \beta_0}\frac{\partial A}{\partial P}\varphi(\lambda_0), \tag{26}$$

where

$$\varphi(\lambda_0)=3\lambda_0\left(1-\sqrt{\lambda_0-1}\,\arctan\frac{1}{\sqrt{\lambda_0-1}}\right)-1-\frac{2}{5\lambda_0}, \tag{27}$$

$\lambda_0^{-1}=4x_0(1-x_0)T_c/T$, and the molar volume V_0 and compressibility β_0 are determined by relations (8) and (9), respectively: $V_0=V_d(x_0)$, $\beta_0=\beta_d(x_0)$. It follows from (27) that in the temperature region corresponding to the homogeneous solution, for any fixed T the fluctuation contribution to the pressure will be the larger the higher the initial concentration of the impurity component ($x_0\leqslant 50\%$) in the solution. Figure 7 shows the dependence $\varphi(\lambda_0(x_0))$ for three values of temperature. Analysis shows that in the concentration region $0\leqslant x_0\leqslant 0.45\%$ the function $\varphi(\lambda_0(x_0))$ is very well approximated by a dependence $\varphi(\lambda_0(x_0))=Ax_0^B$, where the parameters A and B depend weakly on temperature, and at $T=T_c$ they take the values $A=5.46$ and $B=2.11$.

VI. COMPARISON OF THEORY WITH EXPERIMENT

The total pressure in the system can be represented as the sum

$$P=P_0-\Delta P_{\rm fl}+\Delta P_{\rm ph}, \tag{28}$$

where P_0 is the pressure of the solution at $T=0$, and $\Delta P_{\rm ph}$ is the phonon contribution to the pressure.

Since the Debye temperature Θ of solid helium is much higher than its melting temperature, the phonon contribution to the pressure can be described adequately in the Debye approximation (see, e.g., Ref. 15:

$$\Delta P_{\rm ph}=-\frac{3\pi^4}{5V}\gamma_0 T\left(\frac{T}{\Theta}\right)^3, \tag{29}$$

where $\gamma_\theta=\partial\ln\Theta/\partial\ln V$ is the Grüneisen constant. Since the Grüneisen constants for the pure components ^{3}He and ^{4}He are quite close,[16,17] we take for γ_Θ the average value ($\gamma_\Theta\simeq 2.8$) corresponding to the molar volume of the solution under study. As to the Debye temperature there is as yet no reliable data on its value for ^{3}He–^{4}He solid mixtures, and one should therefore take Θ in formula (29) as an adjustable parameter.

Figure 6 shows the theoretical and experimental temperature dependence of the pressure for a solution with a ^{3}He concentration of 32.3%. It is seen that the agreement between theory and experiment is very good over the entire temperature range. Figure 8 demonstrates the temperature dependence of the fluctuation and phonon contributions. The fluctuation contribution is dominant across the entire temperature region in which measurements were made.

For comparison of the theory with experiment we fit three parameters: P_0, z, and Θ. Their values found from the condition of best agreement of the theory and experiment are presented in Table III, from which it is seen that P_0 is extremely close to the experimental values of the initial pressure P_i of the homogeneous solution; this is quite natural, since the measurements were made at rather low temperatures. The Debye temperatures turned out to be equal to (24.3 ± 1.8)K and (24 ± 3)K at molar volumes of 21.22 and 21.84 cm^3/mole, respectively. These values agree precisely with the values of Θ found under the assumption that the rule of additivity holds for the Debye temperature.

From a comparison of the experimental data with the theory we also determined the fundamental parameter of the theory—the effective coordination number z, which has the meaning of the number of atoms enclosed in a sphere of radius R_0 [the correlation radius, which determines the spatial scale of the interactions (12)]. The mean value of this parameter for the solutions with $V=21.22$ cm^3/mole and $V=21.84$ cm^3/mole is found to be approximately 800. Although the values found for z agree in order of magnitude with those found previously[10,11] through an interpretation of experiments on the heat capacity of concentrated ^{3}He–^{4}He solid solutions, they exceed the latter by a factor ranging

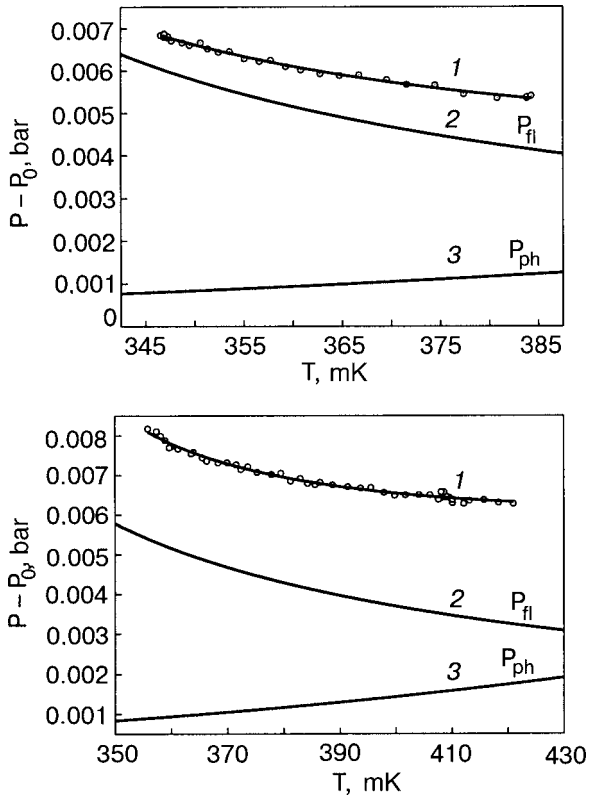

FIG. 8. Fluctuation and phonon contributions to the pressure variation for samples with molar volumes $V=21.22$ cm^3/mole (a) and $V=21.84$ cm^3/mole (b). *1*—Total pressure variation; *2*—$\Delta P_{\rm fl}$ according to Eq. (26); *3*—$P_{\rm ph}$ according to Eq. (29).

TABLE III. Values of the adjustable parameters in the theory.

Exper. No.	P_0, bar	Θ, K	z
Sample A			
V = 21,22 cm^3 / mole			
1	36.0937	20.7	774
2	36.0948	22.6	760
3	36.0959	26.1	917
4	36.0948	23.7	839
5	36.0938	25.6	879
6	36.0866	23.6	805
7	36.0864	27.6	831
8	36.0870	24.3	804
9	36.0852	26.4	912
10	36.0901	23.7	762
11	36.0892	24.3	821
12	36.0877	23.5	795
Sample B			
V = 21,84 cm^3 / mole			
13	30.0146	18.9	720
14	30.0191	21.9	723
15	30.0153	29.3	660

from of about two and one-half to three. This discrepancy may be due to the fact that, unlike the heat capacity, which depends only on z and T_c, the fluctuation correction to the pressure depends on three parameters: Eq. (26) contains not only z but also $\partial T_c/\partial V$, which is known to lower accuracy than T_c, and also the compressibility β_T, for which no experimental data have been published and whose value we therefore estimated essentially from phenomenological arguments of the type in Eq. (7). One might also note a more physical cause of the discrepancy, due to the different experimental conditions. In the present study we measured the heat capacity of a bulk sample, while the heat capacity of a solution found in pores of the coolant was measured in Ref. 1. It is quite possible that under conditions of restricted geometry the fluctuation effects are weakened, and that leads to a lowering of z. Thus the agreement in the values of z extracted from heat-capacity and pressure data can be regarded as reasonable, corresponding to a radius R_0 of six to eight coordination spheres.

On the other hand, such a large value of z and, consequently, of the number of atoms that effectively interact with each other, means that viable new-phase nuclei arise against the background of large-scale fluctuations that promote the realization of a phase transition. The fluctuation contribution is particularly significant at large impurity concentrations, when the distance between impurity atoms is comparable to the interatomic distance, the elastic fields of the impurities overlap, and the effective interaction between them becomes quasi-isotropic while retaining its long-range character. The good agreement of the experimental and calculated temperature dependence of the excess pressure in both the preseparation and metastable regions attests that the model proposed in Refs. 10,11 for taking into account correlation effects in ^{3}He–^{4}He solid solutions is faithful to the real thermodynamic behavior of the systems under discussion.

We note that for dilute solutions of ^{3}He and ^{4}He or ^{4}He in ^{3}He the contribution of fluctuation effects to the pressure variation is small, in proportion to to the small concentration of the impurity component, and the pressure variations due to that contribution can be registered experimentally only at a substantially higher accuracy of measurement. As a result, in a homogeneous dilute solution only the phonon contribution to the pressure is observed in experiment. This conclusion also follows directly from an analysis of the function $\varphi(\lambda_0(x_0))$ (see Fig. 7). Thus, at a fixed temperature for dilute solutions with a concentration of the impurity component of the order of 2–3%, the value of the function φ turns out to be two orders of magnitude smaller than the corresponding value for the concentrated solutions investigated in the present study. It should be kept in mind, however, that in the transition to dilute solutions there is a decrease in the value of the effective coordination number z, which appears in the diameter of relation (26) from which $\Delta P_{\rm fl}$ is determined. A detailed analysis in Refs. 10,11 showed that starting from an x_0 value of the order of a few percent, the value of z depends

weakly on the initial concentration of the solution, so that the dependence of ΔP_{fl} on x_0 will be determined mainly by the behavior of the function $\varphi(\lambda_0(x_0))$.

VII. CONCLUSION

Our experimental and theoretical investigations of the behavior of the pressure in homogeneous concentrated ^{3}He $-^4$He solid solutions near the phase separation region unambiguously attests to the presence of anomalous temperature dependence of the pressure due to correlation effects in the subsystem of the impurity atoms. The analysis done has also led to the clear conclusion that the available experimental results can be interpreted successfully under the assumption that the interaction between impurities is of a long-range character. This long-range character is taken into account directly by the introduction of an effective interaction radius R_0 (or the related parameter z). Fluctuations in the impurity subsystem give rise to new-phase nuclei in the form of compact formations (clusters) containing hundreds of atoms. This effect leads to an increase of the pressure in the solution long before the phase transition temperature is reached.

The increase of the pressure due to fluctuations of the order parameter (density) as the phase separation point is approached from the side of the homogeneous solution in solid mixtures undergoing decomposition at low temperatures is in principle an effect that follows from general thermodynamic arguments and should therefore be expected to appear in other systems, such as dispersion-hardened metal alloys. However, there are no data in the literature on the observation of pressure-fluctuation effects in classical (nonquantum) solutions. The reason is that decomposition in classical systems occurs at high temperatures, where the contribution from density fluctuations is overwhelmed by the much stronger phonon contribution. In the quantum solid solutions ^{3}He$-^4$He phase separation occurs at much lower temperatures, where the phonon energy and, hence, the phonon contribution to the effects under discussion are small, and at high enough densities of the impurity component in the solution the order-parameter fluctuations, which grow with decreasing spinodal temperature, will be dominant.

This study was supported by the Ukrainian Government Foundation for Basic Research (Project 02.07/00391, Contract F7/286-2001).

[a)]E-mail: rudavskii@ilt.kharkov.ua

[1]D. O. Edwards, A. S. McWilliams, and J. G. Dount, Phys. Rev. Lett. **9**, 195 (1962).
[2]W. J. Mullin, Phys. Rev. Lett. **20**, 254, (1968).
[3]M. F. Panczyk, R. A. Scribner, J. R. Gonano, and E. D. Adams, Phys. Rev. Lett. **21**, 594 (1968).
[4]D. O. Edwards and S. Balibar, Phys. Rev. B **39**, 4083 (1989).
[5]R. P. Haley and E. D. Adams, J. Low Temp. Phys. **110**, 121 (1998).
[6]S. C. J. Kingsley, V. Maidanov, J. Saunders, and B. Cowan, J. Low Temp. Phys. **113**, 1017 (1998).
[7]A. N. Gan'shin, V. N. Grigor'ev, V. A. Maĭdanov, N. F. Omelaenko, A. A. Penzev, E. Ya. Rudavskiĭ, A. S. Rybalko, and Yu. A. Tokar, Fiz. Nizk. Temp. **25**, 796 (1999) [Low Temp. Phys. **25**, 592 (1999)].
[8]A. Smith, V. Maidanov, E. Rudavskii, V. Grigor'ev, V. Slezov, M. Poole, J. Saunders, and B. Cowan, Phys. Rev. B **67**, 245314 (2003).
[9]V. N. Grigor'ev, V. A. Maĭdanov, A. A. Penzev, Ye. Ya. Rudavskii, A. S. Rybalko, V. V. Slezov, and E. V. Syrnikov, Fiz. Nizk. Temp. **30**, 177 (2004) [Low Temp. Phys. **30**, 128 (2004)].
[10]T. N. Antsygina, V. A. Slyusarev, and K. A. Chishko, Fiz. Tverd. Tela (St. Petersburg) **40**, 355 (1998) [Phys. Solid State **40**, 325 (1998)].
[11]T. N. Antsygina, K. A. Chishko, and V. A. Slusarev, J. Low Temp. Phys. **111**, 577 (1998).
[12]V. N. Grigor'ev, V. A. Maidanov, A. A. Penzev, A. V. Polev, S. P. Rubets, E. Ya. Rudavskii, A. S. Rybalko, and E. V. Syrnikov, Fiz. Nizk. Temp. **31**, 43 (2005) [Low Temp. Phys. **31**, 32 (2005)].
[13]R. H. Brout, *Phase Transitions*, Benjamin, New York (1965), Mir, Moscow (1967).
[14]I. Prigogine, *The Molecular Theory of Solutions*, Amsterdam, North–Holland (1957).
[15]S. Trickey, W. Kirk, and E. Adams, Rev. Mod. Phys. **44**, 668 (1972).
[16]D. S. Greywall, Phys. Rev. B **16**, 5127 (1977).
[17]D. S. Greywall, Phys. Rev. B **15**, 2604 (1977).

Translated by Steve Torstveit

SHORT NOTES

Relaxation of the magnetization of superconducting YBCO samples in weak magnetic fields

V. P. Timofeev[a] and A. N. Omel'yanchuk

B. I. Verkin Institute for Low Temperature Physics and Engineering of the National Academy of Sciences of Ukraine, pr. Lenina 47, Kharkov 61103, Ukraine

Yu. T. Petrusenko

National Science Center "Kharkov Physicotechnical Institute," ul. Akademicheskaya 1, Kharkov 61108, Ukraine

(Submitted June 17, 2005)

The first investigations are performed of the magnetization and isothermal relaxation of the magnetization of high-temperature superconducting samples with different crystal structure in very weak constant fields ($H \leqslant 0.5$ Oe) at temperatures close to the critical value. It is shown that the twinning boundaries in YBCO single crystals strongly influence the relaxation rate of the magnetization. The collective pinning model is used to estimate the effective pinning potential under these conditions. This estimate can be used to characterize the degree to which artificially produced point defects affect the critical currents of MgB_2 samples. © *2005 American Institute of Physics*. [DOI: 10.1063/1.2144460]

1. Experimental works studying the pinning of magnetic flux in type-II superconductors (SPs) focus on determining the maximum current-carrying capacities in strong magnetic fields.[1,2] The use of highly sensitive squids in contact-free magnetic susceptibility meters makes it possible to perform investigations in weak fields (0.01–0.1) Oe and even observe spontaneous magnetic moments.[3,4] In developing high-temperature superconductor (HTSC) squids, the investigations of the dynamics of magnetic vortices in weak magnetic fields ($\leqslant 1$ Oe) are especially important for decreasing in sensors the intrinsic noise which is often associated with creep and hops of vortices. This noise is decreased, in part, by producing artificial pinning centers.[5]

The objective of the present communication is to present the characteristics of the behavior of the magnetization $M(T,t)$ of $YBa_2Cu_3O_{7-x}$ (YBCO) single crystals in very weak constant magnetic fields ($\mathbf{H} \ll 0.5$ Oe) near the SC transition. Samples with different crystal structure were investigated to determine the influence of thermally activated transformation of Josephson weak links on the potential of pinning centers in a system of unidirectional twin boundaries (TBs). The main measurements were performed at temperatures close to 77 K so that the results obtained could be used in the development of liquid-nitrogen-cooled SC electronics.

2. The resistive state in the superconductors investigated arises at the outset of the motion of magnetic vortices, when the Lorentz force acting on a vortex starts to exceed the pinning force. Under the action of this force and thermal activation, occurring with probability $\sim \exp(-U/kT)$, the vortices start to move, and energy dissipation arises (U—effective activation energy of vortex hopping, equal to the average depth of the pinning potential; k—Boltzmann's constant; T—temperature). These processes also determine the critical current of the SC (I_c).

An ideal SC placed in a weak magnetic field should be in a Meissner state. In real SCs of finite size, as a result of the presence of surface and volume defects the magnetic field at temperatures close to the critical value starts to penetrate into the sample even for $\mathbf{H} < \mathbf{H}_{c1}$ ($\mathbf{H}_{c1}$ is the first critical field of an ideal defect-free ellipsoidal SC).[6] Thermally activated creep of individual vortices results in redistribution and damping of the supercurrents and relaxation of M.

The data from the investigation of magnetic relaxation in SCs are used to obtain the most important parameters of the vortex pinning mechanism. In the simplest case the effective depth of the pinning potential can be estimated from measurements of the rate of isothermal relaxation of $M(t)$:

$$1/M_0(dM/d\ln t) = -kT/U, \tag{1}$$

where M_0 is the initial value of the magnetization, which, as a rule, is taken to be the magnetization in Bean's critical state.[2] However, virtually all published studies concerning the relaxation of the magnetization of SCs have been performed in strong magnetic fields (hundreds of Oe or even several kOe), when complicated processes in rigid, well-formed lattice of magnetic vortices play a large role. As shown in Ref. 7, from the standpoint of the theory of collective pinning in weak magnetic fields, creep of noninteracting vortices occurs, the velocity of the magnetic flux is independent of the magnitude of the magnetic field, and the results of the measurements are insensitive to the deviation of the magnetic field from the direction of the c axis of the HTSC sample.

3. Impurity-free oriented YBCO single crystals were chosen as the main object of the investigations.[8] Annealing, required to obtain optimal doping, in oxygen results in a transformation of the initial structure of the crystals and, in consequence, the formation of TBs. We chose two types of samples (with dimensions close to 1×1 mm, thickness

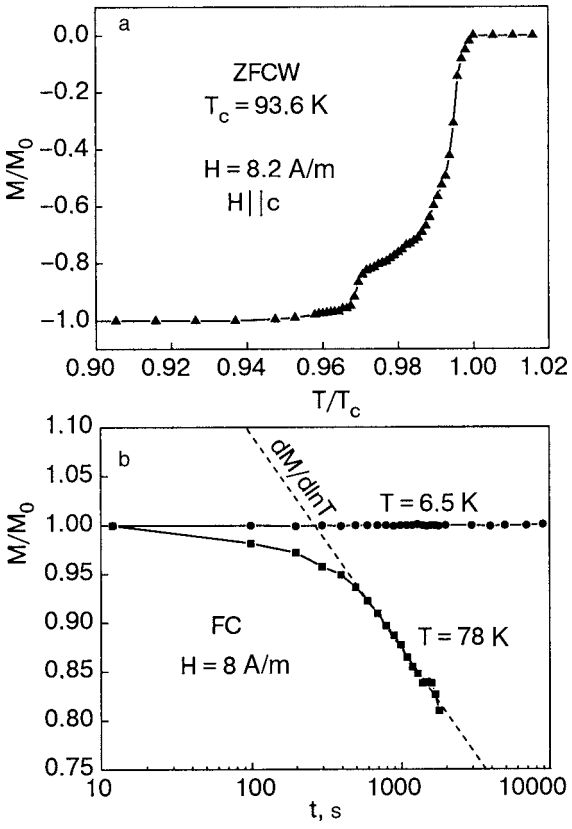

FIG. 1. Normalized function $M(T)$ in the region of the superconducting transition in YBCO single crystal No. 1 with unidirectional TBs (a) and magnetization dynamics of the same sample in a magnetic field 8 A/m (≈0.1 Oe) for two values of the temperature (b). The dashed line shows the average slope of the linear section of the dependence. This slope is used to estimate the effective pinning potential. ZFCW—zero field cooled warming.

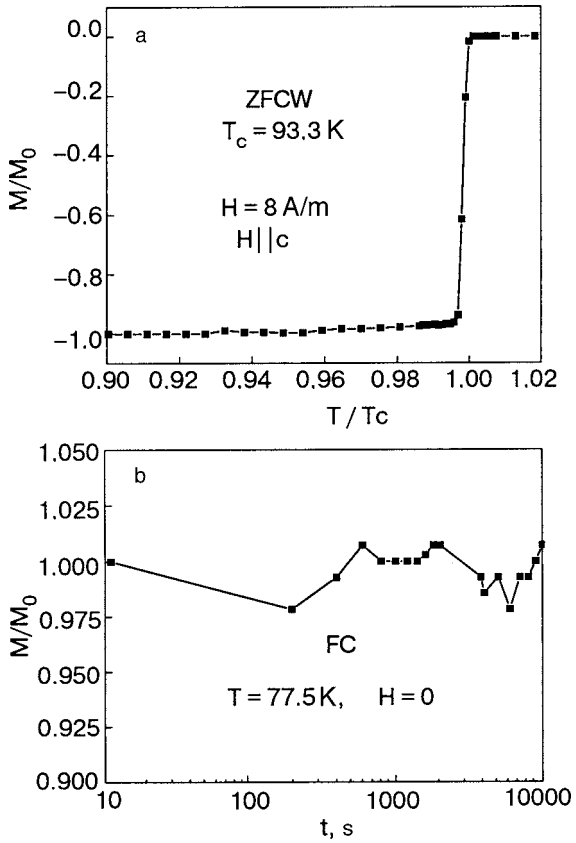

FIG. 2. Magnetic response near the superconducting phase transition in single-crystal YBCO sample No. 4 with multidirectional twin boundaries in magnetic field 8 A/m parallel to the c axis of the crystal (a) and time dependence of the magnetization of a $Bi_2Sr_2Ca_2Cu_3O_{10}$ polycrystal in zero field at temperature 77.5 K (b).

≈0.015 mm) to investigate the role of these planar defects on pinning processes: in some samples unidirectional TBs were oriented parallel to the c axis of the crystal over its entire thickness and other samples contained blocks with multidirectional TBs. For comparison the magnetic responses and the relaxation of the magnetization of polycrystalline YBCO samples with randomly oriented grainy structure and textured $Bi_2Sr_2Ca_2Cu_3O_{10}$ ceramics are discussed.

The investigations of the dependences $M(T,t)$ near a phase transition in weak fields were performed using a magnetic susceptibility meter based on a squid-gradiometer with liquid-helium level cooling. The standard procedure for measuring M with a constant current in a uniform magnetic field of a solenoid was used. The Earth's residual magnetic field in this region was screened and did not exceed 0.5 mOe. This made it possible to cool the sample and transfer it into the SC state using ZFC (Zero Field Cooling), which is preferable for investigating $M(T)$. To analyze $M(t)$ the sample was cooled to ≈77 K in a magnetic field ≈0.5 Oe, i.e. according to the FC method (Field Cooling), after which the field was screened, a chosen value of T was set, and the behavior of $M(t)$ was recorded.

Figure 1a shows the normalized function $M(T)$ with temperature increasing in the region of the superconducting transition in one of the experimental YBCO single crystals with unidirectional TBs. The magnetic field of the solenoid is oriented along the c axis of the single crystal and its magnitude is 8.2 A/m (≈0.1 Oe). For this direction the field is parallel to the planes of the TBs, and Abrikosov vortices are pinned most effectively. As seen in Fig. 1a the curve of the SC transition, in contrast to the data from resistive measurements,[8] is nonmonotonic and occupies a substantial temperature interval $\Delta T \approx 5$ K. A smoothed step is observed in this dependence. This step cannot be explained by the theory of melting of a vortex lattice,[1] considering the low values of H used in the experiment. Figure 1b shows the temporal dynamics of $M(t)$ of this single crystal. For sample temperature $T=78$ K, initially, $M(t)$ is nonlogarithmic and at long times it behaves according to the Anderson–Kim model. The value of U estimated from the expression (1) is of the order of 0.2 eV, which agrees with data obtained by other authors for HTSC samples in strong magnetic fields.[2] The behavior of $M(t)$ of the same sample at low temperature ($T=6.5$ K) is presented in this figure. As one can see, relaxation of supercurrents is not observed. This can be explained by the exponential decrease of the thermal creep of magnetic flux and the presence of Josephson links, which are not suppressed by a magnetic field, near the TBs.[3] An additional argument in support of the latter assertion are the data in Fig. 2a, which shows the normalized function $M(T)$ for a YBCO single crystal which contains blocks of multidirectional TBs. The boundaries of the blocks with mutually perpendicular planes of the TBs give rise to the formation of strong pinning centers. The superconducting phase transition becomes

sharper ($\Delta T_c \approx 0.3$ K), and no magnetization relaxation is observed in this sample at 78 K.

For comparison, the polycrystalline HTSCs $YBa_2Cu_3O_{7-x}$ and $Bi_2Sr_2Ca_2Cu_3O_{10}$ were investigated in weak magnetic fields. The superconducting granules of a polycrystal are coupled with one another randomly by barriers with different transmissivities, forming statistically distributed networks with circulating induced or spontaneous supercurrents. The latter can exist under certain conditions in chaotic current loops of HTSCs, engendering paramagnetic responses. Figure 2b shows the behavior of the normalized magnetization of a polycrystalline $Bi_2Sr_2Ca_2Cu_3O_{10}$ sample at 77.5 K.

The results of our experiments with single crystal samples of YBCO give a basis for supposing that the planes of the TBs create the conditions required for the formation of Josephson networks with randomly distributed parameters. The TBs have a strong local effect on the suppression of the superconducting order parameter, and they lower the energy of the trapped vortex lines. Considering the fact that in a 0.1 Oe field the intervortex distance ($\approx 10^4$ nm) is greater than the intertwin distance ($\approx 10^3$ nm) and is comparable to the penetration depth of the field in the given temperature interval ($\approx 10^4$ nm), it can be expected that all vortices are localized on TBs.

4. In summary, we have performed the first investigations of $M(T)$ and $M(t)$ of HTSC samples with different crystal structure in very weak fields ($\leqslant 0.1$ Oe) and at temperatures close to the critical value. It was shown that TBs in single crystals have a strong effect on the relaxation rate of the magnetization, and the collective pinning model was used to estimate the effective pinning potential under these conditions. The method of contact-free determination of U, described above, is now used to estimate the degree to which artificially created pinning centers influence I_c in MgB_2 samples. Point defects were produced in the volume of a SC using controlled doses of irradiation from a linear electron accelerator.

We thank A. V. Bondarenko for providing the single-crystal samples and V. N. Samovarov for fruitful discussions. This work was partially supported by a UNTTS grant under project No. 655A.

[a)]E-mail: timofeev@ilt.kharkov.ua

[1]G. Blatter, M. V. Feigel'man, V. B. Geshkenbein, A. I. Larkin, and V. M. Vinokur, Rev. Mod. Phys. **66**, 1125 (1994).
[2]Y. Yeshurun, A. P. Malozemoff, and A. Shaulov, Rev. Mod. Phys. **68**, 911 (1996).
[3]V. P. Timofeev and A. V. Bondarenko, Fiz. Nizk. Temp. **30**, 810 (2004) [Low Temp. Phys. **30**, 610 (2004)].
[4]Yu. A. Kolesnichnko, A. N. Omel'yanchouk, and A. M. Zagoskin, Fiz. Nizk. Temp. **30**, 714 (2004) [Low Temp. Phys. **30**, 535 (2004)].
[5]N. N. Bogatina and S. I. Bondarenko, Fiz. Nizk. Temp. **20**, 100 (1994) [Low Temp. Phys. **20**, 81 (1994)]; P. Selders, A. M. Castellanos, M. Vanpel, and R. Wordenweber, IEEE Trans. Appl. Supercond. **9**, 2967 (1999).
[6]R. Liang, D. A. Bonn, W. N. Hardly, and D. Broun, Phys. Rev. Lett. **94**, 117001 (2005).
[7]A. V. Bondarenko, A. A. Prodan, M. A. Obolenskiĭ, R. V. Vovk, and T. R. Arouri, Fiz. Nizk. Temp. **27**, 463 (2001) [Low Temp. Phys. **27**, 339 (2001)].
[8]M. A. Obolenskiĭ, A. V. Bondarenko, V. A. Shklovskiĭ, R. V. Vovk, and A. A. Prodan, Fiz. Nizk. Temp. **24**, 71 (1998) [Low Temp. Phys. **24**, 53 (1998)]; M. A. Obolenskiĭ, A. V. Bondarenko, and M. O. Zubareva, Fiz. Nizk. Temp. **15**, 1152 (1989) [Low Temp. Phys. **15**, 635 (1989)].

Translated by M. E. Alferieff

PERSONALIA

Igor' Vadimovich Svechkarev (On his 70th birthday)

[DOI: 10.1063/1.2144461]

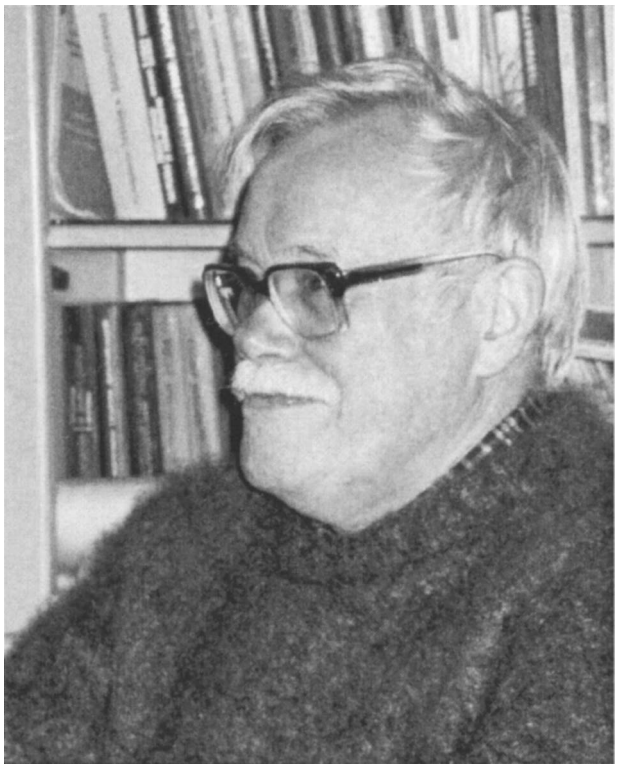

Professor Igor' Vadimovich Svechkarev, a prominent scientist in the field of the physics of weak magnetism of metals and the director of a division of the B. I. Verkin Institute for Low Temperature Physics and Engineering of the National Academy of Sciences of Ukraine, celebrated his 70th birthday on December 16, 2005. His work on the investigation and explanation of the nature of the anomalies of the magnetic susceptibility in simple metals and their relation to the energy spectrum of the conduction electrons and his work on determining the basic dependences in the variation of the parameters of the electronic band spectrum of transition and rare-earth metals under pressure won him wide international acclaim in physics. Prominent physicists from universities in Oregon and Maryland (USA), Toronto (Canada), Amsterdam (Netherlands), and elsewhere repeatedly visited the division of which he is the director to perform joint studies. Igor' Vadimovich celebrates his birthday among young colleagues, researchers, and graduate students, guiding whom is his special concern. I. V. Svechkarev was an active member of the editorial board of this journal for many years.

We warmly congratulate Igor' Vadimovich on his birthday and wish him good health, success, and many years of fruitful scientific work.

Editorial Board

